NTNU

Norwegian University of
Science and Technology

Blade Dynamic Response for Downwind Turbines

Marie Salthaug

Master of Science in Product Design and Manufacturing
Submission date: June 2011
Supervisor: Per-Åge Krogstad, EPT

Norwegian University of Science and Technology
Department of Energy and Process Engineering

Abstract

A MATLAB script has been developed to investigate dynamics in the blades of a 10 MW downstream wind turbine, with both a tubular- and a truss tower. The classical Beam element momentum method with additional correction factors are used to determine forces on the blade. Centrifugal loading have been applied by use of an iteration method. Blade dynamic response is investigated in terms of Modal analysis. In addition, the dynamic response of a blade with adjusted stiffness has been investigated.

Three approaches to obtain the wind velocity field in the rotor plane are studied; averaged Blevins model with input from a study in ANSYS FLUENT, Wind files extracted from ANSYS FLUENT, and results from a small scale wind tunnel experiment. The three cases provide ambiguous results with regards to blade deflection and root flapwise bending moment.

Results indicates that vortex shedding have large effect in a tubular tower configuration, but small effect in a truss tower configuration.

Based the most the most trusted input, the wind tunnel case, the results indicates that a truss tower would provide more desired values in terms of root flapwise bending moment and fatigue loading.

Trondheim, June 2011 Marie Salthaug

Preface

This thesis constitutes the written work related to the subject TEP4925: *Engineering Fluid Mechanics, Master Thesis* at the Norwegian University of Science and Technology (NTNU). My supervisor has been professor Per-Åge Krogstad at the Department of Energy and Process Engineering, NTNU.

I would like to thank scholarship holder Lars Frøyd for providing data and sharing knowledge regarding wind turbine blades. Important advice on how to best model a blade has been provided by Professor Geir Moe.

I am grateful for the patience Erlend Schou Fævelen has showed during the semester and for his help with proofreading the paper. Thanks to M.Sc. Leif Salthaug at Salcon AS for his tips and general expertise.

Finally, I wish to express sincere gratitude to scholarship holder Marit Reiso and researcher Michael Muskulus at the Department of Civil and Transport Engineering for assistance throughout the semester. They have provided insight in the field of downwind turbines and structural analyses, and their positive attitude and thorough follow up has been a source of inspiration during the work.

Table of Contents

List of figures

List of Tables

List of Symbols

Symbol	Unit	Description
A	m^2	Area
a	-	Axial induction factor
a_c	-	Critical value of a in Glauert correction
a’	-	Tangential induction factor
B	-	Number of blades
b	m	Distance to one half centerline deficit
C	kg/s	Damping matrix
c	m	Damping
C_D	-	Drag coefficient
C_L	-	Lift coefficient
C_N	-	Normal force coefficient
C_P	-	Power coefficient
C_T	-	Tangential force coefficient
D	m	Diameter
d_c	m/s	Centerline deficit
dD	N/m	Sectional drag
dL	N/m	Sectional lift
dT	N/m	Sectional Thrust
dQ	N/m	Sectional force in torque direction
E	N/m^2	Modulus of elasticity
E_{kin}	J	Kinetic energy
F	N	Force

F_{CF}	N	Centrifugal force
F_{CF}	N	Centrifugal force in flapwise direction
F_{CR}	N	Centrifugal force in radial direction
F	-	Tip loss factor
G	N/m^2	Shear modulus of elasticity
I_y	m^4	Second moment of area (flapwise)
I_z	m^4	Second moment of area (edgewise)
J	m^4/rad	Torsional stiffness constant
K	N/m	Stiffness matrix
K_G	-	Coefficient in Glauerts Correction
k_j	N/m	Generalized stiffness
k_y	-	Timoshenko Shear coefficient (flapwise)
k_z	-	Timoshenko Shear coefficient (edgewise)
L	m	Sectional length
L_C	m	Chord length
M	kg	Mass matrix
M_{edge}	Nm	Edgewise bending moment
M_{flap}	Nm	Flapwise bending moment
M_Q	Nm	Torque
m	kg	Mass
m_j	kg	Generalized mass
$\dot{m}$	kg/s	Mass flow
P	w	Power
p	Pa	Pressure
Q	Nm	Force in torque direction
R	N	Load vector
Re	-	Reynolds number
r	m	Radius
s	m	Distance
T	N	Thrust
t	s	Time
$\vec{u}$,U	m/s	Wind velocity
U_{rel}	m/s	Relative wind velocity
V	m^3	Volume

v	m	Degrees of freedom/Deflection in edge direction
w	m	Deflection in flap direction

Greek Symbols

Symbol	Unit	Description
α	rad	Angle of attack
β	rad	Cone angle
φ	rad	Angle between plane of rotation and relative wind
θ	rad	Deflection angle
θ_P	rad	Section pitch angle
$\theta_{P,0}$	rad	Blade pitch angle
θ_T	rad	Section twist angle
λ	-	Tip speed ratio
λ_r	-	Local speed ratio
ρ	kg/m^3	Density
σ	-	Solidity
ψ	-	Mode shape
Ω	rad/sec	Rotational speed
ω	rad/sec	Added rotational wind speed
ω_n	Hz	Natural frequency
ζ	-	Damping ratio
μ	kg/m-s	Air viscosity

1 Introduction and Theory

Wind energy has a great potential as a viable energy source. Onshore wind turbine parks are today well developed. Lack of space, visual impact as well as stronger and more consistent winds has created a focus on offshore development; though the main argument by critics is high development cost.

Currently, wind turbines that are able to deliver 10 MW are in the making. These turbines will have more than 60 meters long rotor blades. A large mass is necessary to obtain sufficient stiffness in these blades. Offshore turbines must endure strong forces from wind and waves. Some designs even involve a floating turbine. One is therefore looking to minimize mass in nacelle and rotor.

In addition to the extensive research and development, installation and maintenance are demanding and expensive offshore. Offshore wind energy is still in an early face, and minimizing cost is of major focus in all areas.

One possible solution is the downwind turbine concept, where blades are placed downstream of the tower. The basic advantage of this design is the reduced risk of tower strike. The blades can be made softer and, as a result, lighter. This would in turn reduce the load on nacelle and tower. The design has been considered a poor design because of the tower shadow effect; the blades are subjected to a cyclic load for every revolution.

The scope of this paper is to survey the rotor blade dynamic with the presence of different tower shadows; a Matlab script is made to model the blade dynamic response with both a tubular and a truss tower.

The paper starts off with a quick overview of truss design in offshore wind energy. Following is an overview of the theory connected with forces on the wind turbine rotor. The resulting Matlab model is described and the results are discussed and concluded.

1.1 Truss Design in Downwind Turbines

Tower and foundation are important parameters in offshore wind turbines. They must be able to withstand external forces such as wind and waves, in addition to the forces generated from rotation of the rotor. In downwind turbines the tower shadow effect must be minimized.

Truss towers consist of columns, bracings and horizontal beams. Steel pipes or square hollow sections are most common to use, but open steel H- or channel sections are to some extent used [1].

According to the Danish Wind Industry Association, the basic advantage of truss towers is cost, as a truss tower requires only half as much material as a freely standing tubular tower with a similar stiffness. The disadvantage of truss towers is their visual appearance. When moving the wind turbines offshore, this will no longer be an issue [2]. To the authors knowledge there are currently no complete truss structure towers in offshore downwind turbine projects.

However, there are some examples of incorporating truss structures wind turbines. The Owec tower has been used in Alpha Ventus and Beatrice Wind Farm Demonstrator Project 25 km off the east coast of Scotland where the first turbine was installed in 2006. This is a complete substructure that contains a tubular tower, middle section, and truss foundation with piles. The middle section transfers forces from the tubular tower to the truss foundation [3].

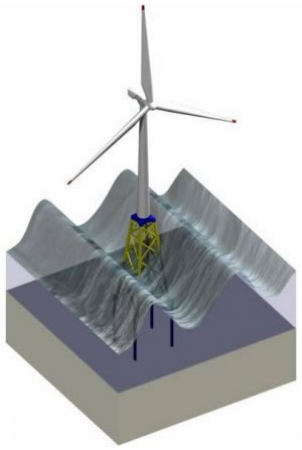

Figure 1 Owec tower with truss foundation in Beatrice Project [4]

The basic advantages and disadvantages of truss towers [5]:

Advantages:

- Low material costs
- Low hydrodynamic forces
- Low wind forces

Disadvantages

- Demanding fabrication process
- Maintenance demands can be wide-ranging (control of welds etc.)
- Low torsional stiffness
- Access to the nacelle becomes difficult after erection

1.2 Energy from Wind

To understand the behavior of the rotor, it is necessary to know a few basic physical relations of a body in motion. The following is background for the blade element momentum theory described in chapter 1.2.6. The theory in chapters 1.2.1 to 1.2.3 is based on Manwell et al. [6].

1.2.1 Energy and Power in Wind Inflow

Consider air is flowing through a disc shaped energy extraction device. The kinetic energy, E_{kin}, from the air is given as:

$$E_{kin} = \frac{1}{2} m \vec{u}^2 \quad (1)$$

Here $\vec{u}$ is the constant velocity of the incoming wind and m is mass of air. The mass described are the total mass of air that moves through the energy extracting device in a given time, t:

$$m = \rho A s = \rho A \vec{u} t \quad (2)$$

Here ρ is density of air, A is the area of the disc, s is distance, and t is the given time (see Figure 2).

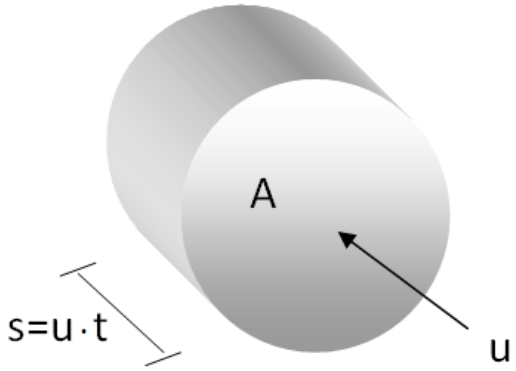

Figure 2 The Energy extracting disc with area *A*, incoming wind velocity *u*, at given time, *t*, and resulting distance s.

Energy of the flow that passes through the disc during a unit time gives the power, *P*:

$$P = \frac{dE_{kin}}{dt} = \frac{1}{2}\dot{m}\vec{u}^{2} \tag{3}$$

Where $\dot{m}$ is mass flow, given by:

$$\dot{m} = \frac{dm}{dt} = \rho A\vec{u} \tag{4}$$

Combining equations (3) and (4) gives the following expression for power in the wind, *P*, through area *A*:

$$P = \frac{1}{2}\rho A\vec{u}^{3} \tag{5}$$

Form equation 5 it can be seen that the power of the wind is proportional to the cube of the wind speed, and is an important factor when evaluating sites for placing wind turbine parks. The power varies linearly with the area of the disc.

1.2.2 Betz Limit

A turbine can never reach 100% efficiency. Total utilization of the available energy in the wind would mean that the wind speed downstream of the rotor would be zero, which is physically impossible.

Consider an idealized rotor with an infinite number of blades, with following assumptions:

- Homogeneous, incompressible and stable flow
- No friction
- Uniform thrust across rotor area
- Non rotating wake
- Static pressure is the same far upstream and far downstream of the rotor.

A tubular control volume goes far upstream and far downstream of the rotor (see Figure 3). Looking at momentum far upstream and far downstream, respectively point 1 and 4 in Figure 3, the net change of force can be obtained. This force is equal the force thrust force, *T*, on the rotor.

$$T = \vec{u}_1 \left(\rho \vec{u} A\right)_1 - \vec{u}_4 \left(\rho \vec{u} A\right)_4 \tag{6}$$

Where *A* is the area the control volumes cross section.

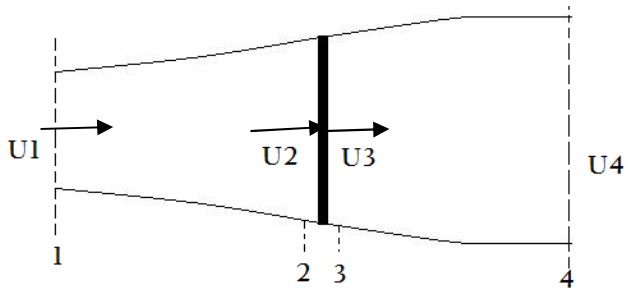

Figure 3 Control volume for rotor disc with wind velocities, U, at four different control points [6]

For steady state flow the mass flow rate, $\dot{m}$, is constant:

$$\left(\rho \vec{u} A\right)_1 = \left(\rho \vec{u} A\right)_4 = \dot{m} \tag{7}$$

Combining equations (6) and (7) gives another expression for thrust:

$$T = \dot{m}\left(\vec{u}_1 - \vec{u}_4\right) \tag{8}$$

The disc extracts energy, i.e. velocity will be lower downstream of the rotor.

No work is done upstream or downstream of the rotor. The energy here is therefore constant. Bernoulli's equation can accordingly be used in regions upstream (point 1 to 2) and downstream of the rotor (point 3 to 4).

Upstream:

$$p_1 + \frac{1}{2}\rho \vec{u_1}^2 = p_2 + \frac{1}{2}\rho \vec{u_2}^2 \tag{9}$$

Downstream:

$$p_3 + \frac{1}{2}\rho \vec{u_3}^2 = p_4 + \frac{1}{2}\rho \vec{u_4}^2 \tag{10}$$

Here *p* is pressure.

It is assumed the pressure far upstream and far downstream is the same ($p_1=p_4$) and that wind velocity is equal right before and after the disc ($u_2=u_3$). Using these assumptions and combining equations (9) and (10) gives:

$$p_2 - p_3 = \frac{1}{2}\rho\left(\vec{u}_1^2 - \vec{u}_4^2\right) \tag{11}$$

Continuity gives that thrust force can be expressed using difference of forces over the rotor. Assuming the area in point 3 in Figure 3 is equal to the area of point two gives the following expression for thrust:

$$T = A_2\left(p_2 - p_3\right) \tag{12}$$

Using Bernoulli combined with continuity gives thrust force one the rotor, i.e. combining equations (11) and (12):

$$T = \frac{1}{2}\rho A_2\left(\vec{u_1}^2 - \vec{u_4}^2\right) \tag{13}$$

The existing power, P, is thrust force multiplied with wind velocity at the disc:

$$P = \frac{1}{2}\rho A_2 \left(\vec{u}_1^{\,2} - \vec{u}_4^{\,2} \right) \vec{u}_2 \tag{14}$$

Setting the equation for thrust in equation (8) equal the equation for thrust in (13), and inserting that mass flow rate, $\dot{m} = \rho \vec{u}_2 A_2$, gives:

$$\frac{1}{2}\rho A_2 \left(\vec{u}_1^{\,2} - \vec{u}_4^{\,2} \right) = \rho \vec{u}_2 A_2 \left(\vec{u}_1 - \vec{u}_4 \right) \tag{15}$$

Resulting in an expression for the wind velocity in point to in Figure 3:

$$\vec{u}_2 = \frac{\vec{u}_1 + \vec{u}_4}{2} \tag{16}$$

Thus, the wind velocity at the rotor plane, using this simple model, is the average of the upstream and downstream wind speed.

Introducing the axial induction factor, *a,* as the fractional decrease in wind velocity between the free stream and the rotor plane:

$$a = \frac{\vec{u}_1 - \vec{u}_2}{\vec{u}_1} \tag{17}$$

Rearranging this equation:

$$\vec{u}_2 = \vec{u}_1 (1 - a) \tag{18}$$

Combining equations (16) and (18) gives and solving for u_4 gives:

$$\vec{u}_4 = \vec{u}_1(1-2a) \tag{19}$$

Inserting the expression for u_4 in equation (13) gives a new equation for thrust:

$$T = \frac{1}{2}\rho A\vec{u}_1^2\left[4a(1-a)\right] \tag{20}$$

Combining equations (16) and (17) gives equations for $\vec{u}_1$ and $\vec{u}_4$. Inserting into (14) gives:

$$P = \frac{1}{2}\rho A\vec{u}^3 4a(1-a) \tag{21}$$

Note that in equations (20) and (21) A_2 has been replaced by *A*, overall area swept by the rotor.

The turbines performance is characterized by a power coefficient, C_P. It is given as:

$$C_P = \frac{P}{\frac{1}{2}\rho\vec{u}^3} = 4a(1-a)^2 \tag{22}$$

The maximum C_P is determined by taking the derivative of the power coefficient with respect to *a* and setting it equal to zero.

$$\begin{aligned} &\frac{dC_P}{da} = 0 \\ &\rightarrow 4(1-a)^2 - 8a\cdot(1-a) = 0 \\ &(3a-1)(a-1) = 0 \end{aligned} \tag{23}$$

Cp reaches a minimum with a=1 and a maximum with a =1/3. The Corresponding maximum C_P value is 16/27 or 59 %. This is the so called Betz limit. The turbine can theoretically capture 59% of the kinetic energy in the wind. In reality there are many limiting factors that contribute to making this limit impossible to reach. Examples include a finite number of blades, rotating wake and tip loss[6].

1.2.3 Corrections for Betz Limit

In the case of a rotating wind turbine rotor, the flow behind the rotor rotates in the opposite direction to the rotor (see Figure 4). This is in reaction to the torque exerted by the flow on the rotor. This added kinetic energy to the downstream wind serves as a loss in extractable turbine energy.

Assuming the wind rotational velocity is small compared to the rotor rotational velocity, one can still assume that the pressure far upstream and downstream of the turbine is equal.

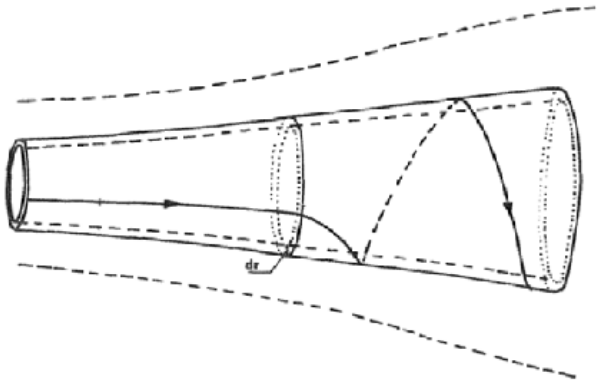

Figure 4 Spin induced in wind with Wake Rotation [6]

The analysis that follows is based on the use of an annular stream tube with a radius r and a thickness dr, resulting in a cross-sectional area equal to $2\pi rdr$ (see Figure 5).

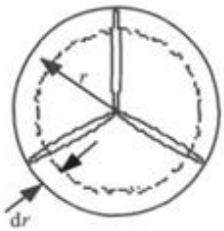

Figure 5 Cross section of stream tube with annular sections of thickness dr with distance r from the centre [6].

Using a control volume that moves with the angular velocity of the blades, the energy equation can be applied to the sections before and after the blades to derive an expression for the pressure difference across the blades:

$$p_2 - p_3 = \rho\left(\Omega - \frac{1}{2}\omega\right)\omega r^2 \tag{24}$$

Where Ω is rotational speed of the rotor and ω is added angular velocity of the air.

The resulting thrust force on an annular element, dT, is:

$$dT = (p_2 - p_3)\,dA = \rho\left(\Omega - \frac{1}{2}\omega\right)\omega r^2 2\pi r dr \tag{25}$$

Angular induction factor, a', is defined as:

$$a' = \frac{\omega}{2\Omega} \tag{26}$$

Inserting the expression for angular induction factor in equation (25):

$$dT = 4a'(1+a')\frac{1}{2}\rho\Omega^2 r^2 2\pi r dr \tag{27}$$

By using that the area, *A,* for a cross sectional area is *2πrdr*, the equation for thrust force from the analysis without wake rotation (equation (20)) gives an expression for thrust on an annular element:

$$dT = 4a(1-a)\rho\vec{u}^2\pi r dr \tag{28}$$

Note that $\vec{u}_1$ has been replaced by $\vec{u}$, free stream velocity.

An expression for the torque on the rotor can be found by applying the conservation of angular momentum. By this, torque exerted on the rotor, dM_Q, must equal change in angular momentum of the wake. On an incremental annular area element this gives:

$$dM_Q = d\dot{m}(\omega r)(r) = \rho U_2 2\pi dr(\omega r)(r) \tag{29}$$

Inserting that U_2=U(1-a) and a'=ω/2Ω, this expression reduces to:

$$dM_Q = 4a'(1-a)\rho u\Omega r^2\pi r dr \tag{30}$$

The force in torque direction, dQ, is equal to the torque divided by *r*:

$$dQ = 4a'(1-a)\rho u\Omega r^2\pi dr \tag{31}$$

1.2.4 Airfoils and Aerodynamics

Wind turbine blades act in principle as wings on an airplane. Pressure difference above and below the blade creates a lift. The basic theory is that streamlines separate at the beginning of the blade and merges on a point behind the blade (see Figure 6). Because of asymmetry in the cross section, the flow over the wing must have higher velocity to reach the merging point.

Bernoulli gives:

$$\frac{1}{2}\rho u^2 + p = \text{constant for a streamline.} \quad (32)$$

The result is that pressure is lower on the top of the wing, creating a lift force [7].

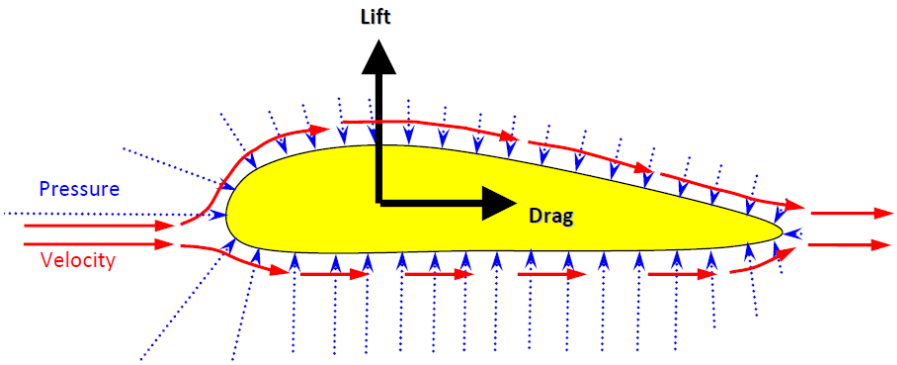

Figure 6 Pressure and velocity profile over blade cross section. Lower pressure on the top of the cross section creates a lift force. [7]

Design of airfoils is not considered to be within the scope of this paper. Only a brief explanation of important parameters is presented [6]:

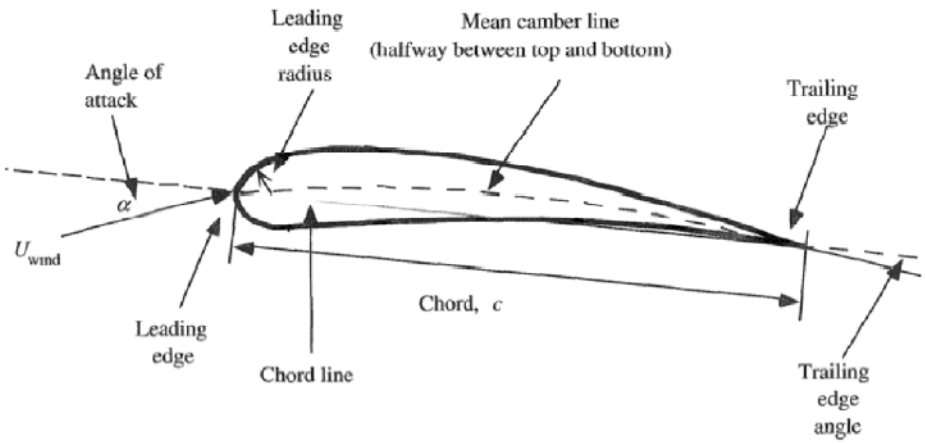

Figure 7 Terminology used to describe an airfoil [6]

- The chord line is a straight line between the leading edge and trailing edge.
- Angle of attack is the angle between the chord line and the relative wind
- Mean camber line is the locus of points halfway between the upper and lower surfaces of the airfoil
- Camber the distance from the chord line to mean camber line, measured perpendicular to the chord line.
- Thickness is the distance between lower and upper surfaces, measured perpendicular to the chord line.

The geometric parameters that have an effect on the aerodynamic performance of an airfoil include: the leading edge radius, mean camber line, maximum thickness and thickness distribution of the profile and the trailing edge angle[8].

Angle of attack (AoA) is the factor that has the greatest influence on rotor performance. Drag increases with increasing AoA, so does lift, up to a critical point where stall begins to form. Stall occurs when the flow gets separated from the blade (see Figure 8). This is when the angle of attack becomes too big, and the airstream do not have enough energy to follow the blade surface. Stall creates turbulence and backflow, resulting in loss of lift [7].

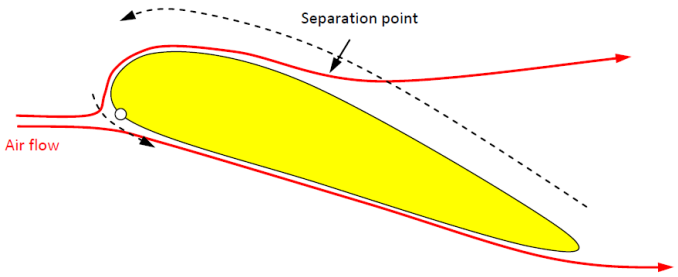

Figure 8 Separation of stream lines and resulting stall on cross section. Red lines illustrate air stream, dotted line illustrate backflow [7].

1.2.5 Blade Element Method

The idea behind the blade element method (BEM) is to divide the blade in sections, and assume no aerodynamic interaction between the sections. Lift and drag are the only forces acting on the blade. Note that lift is the force perpendicular to the relative incoming wind, and drag is a force parallel to the relative incoming wind.

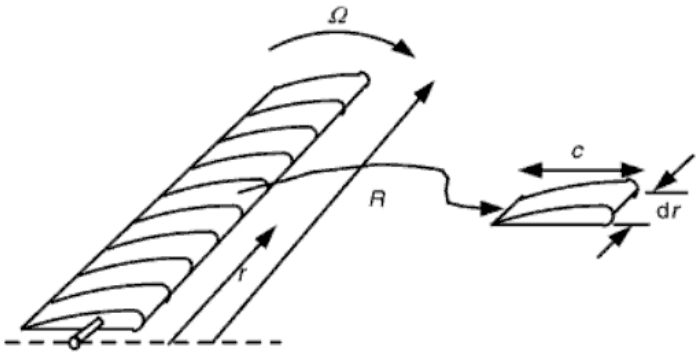

Figure 9 Blade Element Method: no aerodynamic interaction between sections. Displaying section of length *dr* and chord length *c* at a distance *r* from center rotating with velocity Ω. R total blade radius[6].

Looking at a blade cross section, one can analyze forces and determine geometric relations (see Figure 10)

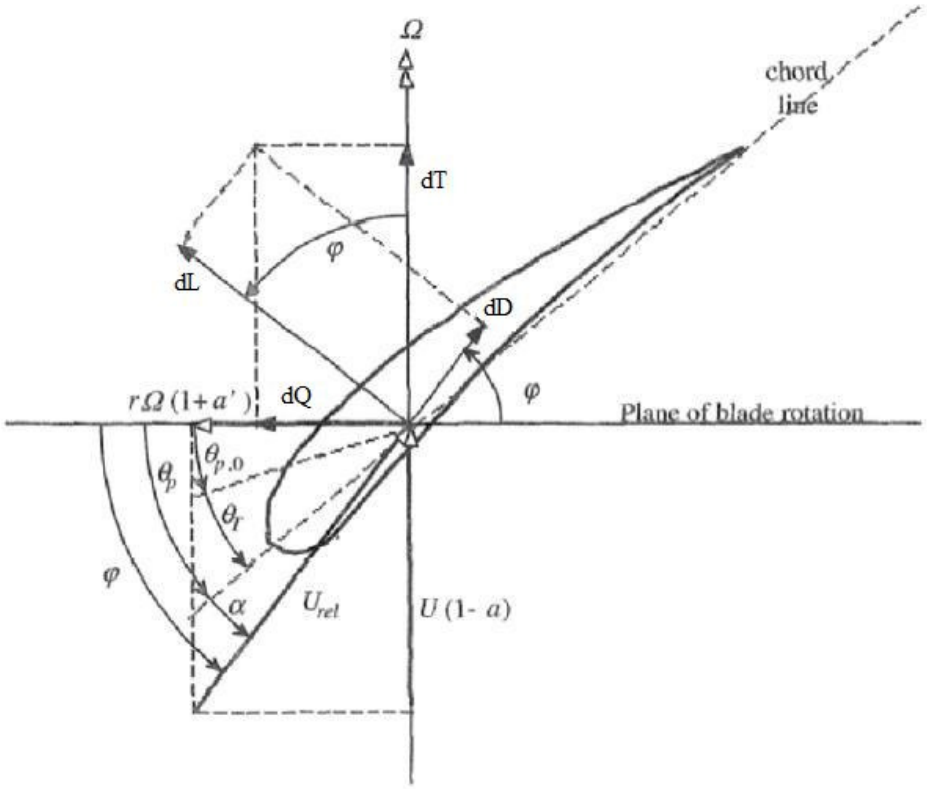

Figure 10 Geometric relations and aerodynamic forces on cross section [6]

Where:

U(1-a): Incoming wind velocity

U_{rel}: Relative wind velocity

θ_p : Section pitch angle, i.e. angle between chord line and plane of rotation

$\theta_{p,0}$: Blade pitch angle

θ_T : Section twist

α: Angle of attack

φ: Angle between plane of rotation and relative wind

dL: Incremental lift

dD: Incremental drag

dT: Incremental force normal to plane of rotation (Thrust).

dQ: Incremental force tangential to plane of rotation. This is the force that creates electric power.

From Figure 10, the following geometric relations apply (equations (33) to (37)):
The angle between the plane of rotation and the relative wind is the sum of angle and attack and the twist:

$$\varphi = \theta_T + \alpha \tag{33}$$

The same angle can also be defined as:

$$\tan\varphi = \frac{U(1-a)}{\Omega r(1+a')} \tag{34}$$

Before a blade is pitched, one can find the angle of attack by:

$$\alpha = \tan^{-1}\left(\frac{U(1-a)}{\Omega r(1+a')}\right) - \theta_T \tag{35}$$

The velocity of the relative wind can be found by:

$$U_{rel} = \frac{U(1-a)}{\sin\varphi} \tag{36}$$

or:

$$U_{rel} = \frac{\Omega r(1+a')}{\cos\varphi} \tag{37}$$

1.2.5.1 Blade Element Momentum Method

Lift- and drag per unit length for flow around two dimensional objects are given as:

$$dL = \frac{1}{2}\rho \cdot U_{rel}{}^2 \cdot L_C \cdot C_L \tag{38}$$

$$dD = \frac{1}{2}\rho \cdot U_{rel}{}^2 \cdot L_C \cdot C_D \tag{39}$$

Here L_C the local chord length, and C_L and C_D are lift and drag coefficients. C_L and C_D are dependent on the airfoil geometry, and vary with angle of attack. Tables displaying angle of attack and the belonging lift and drag forces are usually determined by wind tunnel experiments or blade design software[6].

Lift and drag coefficients projected into directions normal and tangential to the rotor plane:

$$C_N = C_L \cos(\varphi) + C_D \sin(\varphi) \tag{40}$$

$$C_T = C_L \sin(\varphi) - C_D \cos(\varphi) \tag{41}$$

Hence, forces per unit length in directions normal to and tangential to the rotor plane are:

$$dT = \frac{1}{2}\rho \cdot U_{rel}{}^2 \cdot L_C \cdot C_N \tag{42}$$

$$dQ = \frac{1}{2}\rho \cdot U_{rel}{}^2 \cdot L_C \cdot C_T \tag{43}$$

Using equation (36) for U_{rel} and multiplying with sectional length and number of blades, *B*, gives the following expression for total thrust on the rotor:

$$dT = \frac{1}{2}\rho B \frac{U_0^2(1-a)^2}{\sin^2\varphi} L_C C_N dr \tag{44}$$

Similarly, equations (36) and (37) for U_{rel} gives the expression for force in torque direction:

$$dQ = \frac{1}{2}\rho B \frac{U_0(1-a)\Omega r(1+a')}{\sin\varphi\cos\varphi} L_C C_T dr \tag{45}$$

Referring to the equations derived for thrust (28) and torque (31) in chapter 1.2.3. These are called the momentum equations:

$$dT = 4a(1-a)\rho\vec{u}^2\pi r dr \tag{46}$$

$$dQ = 4a'(1-a)\rho u\Omega r^2\pi dr \tag{47}$$

Solidity is defined as the fraction of the annular area that is covered by blades:

$$\sigma(r) = \frac{L_C(r)B}{2\pi r} \tag{48}$$

Here *B* is number of blades.

Setting equation for thrust from the blade element method (44) equal to the thrust from the momentum equation (46), and include the expression for solidity gives an expression for the axial induction factor:

$$a = \left[\frac{4\sin^2 \varphi}{C_N \sigma} + 1 \right]^{-1} \tag{49}$$

Similarly, setting equation (45) equal (47) gives an expression for the tangential induction factor:

$$a' = \left[\frac{4\sin \varphi \cos \varphi}{C_T \sigma} - 1 \right]^{-1} \tag{50}$$

The induction factors will depend on the characteristics and size of the airfoil used. Since the different blade sections are assumed to be aerodynamically independent of each other, each section can be treated separately.

1.2.5.2 Tip Loss

Ideally the air would flow straight across the wing, parallel with the airfoil. However, at the tip of the blade, this is not the case.

There is a pressure difference above and below the blade. At the tip of the wing, the shortest route the airflow can take to equate this pressure difference is around the tip of the airfoil (see Figure 11). This has two effects [7]:

- The lift is reduced as the air pressure is equated at the tip
- A vortex is created in the wake of the blade tip

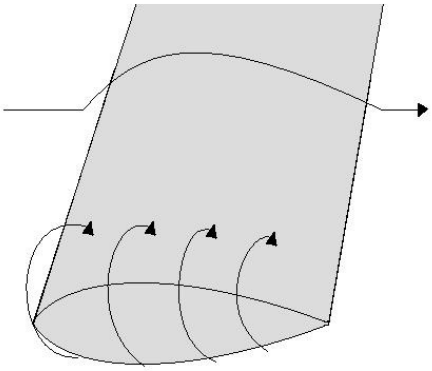

Figure 11 Flow of air with tip loss

The tip loss effect can be accounted for by Prandt'l's tip loss factor. Prandt'l's tip loss factor assumes that the wake does not expand. This is a simplification, but the error is assumed to be small and can be neglected. Prandt'l's tip loss effect factor is:

$$F = \frac{2}{\pi}\cos^{-1}\left(\exp\left(-\frac{B}{2}\cdot\frac{1-\left(\frac{r}{R}\right)}{\left(\frac{r}{R}\right)\sin\varphi}\right)\right) \tag{51}$$

Here *R* is the total blade radius, and *r* is the sectional radius.

The factor will be used to correct expressions for induction factors and forces; i.e. equations (49) and (50) becomes:

$$a = \left[\frac{4F\sin^2\varphi}{\sigma C_N} + 1\right]^{-1} \tag{52}$$

And

$$a' = \left[\frac{4F\sin\varphi\cos\varphi}{\sigma C_T} - 1\right]^{-1} \tag{53}$$

Note that at the tip of the blade tip loss factor approaches zero. As a result the axial induction factor will approach 1 and tangential induction factor to become -1. This means that the wind speed at the tip of the blade would be zero. The reason behind this is that one is operating with two different induction factors, one local to the blade where the wind is affected the most, and one average value. To find the average induction factors, axial and tangential induction factors must be multiplied with the tip loss factor. Thus the factors would approach zero as the tip loss factor approaches zero. The azimuthally average is the ones to be used in the energy and efficiency equations [7].

1.2.5.3 Glauerts Correction for Heavy Loaded Turbines

From equation (20) it is clear that C_T will approach zero when the axial induction factor approaches 1. In reality the trust force on the turbine would not approach zero but increase above 1. The trust on a turbine can be higher than the static pressure in the wind [7].

Glauert suggested a model to correct this based on empirical data. The model is only to be used for values of a above a certain level; a_c. Glauert suggested a_c to be 0.2. This model should be used instead of (52) when the axial induction factor is higher than the critical limit [7]:

$$a = \frac{1}{2} \cdot \left[2 + K\left(1 - 2a_c\right) - \sqrt{\left(K_G\left(1-2a\right)+2\right)^2 + 4\left(Ka_c^2 - 1\right)} \right] \tag{54}$$

Where:

$$K_G = \frac{4F\sin^2\varphi}{\sigma C_N} \tag{55}$$

The final result is an algorithm determining axial and tangential induction factors based on both blade element method and the momentum equations. The induction factors are affected by the tip loss factor and Glauerts corrections [7]:

I. Initialize a and a'
II. Compute local air flow angle using (34)
III. Compute Prandtl's tip loss factor using (51)
IV. Compute local angle of attack using (33)
V. Obtain C_L and C_D from table (given angle of attack)
VI. Compute C_N and C_T from (40) and (41)
VII. Calculate a from equation (52). If the axial induction factor is above a_c, use equation (54).
VIII. Calculate a' from equation (53)
IX. If the new values for a and a' have changed more than a certain tolerance, repeat from step II.

The force on blade section can finally be found by including tip loss in the equations from blade element method ((44) and (45)):

$$dT = F\frac{1}{2}\rho B\frac{U_0^2(1-a)^2}{\sin^2\varphi}L_C C_N dr \tag{56}$$

$$dQ = F\frac{1}{2}\rho B\frac{U_0(1-a)\omega r(1+a')}{\sin\varphi\cos\varphi}L_C C_T dr \tag{57}$$

Note that these forces are in the rotor plane; i.e. if the blade is coned, the forces must be projected into the blade coordinate system by multiplying the thrust force by the cosine of the cone angle.

1.3 Tower Shadow

Tower shadow is the area of the rotor plane where the incoming flow pattern has been changed by the tower; i.e. the tower shadow is a region characterized by reduced wind velocity and altered stream lines.

The flow around a cylinder can be characterized an expression of the unitless coefficient called Reynolds number, Re[9]:

$$\mathrm{Re} = \frac{\rho U D}{\mu} \tag{58}$$

Here U is free stream wind velocity, D is diameter of the cylinder (tower), and μ is air viscosity. Reynolds number describes the nature of the stream lines (see Figure 12).

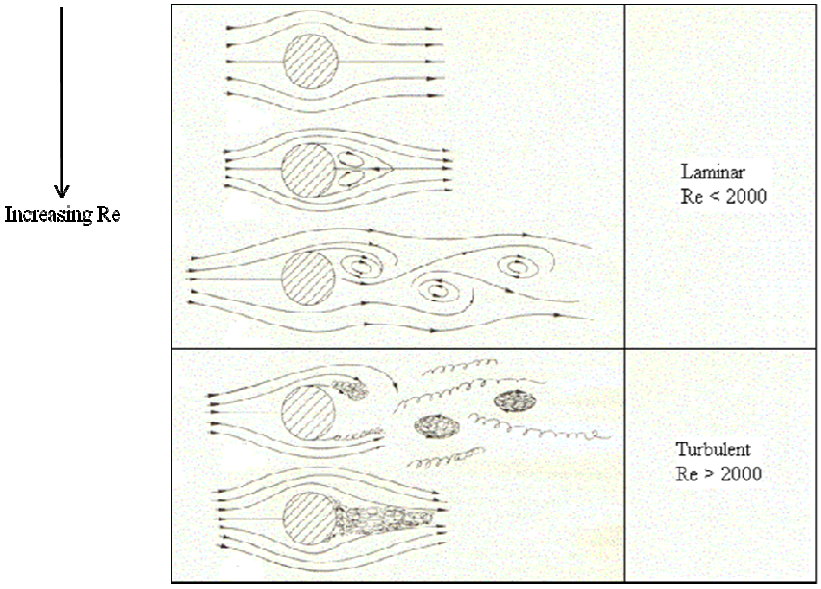

Figure 12 Boundary layer separation with increasing Reynolds number [10].

With Reynolds number below 2000, the flow around the cylinder is laminar [10]. At very low Reynolds numbers (under 0.5), the air streams will flow as seen in topmost case. The air velocity right before and right after the cylinder comes to a stop. If 0.5<Re<70 boundary

layers separate symmetrically on either side of the cylinder. The ends of these separated zones remain attached to the cylinder as shown above. At Reynolds number between 70 and 2000 the ends of the separated zones curl up into vortices and detach alternately from each side forming a trail of vortices on the downstream side of the cylinder [9].

Turbulence starts to form in the region behind the cylinder with Reynolds numbers above 2000, the velocity at a given point can change in magnitude and direction.

Because the free stream wind velocity, density, and viscosity are assumed to be constant in this study, only the diameter of the cylinder will have the dominating impact on the flow pattern behind the cylinder.

1.3.1 Tower Shadow Modeling

A study carried out by Hagen et al. [11] indicated that the most realistic way of modeling the tower shadow is done by Blevins approach.

The model proposed by Blevins is a two parameter model with one parameter describing the distance upstream of the virtual origin the wake, and the second parameter being the drag coefficient of the cylindrical member; tower. Truss tower consists of four such cylinders. The time averaged velocity profiles in Blevins model are given by [12]:

$$b = 0.23\left[C_D D\left(z + z_0\right)\right]^{1/2} \tag{59}$$

$$d_c = 1.02 V_\infty \left(\frac{C_D D}{z + z_0}\right)^{1/2} \tag{60}$$

$$U\left(x, z\right) = U_\infty \left(1 - \frac{d_c}{U_\infty} e^{-0.69 x^2 / b^2}\right) \tag{61}$$

Here *b* is transverse distance to one-half centerline deficit, C_D is the drag coefficient of the tower, *D* is the member diameter, *z* is the distance downstream for the member center, *x* is the transverse distance, z_0 the upstream location of the virtual origin of the wake, d_c is the centerline velocity deficit, U_∞ is free stream wind velocity and *U(x,z)* is the wind velocity distribution downstream of the cylinder (see Figure 13).

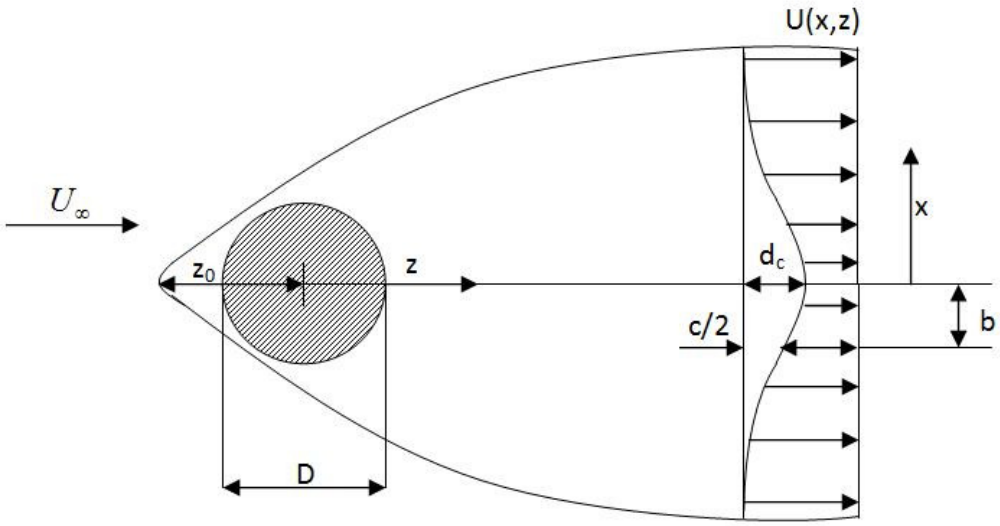

Figure 13 Parameters in Blevins model for determining wind velocity field behind a cylinder.

The model assumes that the wake width grows with the square root of the distance. The advantage of this model is that the virtual origin allows for more flexibility. The location of the origin can be modified to make the wind field match results from wind tunnel tests.

Assuming the wake to be frozen, the axial induced velocity and angular induced velocity are taken as remaining constant over time, at each radius, at the values calculated for steady free stream velocity [13].

1.3.2 Tower Shadow Influence on Blades

The tower shadow does not contribute to considerable loss of power, but the velocity deficit that the blades experience every rotation will have an impact on the blade fatigue life [14].

Fatigue is a failure condition which occurs with the presence of cyclic loading: i.e. it is not the mean stress, but the amplitude of the alternating stress that influence the fatigue life of the material. Larger alternating stress gives shorter time to fatigue[15]. Fatigue calculations of composite wind turbine blades are complex, and will not be carried out in this paper.

When dealing with cyclic force dips, resonance issues can occur. It is important that the natural frequency of the blades does not match the frequency of the force dips induced by the tower shadow.

1.4 Blades

Modern wind turbine blades consist of skin, spar cap and web (see Figure 14). The skin is airfoiled shaped and normally consist of glass-fibre-reinforced plastics (GPRs) or carbon fibre reinforced plastics (CFRPs) [16]. Spar and skin are the main carrying components: The skin carries the main edgewise and torsional loading, while the spar caps carry the main flapwise loading. The purpose of the web is to distribute shear forces under flapwise deflection, but it also contributes to edgewise and torsional stiffness [17].

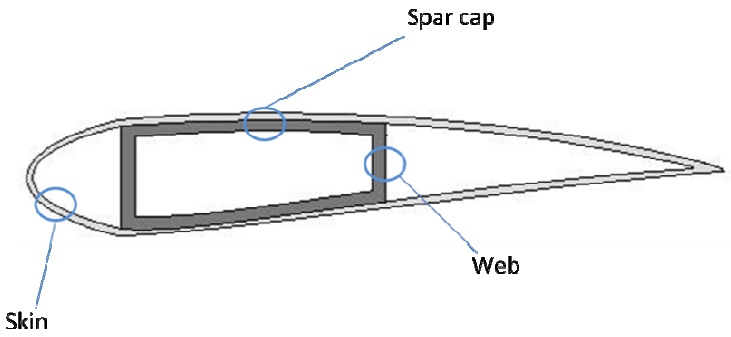

Figure 14 Modern wind turbine blades with aerodynamic skin, and load carrying spar and web.

A wind turbine blade can be modeled as a technical beam. If laminate is symmetric, thin walled and have free Poisson contraction. The beam can be treated as isotropic [18].

1.5 Modal Analysis

The dynamic response of rotating wind turbine blade is best investigated in terms of modal analysis.

First, the fundamental system of differential equations that must be solved in order to assess the response of a structure exposed to dynamic forces is given by:

$$M\ddot{v} + C\dot{v} + Kv = R(t) \tag{62}$$

Here *M* is the mass matrix, *C* is the damping matrix, and *K* the stiffness matrix of the structure. The column vector *v* contains the degrees of freedom (dofs) for the nodes, both translational and rotational. *R* is a vector that contains the forces related to the different dofs in the *v* vector.

Note that equation (62) is valid for linear systems where the stiffness term is governed by the linear elastic stiffness matrix *K* (deformation if proportional to load). If non-linear systems are studied, it is necessary to replace *K* with a stiffness matrix that is dependent of the deformation of the structure, *K(r)*. Load and deformation are no longer proportional, and an incremental/iterative solution must be utilized to solve the equation system [5].

The *M* and *K* matrices are normally established by use of finite element programs. However, as shown later in the paper, it can also be also be determined by calculations.

For a structure vibrating freely without damping loads acting on it, the movement can be described by;

$$M\ddot{v} + Kv = 0 \tag{63}$$

Assuming a solution of the form:

$$v = \mathrm{Im}\{\psi e^{i\omega t}\} \tag{64}$$

Gives:

$$K\psi = \omega^2 M\psi \tag{65}$$

This is the so called general eigenvalue problem in which ψ is the eigenvector and $\omega^2=\lambda$ is the eigenvalue. A solution will be a eigenvalue, $\omega_{n,j}$, and an eigenvector, Ψ_j, pair that satisfies:

$$\left(K - \omega_{n,j}^2 M\right)\psi_j = 0 \tag{66}$$

Setting Ψ_j to zero gives a trivial solution. The condition for obtaining the different frequencies form the equation is:

$$\det\left(K-\omega_{n,j}^2 M\right)=0 \tag{67}$$

The eigenvalue problem can be solved with different algorithms, and it constitutes the computational demanding part of the solution procedure of modal technique. In Matlab, the default algorithm for symmetric *K* and symmetric positive definite *M* uses Cholesky factorization of *M* [19].

The output of the eigenvalue problem is eigenvectors, ψ and eigenvalues ω_n.

The idea of the modal analysis technique is to split the response into a spatial "shape part" and a time dependent part, where the product represents the physical displacement response in the different degrees of freedom. I.e. The solution can be expressed as a summation of the response in all these degrees of freedom [20]:

$$v=\sum_{j=1}^{N}\psi_j x_j(t) \tag{68}$$

Here subscript j indicates mode number.

In matrix form, equation (68) becomes:

$$v=\psi x(t) \tag{69}$$

In which the matrix

$$\psi=\left[\psi_1\,\psi_2\ldots\psi_N\right] \tag{70}$$

Is a NxN matrix in which the columns are the eigenvectors of the system.

The time dependent coefficients of the eigenvectors are collected in a vector:

$$\left[x_1(t)\,x_2(t)\ldots x_n(t)\right] = x(t) \tag{71}$$

Because the response is divided into a shape part and a time dependent part, differentiating the terms from (69) with respect to time is straight forward:

$$v = \psi x(t) \qquad \dot{v} = \psi \dot{x}(t) \qquad \ddot{v} = \psi \ddot{x}(t) \tag{72}$$

Substituting in the general dynamic equation(62):

$$M\psi\ddot{x}(t) + C\psi\dot{x}(t) + K\psi x(t) = R(t) \tag{73}$$

Premultiplying (73) with Ψ^T gives [20]:

$$\psi^T M\psi\ddot{x}(t) + \psi^T C\psi\dot{x}(t) + \psi^T K\psi x(t) = \psi^T R(t) \tag{74}$$

The first and last term of the left side is a diagonal matrix with diagonal terms given as:

$$\psi_j^T M_j \psi_j = m_j \qquad \psi_j^T K_j \psi_j = k_j \tag{75}$$

The subscript j represents the j^{th} solution. The resulting *k* and *m* are now a scalar.

The damping effects can be assumed to be expressed by the damping ratio, ξ_j, in each mode. All off-diagonal damping terms can be neglected [20].

$$\psi_j^T C_j \psi_j = c_j = 2m_j\zeta_j\omega_{n,j} \tag{76}$$

The load is found by summing the modal loads weighed by the shape factor Ψ_j for the actual mode shape.

$$R_j(t) = \psi_j^T R(t) \tag{77}$$

Thus, the general equation in (62) can be replaced by N one degree of freedom equations of the form:

$$m_j \ddot{x}_j + 2m_j \zeta_j \omega_{n,j} \dot{x}_j + k_j x_j = R_j(t) \tag{78}$$

The N degrees of freedom system of the blade is now expressed by N independent one-degree-of freedom system. The sum of these systems describes the movement of the blade.

The equation (78) can be solved by a differential equation solver. A much used and accepted solver is the Runge Kutta method. Runge Kutta is a method of numerically integrating ordinary differential equations (ODE) by using a trial step at the midpoint of an interval to cancel out lower-order error terms [21].

1.5.1 Blade Structural Matrices

To model a turbine blade as a beam, both Euler-Bernoulli and Timoshenko beam elements can be used. Because the latter incorporates an approximate way of handling shear deformations, the blade is modeled based on Timoshenko theory [22].

For the wind turbine case, the blade can be modeled as a 3D beam, with nodes along the elastic axis of the blade. The blade is again divided into sections, and each section is treated as a 3D beam.

One node is placed at each end of the blade section. The node is placed at the point of elasticity in the cross section. The point of elasticity is defined as the point where a normal force (out of the plane) will not give rise to a bending of the beam [16]. The coordinate system is as seen in Figure 15. The blade is originally twisted, but the structural properties have been modified into flap- and edgewise (z and y) directions.

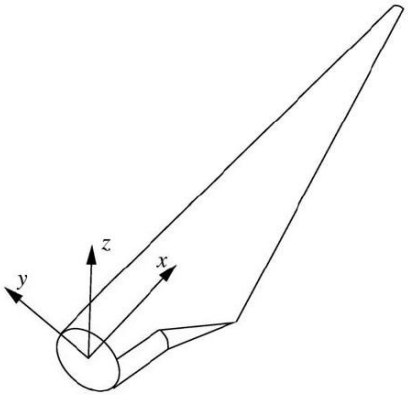

Figure 15 Definition of blade Coordinate System. X in radial distance, y in edgewise-, and z in flapwise direction.

1.5.1.1 Stiffness Matrix

Allowing six degrees of freedom per node: three translations and three rotations, the stiffness matrix for one beam element is given in [22]:

$$[K]=\begin{bmatrix} X & 0 & 0 & 0 & 0 & 0 & -X & 0 & 0 & 0 & 0 & 0 \\ & Y_1 & 0 & 0 & 0 & Y_2 & 0 & -Y_1 & 0 & 0 & 0 & Y_2 \\ & & Z_1 & 0 & -Z_2 & 0 & 0 & 0 & -Z_1 & 0 & -Z_2 & 0 \\ & & & S & 0 & 0 & 0 & 0 & 0 & -S & 0 & 0 \\ & & & & Z_3 & 0 & 0 & 0 & Z_2 & 0 & Z_4 & 0 \\ & & & & & Y_3 & 0 & -Y_2 & 0 & 0 & 0 & Y_4 \\ & & & & & & X & 0 & 0 & 0 & 0 & 0 \\ & & \textit{symmetric} & & & & & Y_1 & 0 & 0 & 0 & -Y_2 \\ & & & & & & & & Z_1 & 0 & Z_2 & 0 \\ & & & & & & & & & S & 0 & 0 \\ & & & & & & & & & & Z_3 & 0 \\ & & & & & & & & & & & Y_3 \end{bmatrix}\begin{bmatrix} u_1 \\ v_1 \\ w_1 \\ \theta_{x1} \\ \theta_{y1} \\ \theta_{z1} \\ u_2 \\ v_2 \\ w_2 \\ \theta_{x2} \\ \theta_{y2} \\ \theta_{z2} \end{bmatrix} \tag{79}$$

Where:

$$X=\frac{AE}{L} \qquad S=\frac{GJ}{L} \tag{80}$$

$$Y_1=\frac{12EI_z}{(1+\phi_y)L^3} \qquad Y_2=\frac{6EI_z}{(1+\phi_y)L^2} \qquad Y_3=\frac{(1+\phi_y)EI_z}{(1+\phi_y)L} \qquad Y_4=\frac{(2-\phi_y)EI_z}{(1+\phi_y)L} \tag{81}$$

$$Z_1=\frac{12EI_y}{(1+\phi_z)L^3} \qquad Z_2=\frac{6EI_y}{(1+\phi_z)L^2} \qquad Z_3=\frac{(1+\phi_z)EI_y}{(1+\phi_z)L} \qquad Z_4=\frac{(2-\phi_z)EI_y}{(1+\phi_z)L} \tag{82}$$

$$\phi_y=\frac{12EI_zk_y}{AGL^2} \qquad \phi_z=\frac{12EI_yk_z}{AGL^2} \tag{83}$$

Where:

- A is cross sectional area
- E is elastic modulus
- L is length of blade section
- G is shear modulus of elasticity
- J is torsional stiffness constant
- I_y and I_z is second moment of area in flapwise and edgewise direction, respectively
- K_y and K_z is the Timoshenko Shear coefficient in flapwise and edgewise direction, respectively

1.5.1.2 Mass Matrix

A mass matrix is a discrete representation of a continuous mass distribution. The mass is treated as a "lumped". This is obtained by placing particle masses at nodes. An obvious advantage of this is computational: less storage space and processing time are required [22].

Rotational degrees of freedom are not supplied with rotational inertia by the mere presence of mass particles. Rotational inertia must be added separately. A beam with a rotary inertia degrees of freedom will have the appurtenant element in the mass matrix[22]. The mass matrix of a 3-d beam element with 12 degrees of freedom is given by ([23]):

$$M = \rho AL \begin{bmatrix}
\frac{1}{3} & 0 & 0 & 0 & 0 & \frac{1}{6} & 0 & 0 & 0 & 0 & 0 & 0 \\
 & \frac{13}{35}+\frac{6I_z}{5Al^2} & 0 & 0 & 0 & \frac{11l}{210}+\frac{I_z}{10Al} & 0 & \frac{9}{70}-\frac{6I_z}{5Al} & 0 & 0 & 0 & -\frac{13l}{420}+\frac{I_z}{10Al} \\
 & & \frac{13}{35}+\frac{6I_y}{5Al^2} & 0 & -\frac{11l}{210}-\frac{I_y}{10Al} & 0 & 0 & 0 & \frac{9}{70}-\frac{6I_y}{5Al} & 0 & \frac{13l}{420}-\frac{I_y}{10Al} & 0 \\
 & & & \frac{J_x}{3A} & 0 & 0 & 0 & 0 & 0 & \frac{J_x}{6A} & 0 & 0 \\
 & & & & \frac{l^2}{105}+\frac{2I_y}{15A} & 0 & 0 & 0 & -\frac{13l}{420}+\frac{I_y}{10Al} & 0 & -\frac{l^2}{140}-\frac{I_y}{30A} & 0 \\
 & & & & & \frac{l^2}{105}+\frac{2I_z}{15A} & 0 & \frac{13l}{420}+\frac{I_y}{10Al} & 0 & 0 & 0 & -\frac{l^2}{140}-\frac{I_z}{30A} \\
 & & & & & & \frac{1}{3} & 0 & 0 & 0 & 0 & 0 \\
 & & & & & & & \frac{13}{35}+\frac{6I_z}{5Al^2} & 0 & 0 & 0 & -\frac{11l}{210}-\frac{I_z}{10Al} \\
 & & & & & & & & \frac{13}{35}+\frac{6I_y}{5Al^2} & 0 & \frac{11l}{210}+\frac{I_y}{10Al} & 0 \\
 & & & & & & & & & \frac{J_x}{3A} & 0 & 0 \\
 & & & & & & & & & & \frac{l^2}{105}+\frac{2I_y}{15A} & 0 \\
 & & & & & & & & & & & \frac{l^2}{105}+\frac{2I_z}{15A}
\end{bmatrix} \quad (84)$$

1.5.1.3 Damping Matrix

It is difficult to establish the amount of damping as it is generally uncertain in advance. This is particularly true for a rotor blade, where aerodynamic damping contributes alongside the structural damping of the blade. Normally a form of Rayleigh damping is used. Damping is in most cases modeled as viscous, which mean that it is proportional to the deformation rate. From the damping equation in modal analysis (76), it has been established that all off diagonal terms can be neglected. The damping matrix is therefore a diagonal matrix:

$$C = c \begin{bmatrix}
1 & 0 & 0 & 0 & 0 & 0 & 0 & 0 & 0 & 0 & 0 & 0 \\
0 & 1 & 0 & 0 & 0 & 0 & 0 & 0 & 0 & 0 & 0 & 0 \\
0 & 0 & 1 & 0 & 0 & 0 & 0 & 0 & 0 & 0 & 0 & 0 \\
0 & 0 & 0 & 1 & 0 & 0 & 0 & 0 & 0 & 0 & 0 & 0 \\
0 & 0 & 0 & 0 & 1 & 0 & 0 & 0 & 0 & 0 & 0 & 0 \\
0 & 0 & 0 & 0 & 0 & 1 & 0 & 0 & 0 & 0 & 0 & 0 \\
0 & 0 & 0 & 0 & 0 & 0 & 1 & 0 & 0 & 0 & 0 & 0 \\
0 & 0 & 0 & 0 & 0 & 0 & 0 & 1 & 0 & 0 & 0 & 0 \\
0 & 0 & 0 & 0 & 0 & 0 & 0 & 0 & 1 & 0 & 0 & 0 \\
0 & 0 & 0 & 0 & 0 & 0 & 0 & 0 & 0 & 1 & 0 & 0 \\
0 & 0 & 0 & 0 & 0 & 0 & 0 & 0 & 0 & 0 & 1 & 0 \\
0 & 0 & 0 & 0 & 0 & 0 & 0 & 0 & 0 & 0 & 0 & 1
\end{bmatrix}$$

After multiplication with the eigenmode, the resulting modal structural damping is

$$c_j = 2m_j\zeta_j\omega_{n,j} \tag{85}$$

The aerodynamic damping is added to this term to provide the total damping of the blade.

1.5.1.4 Assembly of Elements

Each structure node is regarded as a small connector to which elements are attached. Loads applied to a node come from element deformation and external loads distributed over elements. The structure node must be in static equilibrium under the action of all loads applied to it.

For small deformations it is reasonable to treat the beam as stiff, and limit the node constrain to be the placement of the nodes. Large deformations demands that it is treated as a multibody system. In this paper the deformations are assumed to be small, and the blade is treated as stiff.

For the 3D beam, assembly is easily done by realizing that the second node of the first element is the first node in the second element, and so on: i.e. the bottom right 6x6 area (degrees of freedom concerning second node) of the 12x12 matrix of the first beam element is added to the top left 6x6 matrix of the second beam element, and so on (see Figure 16).

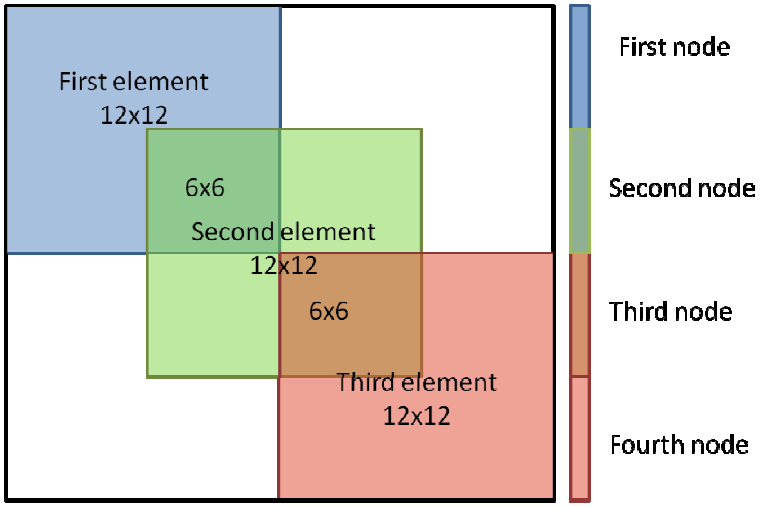

Figure 16 Assembly of Elements in K and M Matrices

Because the load is calculated in a time dependent domain, the blade is kept in the local coordinate system. Instead the wind field is set to be rotating: i.e. the loads are time dependent. The centrifugal loading on the blade is accounted is also accounted for by modifying the aerodynamic loading. This is explained in the next chapter.

1.5.2 Load Vector

During normal operation aerodynamic-, centrifugal-, Coriolis-, and gravity loads are present. Since this paper does not treat yawing motion, the Coriolis effect is assumed to be small and neglected in this study. The gravity load is neglected for simplicity.

The aerodynamic forces are determined in the time domain using the BEM method with Prandtl's tip loss factor and Glauerts correction (see section 1.2).

Centrifugal force is apparent in the radial direction(x direction) of the blade. However, it is present in the flapwise and edgewise direction in the downwind configuration because of the cone and flapwise deflection of the blade (see Figure 17)

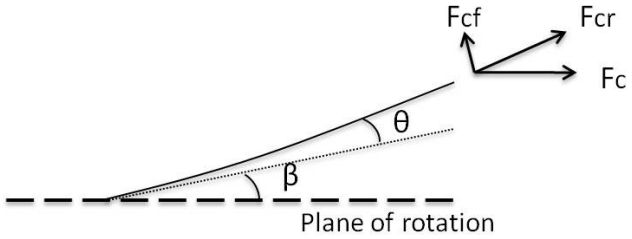

Figure 17 Direction of Centrifugal Forces. Cone angle β, deflection angle θ, total centrifugal force Fc, centrifugal contribution in flapwise (Fcf) and radial direction (Fcr)

Here β is the cone angle, θ is the deflection angle, F_c is the total centrifugal force, F_{cf} is the force in flapwise direction and F_{cr} in radial direction.

The total centrifugal load and its contribution in flap- and radial direction in found by the following equations, respectively:

$$F_{C,i} = m_i \cdot \Omega^2 \cdot r_i \cdot \cos(\beta + \theta_i) \tag{86}$$

$$F_{CF,i} = m_i \cdot \Omega^2 \cdot r_i \cdot \cos(\beta + \theta_i) \cdot \sin(\beta + \theta_i) \tag{87}$$

$$F_{CR,i} = m_i \cdot \Omega^2 \cdot r_i \cdot \cos^2(\beta + \theta_i) \tag{88}$$

The subscript i indicates section number.

Because the centrifugal force depends on the deflection an iteration procedure for determining centrifugal stiffening of the blade has been employed. The method is as follows:

I. Deflection and deflection angles is calculated using only the aerodynamic loads
II. The centrifugal load is calculated based on this deflection
III. The centrifugal load is then added to the aerodynamic load and a new deflection is calculated

Step II and III of this procedure is repeated until the deflection converges.

For simplicity the centrifugal force is calculated for deflections from first mode response. The higher order modes are assumed to have little effect on the centrifugal force.

1.6 Bending Moment Distribution

The bending moment due to nodal displacement is calculated from the curvature of this field. As shown in elementary beam theory, the bending moment field, M=M(r) is [22]

$$M_{flap} = EI_{flap} \frac{d^2 w}{dx^2} \tag{89}$$

$$M_{edge} = EI_{edge} \frac{d^2 v}{dx^2} \tag{90}$$

2. Model

An initial design of a 10 MW offshore turbine is analyzed in this study. The blades are placed on a hub with diameter 5 meters, and rotational speed is set to 12 rotations per minute. The tower is assumed to be rigid in both cases.

2.1 Turbine Blade

10 MW turbine blades have been designed by Frøyd et al. [17]. The overall data is presented in Table 1.

Table 1 Turbine blade properties

Parameter	Value
Length [m]	68
Mass [kg]	23 156
Tip speed ratio [-]	7
Number of airfoils [-]	7
Number of sections [-]	39
Structural damping ratio (all modes) [%]	0.477465
Cone angle [degrees]	2.5

The blade is modeled by use of structural matrices described in chapter 1.5. The choice of 39 sections is a tradeoff between natural frequency converge and computational round off errors in matlab. The round off errors is particularly applicable to Runge Kutta ODE solver.

Data used in the stiffness and mass matrices is based on table found in appendix A-9.

The stiffness properties of the blade are given in points along the blade radius. For illustrating reasons these values are plotted in a graph presented in Figure 18.

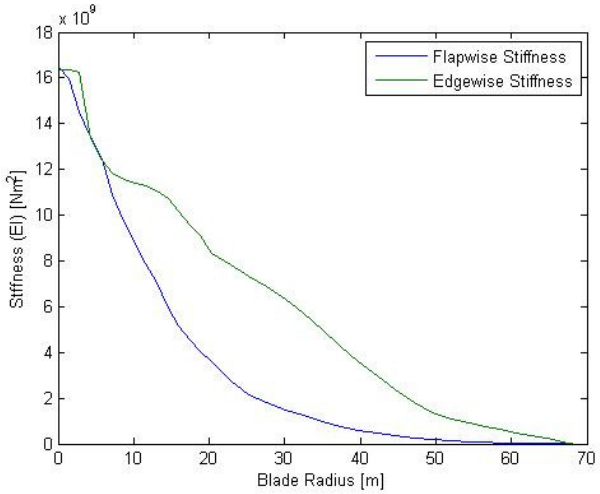

Figure 18 Blade flapwise and edgewise stiffness

The dynamic response is calculated with modal analysis based on the three first eigenmodes. The higher order modes gives smaller contribution and are assumed to give be neglectable.

Analysis has been made by looking at the dynamic response when adjusting the blade stiffness alone, and adjusting both the stiffness and mass.

The aerodynamic modal damping has been set to 1.2 kg/s in all modes. This is merely a guess, as the aerodynamic damping is unknown.

2.1.1 Loads on Blade

Aerodynamic forces are calculated in time domain using classical Blade Element method with Prandtl's tip loss and Glauerts correction. The final procedure is presented in chapter 1.2.5.3. The deduction is shown in chapter 1.2. Centrifugal forces have been implemented by the iteration procedure explained in chapter 1.5.2.

The air density is 1.225kg/m^3, representing wind density offshore. The rotational speed is set to 12 rotations per minute (rpm), corresponding to 5 seconds per rotation. Azimuth angle is set to zero at the vertical line above the hub (see Figure 19), with increasing value as the blade rotates clockwise.

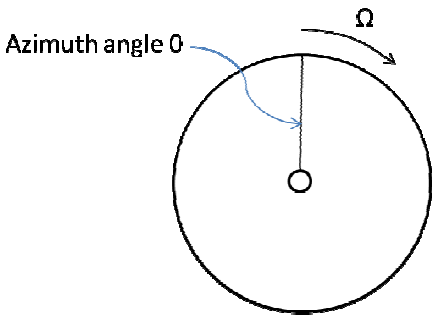

Figure 19 Placement of 0 azimuth angle, and direction of rotation Ω

2.2 Towers

Both a tubular and a truss tower are used in the model. The geometry of the towers and the rotor placement is chosen to be able to compare the results with a study conducted in Ansys Fluent [11].

The tubular tower has a diameter of 4m. The rotor is placed at a distance equal to three tower diameters downstream of the tower center.

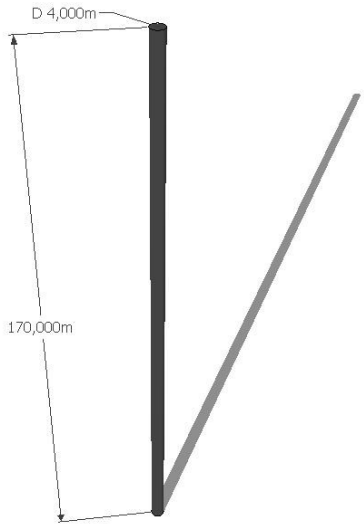

Figure 20 Tubular tower geometry; Diameter 4 meters and height 170 meters

A truss tower based on the truss tower for the 5MW NREL turbine ([24]) is modified for a 10MW turbine by post. doc Paul Thomassen and scholarship holder at NTNU[25].

The modification done is quite coarse, and it is used here merely as a theoretical tower model to analyze the tower shadow (see Figure 21).

The corner columns give the largest effect regarding tower shadow. The corner column diameter is 1350 mm. The bracings have been neglected in this study.

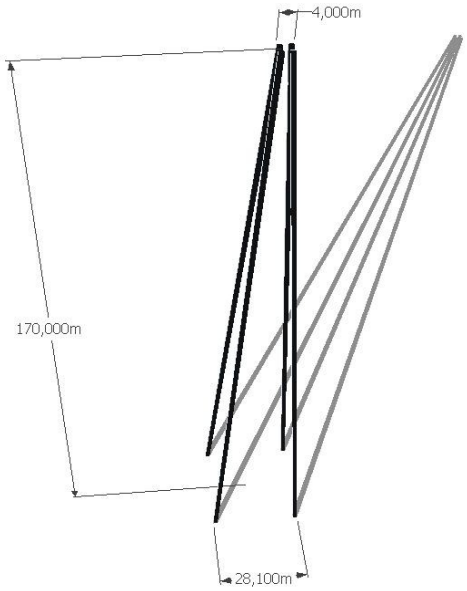

Figure 21 Truss tower geometry. Top width 4 meters, bottom width 28.1 meters, and height 170 meters.

The truss tower is placed at 0 degrees to the wind, and the rotor is placed at a distance equal to 3D (where D is 4m, diameter of the tubular tower) downstream of the centerline (see Figure 22).

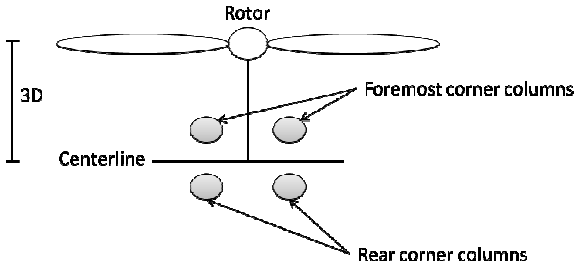

Figure 22 Rotor and tower placement. 3D equals three times the diameter of the tubular tower

2.3 Tower Shadow Models

Blevins model described in chapter 1.3 are used to calculate the time averaged velocity profiles in the tower shadow region. The unknown values c_d and x_0 are obtained from a study by Hagen et al. [11], and presented in Table 2.

Table 2 Parameters used in Blevins model

Parameter	Truss tower	Tubular tower
c_d [-]	0.608	0.399
x_0 [m]	11.544	6.709

The four corner columns have been applied separately in the truss tower.

To the student's knowledge, the only Wind turbine software that handle downstream wind turbines with wake from a truss tower is Garrad Hassans Bladed [26]. An assumption made in this paper as well as in GH Bladed is assuming that the rear corner columns do not affect the incoming wind velocity to the foremost columns.

2.3.1 ANSYS FLUENT Wind Files

Hagen et al., [11] studied the turbulent flow past towers with equal geometry as towers in this paper. The analysis was made in ANSYS FLUENT (version 12.1.4, Ansys Inc., Cantonburg, USA) with a more realistic velocity profile containing turbulent inflow and vortex shedding. To study the effect on the blades from these effects, the time averaged model is compared to wind ANSYS FLUENT wind files from the study provided by Torbjørn Ruud Hagen, Marit Reiso and Michael Muskulus. This will be referred to as the ANSYS Wind File case.

The study is based on 2D simulations, and the wind files contain velocities recorded at a line transverse to the free stream flow at height 42 meters above sea level. This is corresponding to the location where the blades should have the highest energy production.

This data have been modified to a 3D case by extracting the line into the x-y plane in the tower shadow: i.e. the wind profile line in direction transverse to the incoming wind direction is extrapolated along the tower axis. The blade is set in motion with this time dependent velocity profile, with a time step of 0,005s.

The wind file contained velocity profiles in 30 seconds. Both the truss and tubular case was tested in several blade rotations, to include all effects of the vortex shedding.

2.3.2 Wind Tunnel Experiment

Reiso et al. [27] compared wind velocities in the tower shadow for tubular- and truss tower in the wind tunnel at the Norwegian University of Science and Technology. The experiment was carried out in micro scale, and the resulting wind velocities differs from the full scale ANSYS FLUENT results in the study of Hagen et al., [11]. The parameters in Blevins model have been roughly modified to match the wind profile from the wind tunnel experiment behind both the tubular and truss tower. The results from this case will be referred to as the Wind Tunnel case.

2.4 Matlab Script Structure

The software for analyzing blade dynamic response was developed using MALAB version R2010a [21]

The structure of the resulting matlab script determining wind velocities in rotor plane for the averaged Blevins model is presented in Figure 23. Theoretical background information is found in section 0.

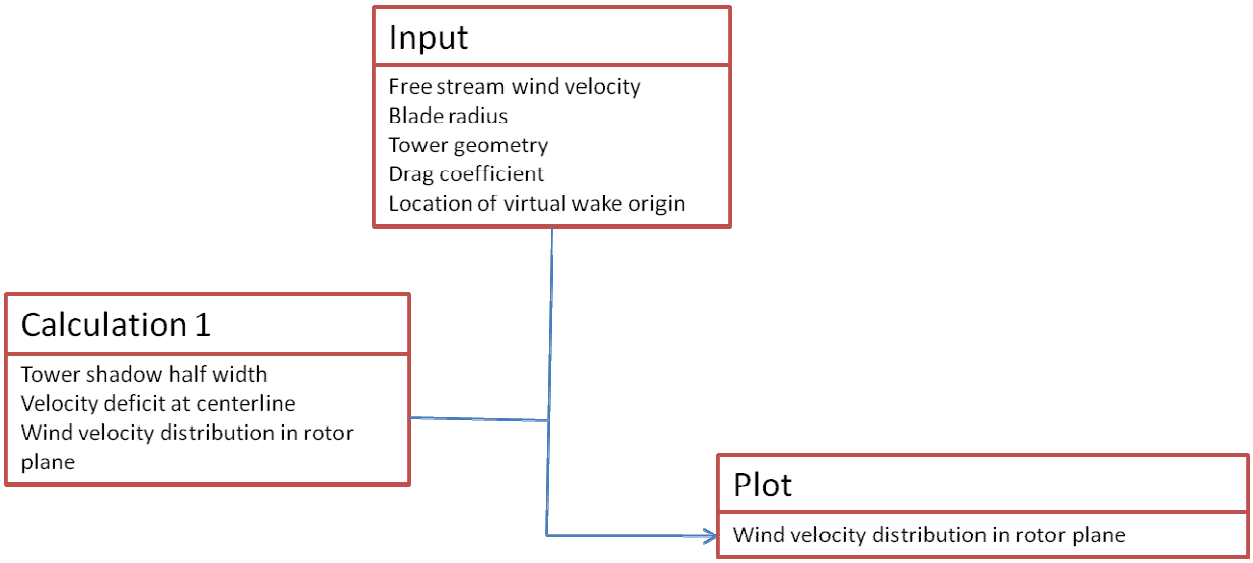

Figure 23 Chart for the Wind Velocity in Rotor Plane script (MATLAB calculation1).

The matlab script is found in appendix A-1 (tubular tower) and A-2 (truss tower).

The wind velocity distribution calculated with Blevins averaged model uses input found in Table 2. The resulting wind distribution contains wind velocities experienced by each section at each time step.

In the wind tunnel case, values in Blevins model (b and c_d) are modified to match the wind profile in the study.

In case of the Ansys Fluent wind files, the wind field is modified for the rotor plane. The time step in the files is 0.005 seconds, resulting in 1000 steps per revolution for the wind turbine blade. For each time step, the blade moves a step of 2π/1000 radians. Hence the resulting wind field displays velocities experienced by the blade section during five revolutions. See appendix A-3 (tubular tower) and A-4 (truss tower) for matlabskript.

The next step is to determine induction factors and lift- and drag coefficients (Figure 24). Theoretical background for the script is found in 1.2.5.3.

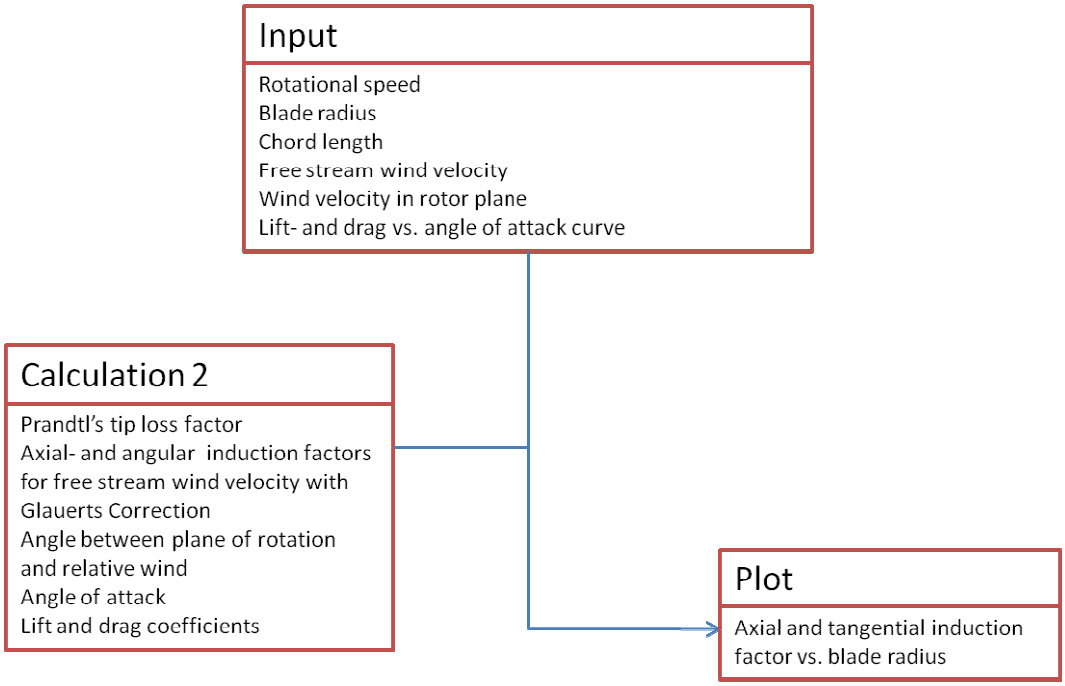

Figure 24 Chart for the Induction Factors, Lift- and Drag Coefficients script (MATLAB calculation 2)

See appendix A-5 for the matlab code.

The induction factors are calculated based on free stream wind velocity, and remains constant throughout the revolution: i.e. they are the same in all three cases.

The angle of attack is dependent on the incoming wind velocities: i.e. the wind velocities in the tower shadow changes the angle of attack. The lift- and drag coefficients for each section are dependent of the angle of attack. For each section, a function in the script finds the angle of attack in the table nearest to the calculated angle of attack. Then, the function picks

out the lift and drag coefficients connected to the specific section with the given angle of attack.

Figure 25 shows the flow in script for determining aerodynamic forces on the blade. Theory behind this script is found in 1.2.5.3.

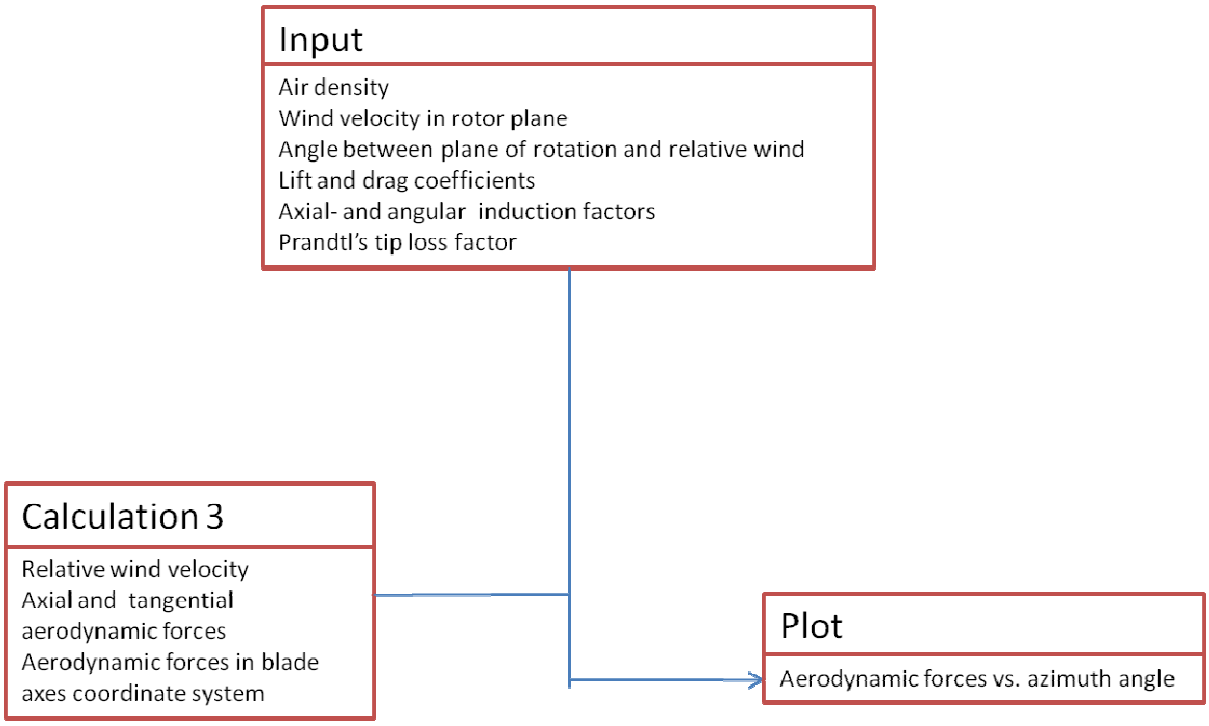

Figure 25 Chart for Aerodynamic Forces Script (MATLAB calculation 3)

See appendix A-6 for the matlab code.

The aerodynamic forces are calculated for each section at each time step of the revolution in all three cases.

The structure of the matlab script determining the blade dynamic response is illustrated in Figure 26. The theory behind this scrip is found in section 1.5.

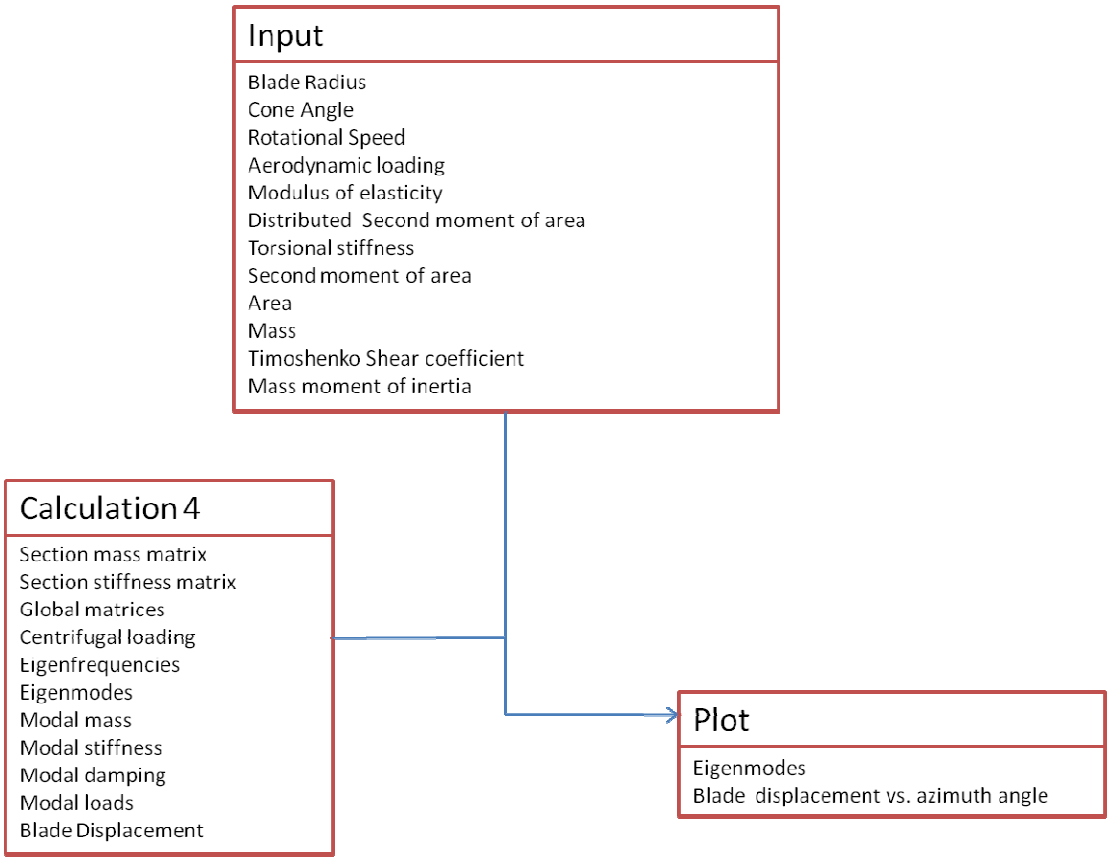

Figure 26 Chart for Blade Dynamic Response Script (MATLAB calculation 4)

See appendix A-7 for matlab script.

The script use iteration to obtain the centrifugal loading throughout the revolution (section 1.5.2). The total loading on the blade is time dependent. The script determines deflection distribution along the blade radius, but for illustrative reasons only the tip deflection is presented in the results.

This script has been used for analyzing dynamic response with reduced blade stiffness, or reduced mass and stiffness; The adjustment have been done by modifying the stiffness (or mass *and* stiffness) in the structural matrices and the dynamic response have been determined. The script for plotting the resulting blade tip deflection and plotting the resulting root flapwise bending moment with adjusted stiffness is presented in Appendix A-

11 and A-12, respectively. The same procedure is followed when adjusting both stiffness and mass.

The last part of the script is determining the blade bending moment distribution (Figure 27). The theoretical background information is found in chapter 1.6.

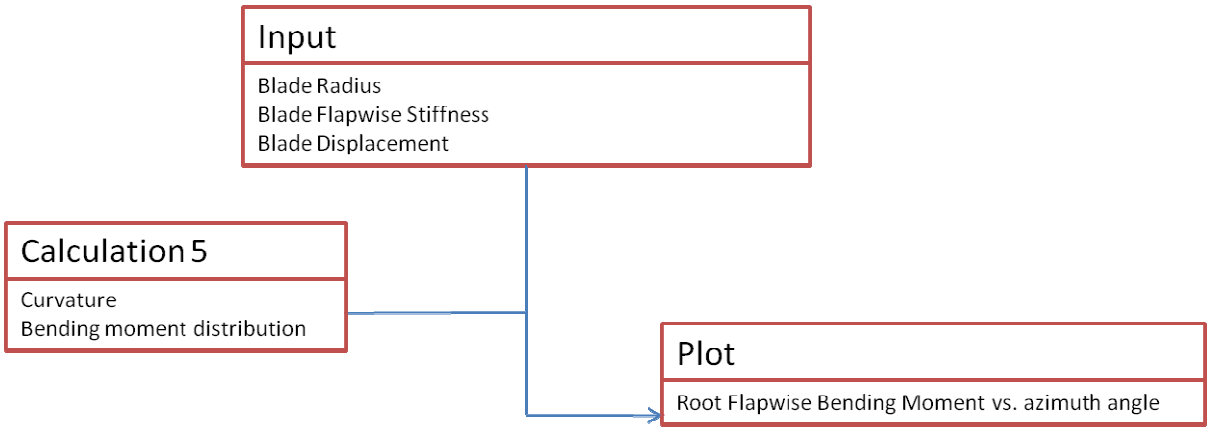

Figure 27 Chart for Bending Moment Distribution Script (MATLAB calculation 5)

Matlab script is presented in appendix A-8.

Figure 28 illustrates the total flow of information between the five different matlab scripts presented in Figure 23 to Figure 27.

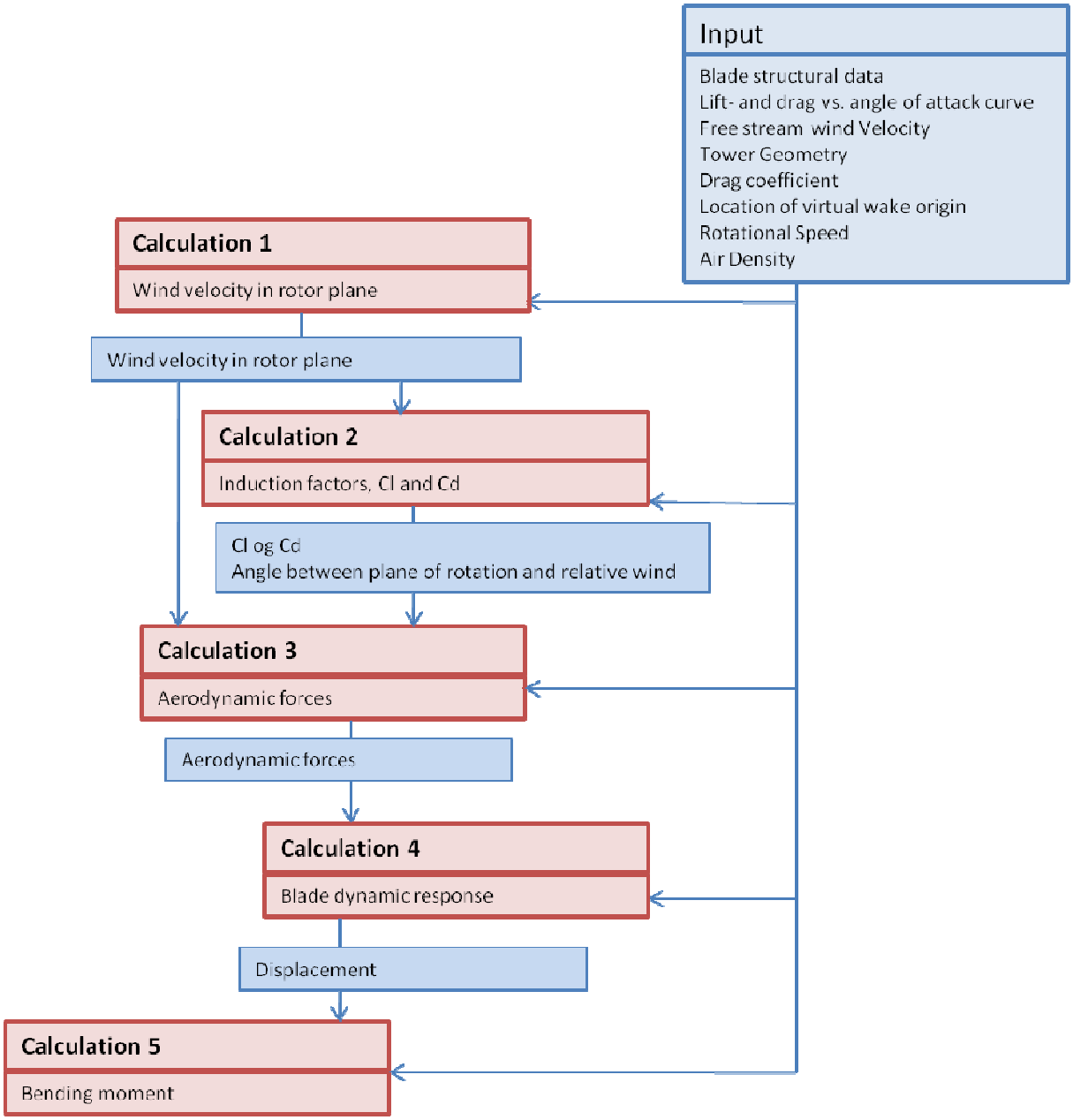

Figure 28 Flow of Information between MATLAB Calculations 1 to 5

The blue boxes between the calculations represent the output and input of data. For example, the output of calculation 1 is a matrix of wind velocities on sections of the blade sections at each time step. This matrix is input in both the calculation 2 and 3.

3. Results

The results presented are all from the model made in MATLAB.

3.1 Axial and Tangential Induction Factors

The resulting induction factors *a* and *a'* from matlab script 2 (Appendix A-5) is plotted along the blade radius (Figure 29). The induction factors are computed with Prandtl's tip loss factor and Glauerts correction for heavily loaded turbines.

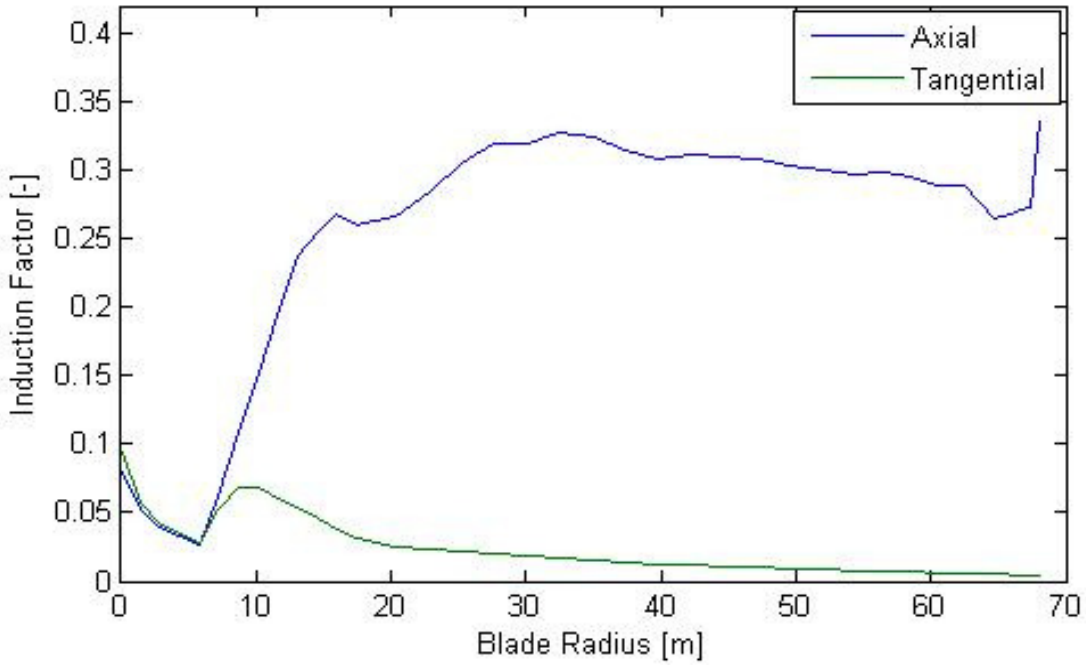

Figure 29 Induction factors along blade radius

The axial induction factor for creating maximum power is 1/3. The induction factors are dependent on the lift and drag coefficients. Near the hub the blade has cylindrical geometry, hence no lift forces. These induction factors are in close to what was found by Frøyd et al. [28]. This is suggesting that the axial factor lies around 0.3 at blade radius more than around 20 meters, and that the tangential induction factor lies below 0.1.

3.2 Aerodynamic Forces

The aerodynamic forces in axial in tangential direction (matlab script 3, appendix A-6) is displayed for incoming wind velocity of 12 m/s (Figure 30). There is a close to linear increase in axial forces from origin to radius 60 meters where it approaches 11 kN/m. The tangential force lies nearly constant at a value of 2 kN/m. The effect of the tip loss factor can clearly be seen near the tip of the blade, where the axial and tangential force approaches zero.

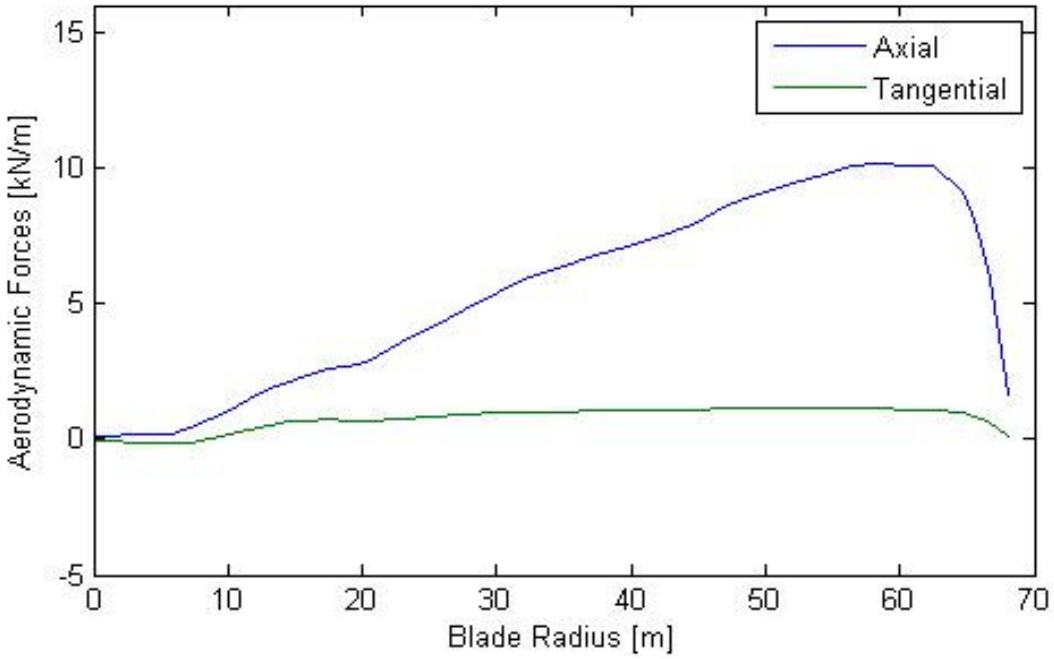

Figure 30 Aerodynamic forces along blade radius

This trend compare well to Frøyd et al. [28], suggesting zero force near the tip and origin.

3.3 Eigenmodes

The first result of matlab scrip calculation 4 is the first four eigenmodes in flap direction and the appurtenant eigenfrequencies (Figure 31).

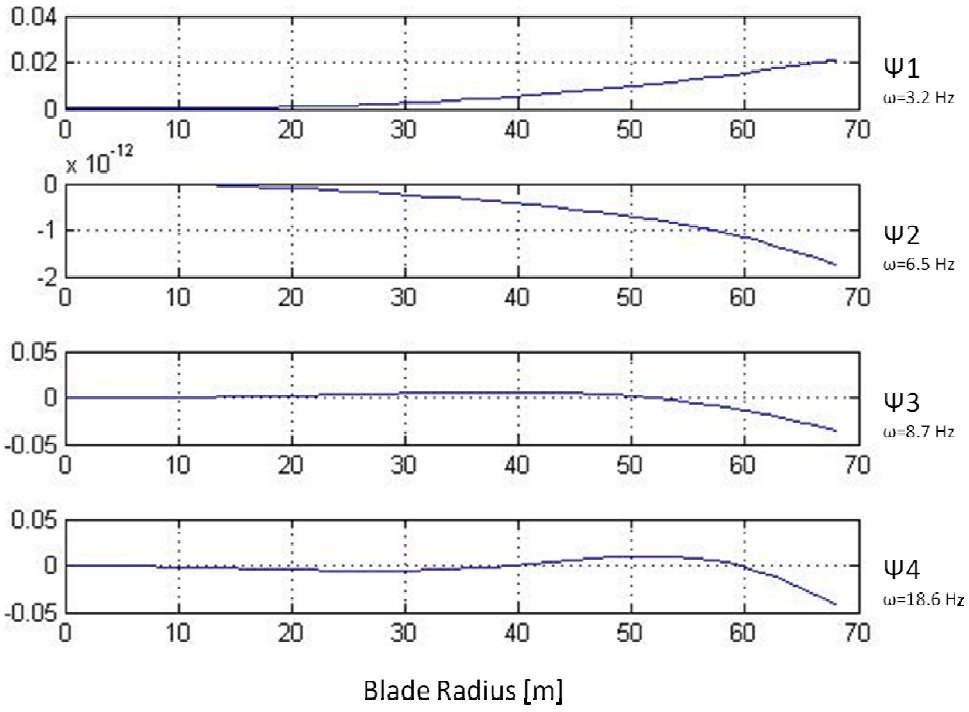

Figure 31 First four flapwise eigenmodes, ψ, and eigenfrequencies, ω_n

In all cases the blade eigenmodes are close to zero until blade radius is 20 meters. This is due to the blade stiffness. Near the hub the geometry of the blade is cylindrical followed by a section with large thickness, resulting in high stiffness. The natural frequency of the first mode in 3.2 Hz, and the maximum eigenmode value is 0.02. The second mode has a frequency of 6.5 Hz, over double the natural frequency of the first mode. The minimum value of the mode is in the order 10^{-12}, providing very little contribution to the flapwise movement. The third mode crosses zero, and has minimum value of about -0.04. The natural frequency of this mode is 8.7 Hz. The fourth mode crosses zero twice, and has a minimal value close to -0.05. However, the natural frequency of 18.6Hz indicates that the contribution from this mode would be small.

Similarly, the eigenmodes in edge direction are presented in Figure 32.

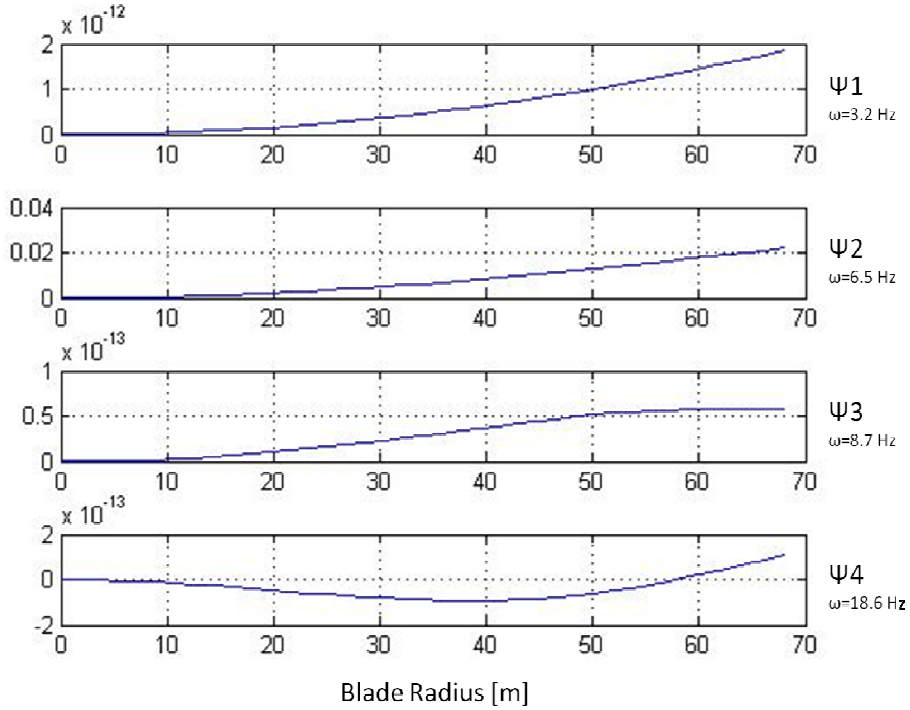

Figure 32 First four edgewise eigenmodes, ψ, and eigenfrequencies, ω_n

The first mode is in the order 10^{-12}, suggesting very little contribution to the edgewise deflection. The second mode resembles the first flapwise mode. This is the mode that gives the largest contribution edgewise. But as the frequency of the mode is considerably higher in the second mode, the deflection in edgewise direction will be smaller than the deflection in the flapwise direction. The third and fourth mode are in the order of 10^{-13} and can be neglected.

3.4 Blevins Time Averaged Model

Chapter 3.4 presents results from Blevins time averaged model. The time step in this analysis is 0.014 seconds, representing one degree azimuth.

3.4.1 Wind Velocity in Rotor Plane

The wind velocity distributions in rotor plane are results from calculation 1 in the matlab script.

The wind velocities in the rotor plane with wake from tubular tower is illustrated in Figure 33; i.e. wind velocities experienced by the blade. The color bar on the right of the figure explains the value of the color code (m/s).

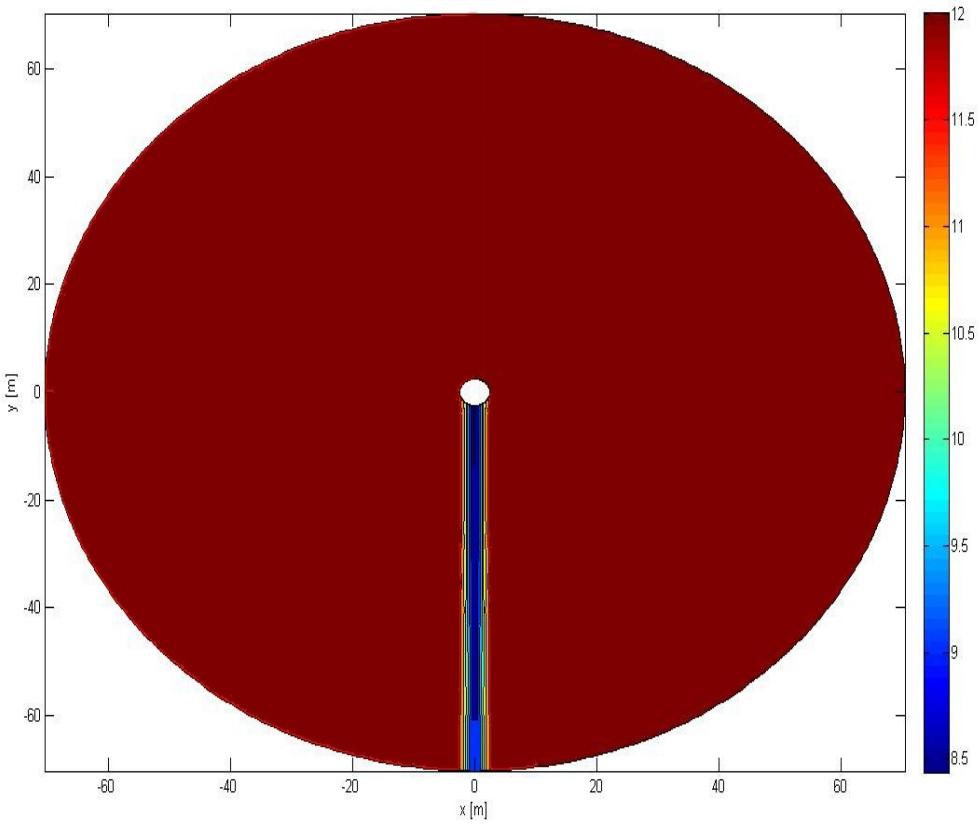

Figure 33 Wind velocity in rotor plane [m/s], averaged Blevins with tubular tower

The center of the tower shadow lies on zero *x*-value. The blades section enters and exits the tower shadow regions at different azimuth angles, depending on the distance from the center; i.e. the section closest to the hub enters the tower shadow first and, and the tip section enters last. At azimuth angle π all sections are in the tower shadow. Finally tip section exits first and hub section last.

When the rotational speed is 5 seconds per rotation, the frequency of the force dip will be 2 Hz.

The wind field for a turbine with truss tower is shown in the similar manner (Figure 34).

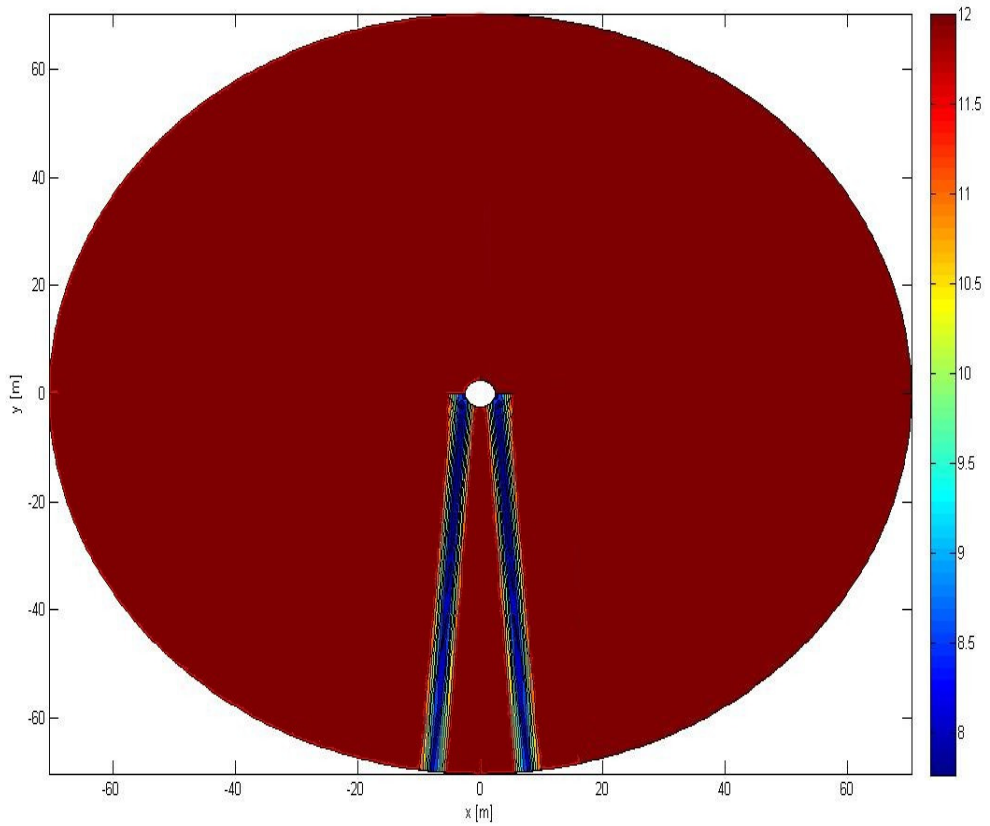

Figure 34 Wind velocity in rotor plane [m/s], averaged Blevins with truss tower

The tower shadow is split in two components, placed on both sides of zero *x*-value. The transverse distance from zero *x*-value to the center varies with *y*-value. The top of the tower shadow is two meters from the rotor center. Hence the blade will not experience maximum tower shadow deficit in all sections at the same time.

Note that the velocity deficit is about 0.7 m/s higher in the truss tower than in the tubular tower. The tower shadow width is about 5 meters behind the tubular tower and about 4 meters behind the corner columns in the truss tower. The difference seems small considering that the diameter of the tubular tower and the corner column in the truss tower are 4m and 1.35m, respectively. This is due to the drag coefficient and location of the virtual wake origin, presented in Table 2.

The wake is wide in truss tower because of the two parallel corner columns, both contributing to the velocity deficit. The shadow is narrow near the hub, and becomes wider as y becomes more negative. This is because the corner columns are placed aslant: i.e. the rear corner columns are further away from the rotor as the y coordinate becomes more negative. At the same time, the foremost corner columns are closer to the rotor, creating a narrow shadow with high wind velocity deficit.

The force dip from the truss tower will have two frequencies. One with a value of about 0.2 Hz representing the period from when the blade exits the second part of the wake, until it hits the first part of the wake again. And one of about and 5Hz, in connection to the time between the two tower shadow parts of the truss tower shadow.

3.4.2 Blade Tip Displacement

The final result from Matlab calculation 4 (Appendix A-7) is the blade tip displacement during one revolution. Figure 35 and Figure 36 shows the tip displacement during one revolution with wake from tubular tower and truss tower, respectively. The deflection is calculated based on response from the first three modes combined. In addition the response based merely on the first mode is presented.

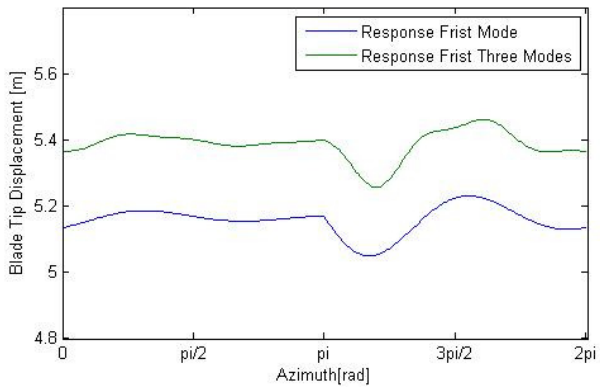

Figure 35 Blade tip displacement with averaged Blevin model based on first three modes and merely first mode, tubular tower

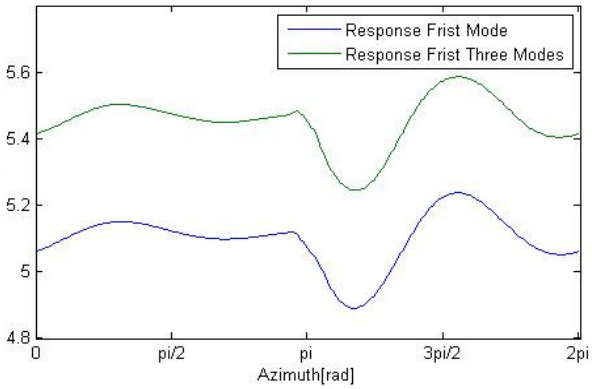

Figure 36 Blade tip displacement with averaged Blevin model based on first three modes and merely first mode, truss tower

Note that in the tubular tower case, the tower shadow induced deflection drop is delayed about π/4 compared to the placement of the tower (azimuth angle π). This is due to the inertia forces, resisting the movement.

Even though the tower shadow is split in the truss tower case, the effect in terms of blade displacement is one dip with considerably large amplitude after azimuth angle pi.

The time lag between the first and second wake from the corner columns in the truss tower is too short for the displacement to recover; second dip merely only enforces the effect of the first dip. The harmonic movement from the second dip may also to affect the first dip.

The higher order modes give an addition in the deflection in the terms of an upward shift of the line and perturbations with higher frequencies. In flapwise direction, the response from the second mode is in the order of 10^{-11}. The difference in deflection mainly comes from the third mode. The upward shift of the curve is about 0.2 meters larger in the truss tower case than in the tubular case.

The perturbations in the higher order modes are larger in the tubular case, seen as difference the curve shape. This may be because the blades experience force dips of 0.2 Hz contributing to fluctuations in the higher modes: i.e. the force dip creates a displacement in the higher mode, and the perturbations are harmonic movement due to this deflection.

The nature of the small perturbations in the truss case may be connected to the two rapid dips in forces on the blade, resulting in a high frequency in “force dips”: i.e. the second force dip cancels out the harmonic motion of the deflection from the first force dip.

The difference between the two towers in blade tip displacement based on the first three modes is shown in Figure 37.

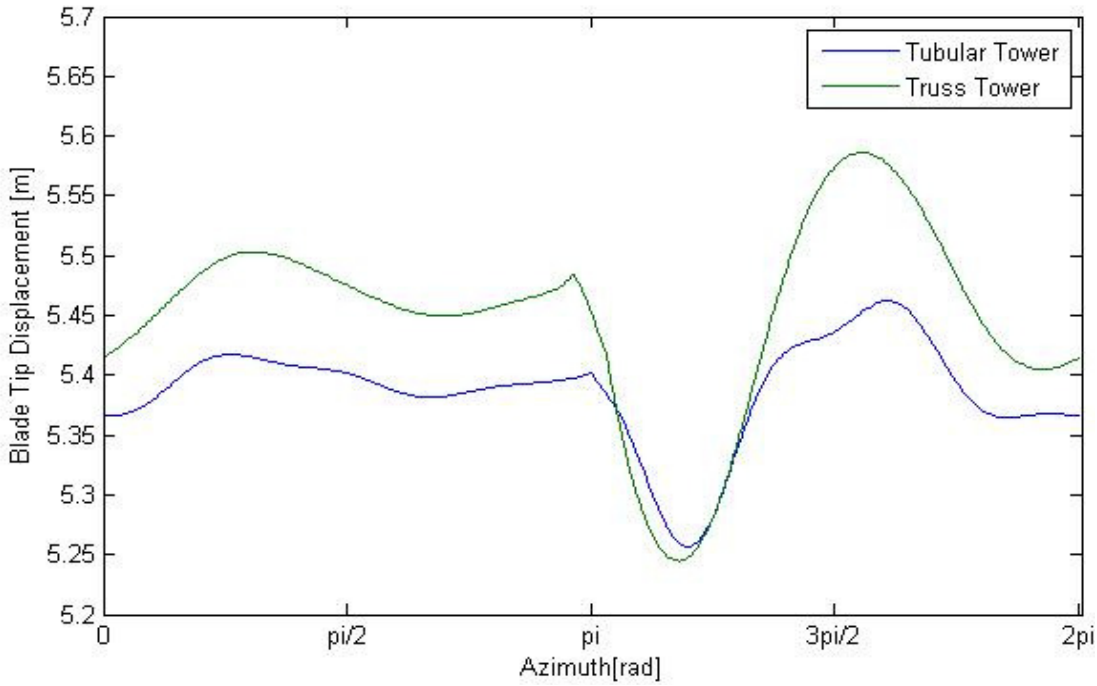

Figure 37 Blade tip displacement, averaged Blevins model with both towers

The truss tower gives rise to amplitude of about 25 cm, while the amplitude in the tubular tower case is about 15 cm. The velocity deficit in the tower shadow is about 0.7 m/s higher is the truss case, contributing to the difference. The general deflection is about 10 cm larger in the truss tower case. The blade deflection has a steeper drop and larger fluctuations with truss tower. The tower shadow induced fluctuation in blade deflection is about 67% larger in the truss tower case compared to the tubular tower configuration.

The effect of the centrifugal loading in Matlab calculation 4 (Appendix A-7) is illustrated with the truss tower wake (Figure 38). The figure shows the response in tip deflection for the first mode, with and without centrifugal stiffening.

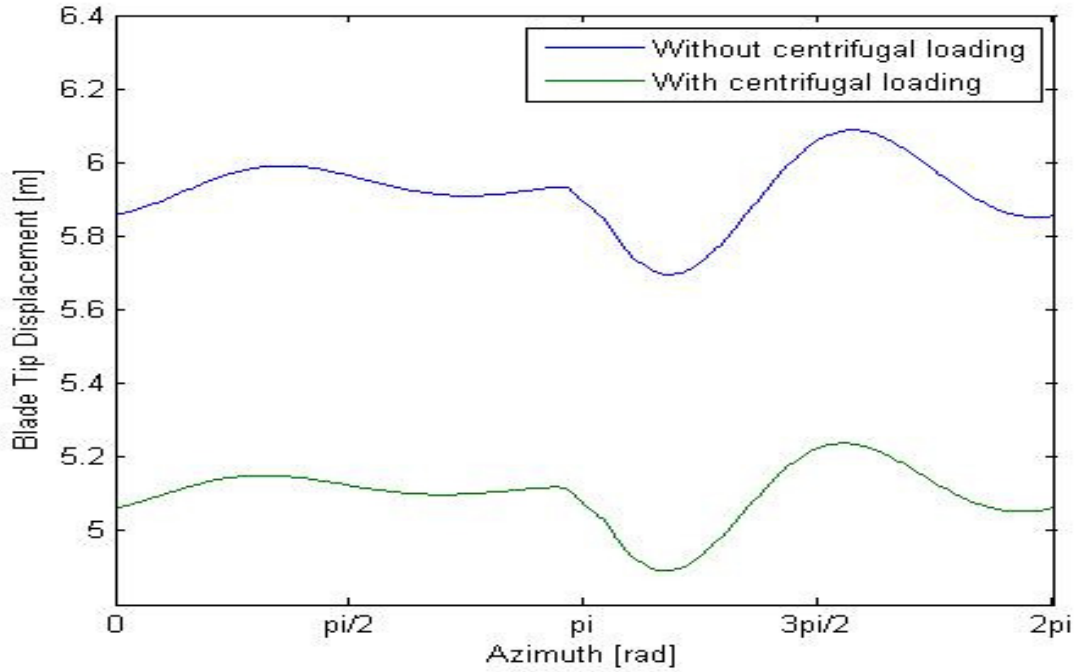

Figure 38 Effect of centrifugal loading, averaged Blevins model first mode, truss tower.

The effect of the centrifugal force is that it stiffens the blade; as can be seen in the downward shift, and the slightly changed shape of the tip deflection curve. The centrifugal force is dependent on the deflection of the blade; the force is smaller in the first deflection dip of the blade (after azimuth angle pi [rad]). The force then increases at azimuth angle around 3pi/2. I.e. the centrifugal loading decreases the blade fluctuating movement.

3.4.3 Root Flapwise Bending Moment

The result of calculation 5 is presented in Figure 39. The figure displays the root flapwise bending moment (RFM) for both towers. The bending moment depends on the curvature of the blade, which is the 2nd derivative of the deflection.

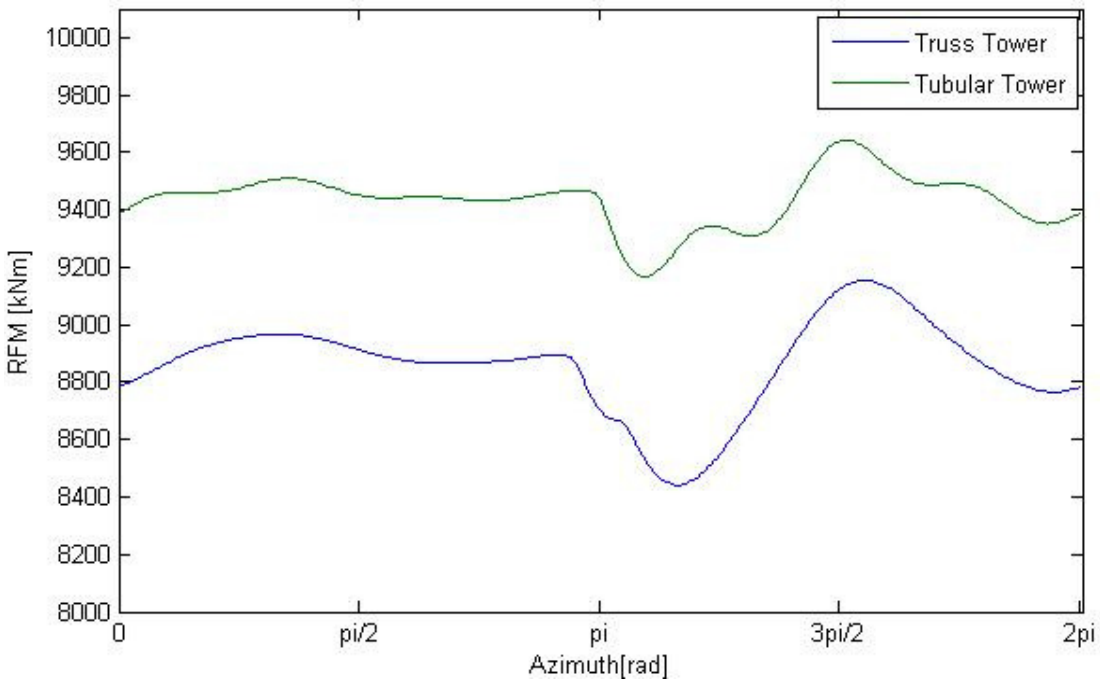

Figure 39 Root flapwise bending moment, averaged Blevins with both towers

The root flapwise bending moment with truss tower configuration generally lies about 600 kNm lower compared to the tubular tower. This is due to the upward shift in tip deflection from the third mode being larger in the truss case, contributing to a different blade curvature around the entire revolution.

The bending moment varies from 9200 to about 9700 kNm in the tubular tower case, a difference of 500 kNm. In the truss case, the bending moment varies from 8400 to 9200 kNm, a difference of 800 kNm. Hence the bending moment fluctuation during a revolution is about 200 kNm larger with the truss tower than with the tubular tower. This is connected to the large variation of the blade deflection in the tubular tower case.

The fluctuations in tip deflection from the third mode are larger in the tubular case, changing the curvature of the blade during the revolution. The result of this is high frequency variation of the root flapwise bending moment, which seems to reduce the amplitude of the fluctuation due to the tower shadow.

The bending moment in the truss tower case generally lies about 7% above the tubular tower case. The truss tower has a steeper drop in RFM after azimuth angle pi and slower recovery of the RFM as the blade leave the tower shadow, resulting in high fatigue loading of the structure.

3.5 ANSYS FLUENT Wind Files

Chapter 3.5 displays results based on time dependent wind files extracted from ANSYS FLUENT (the wind file case). The forces and dynamic response of this input is calculated in the same way as in chapter 3.4, but with a time step of 0.005 seconds, compared to 0.014 seconds before, to obtain the same rotational speed of 12 rotations per minute.

3.5.1 Wind Velocity in Rotor Plane

The wind speeds in the rotor plane experienced by one blade in one revolution is shown at for a randomly chosen starting time in the wind file (Figure 40).

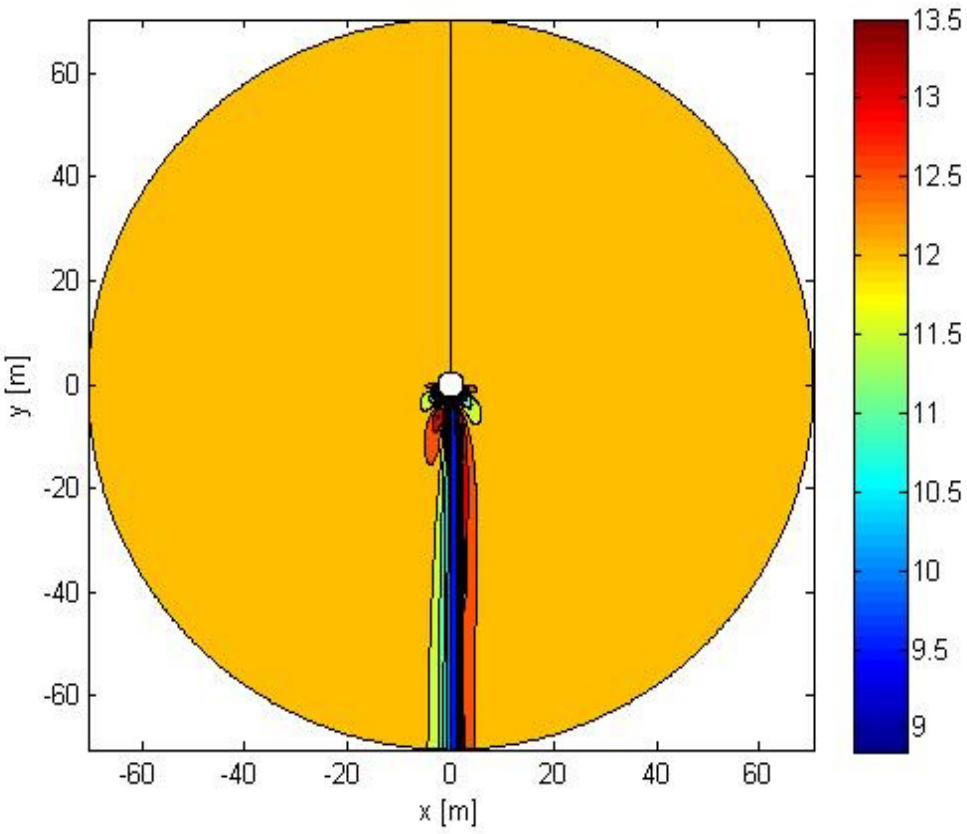

Figure 40 Wind velocity in rotor plane [m/s], ANSYS wind files with tubular tower

The highest wind velocity during this particular revolution is 13.5 m/s, 1.5 m/s higher than in the time averaged model, here taking place at the right side of the tower. The lowest wind speeds here a bit to the right side of the wake. This is due to the vortex shedding.

Figure 41 displays the wind velocities in the rotor plane with wake from the truss tower. It seems as the wind speed here is changing more rapidly than in the tubular tower: i.e. the vortices are of higher frequency compared to the tubular tower.

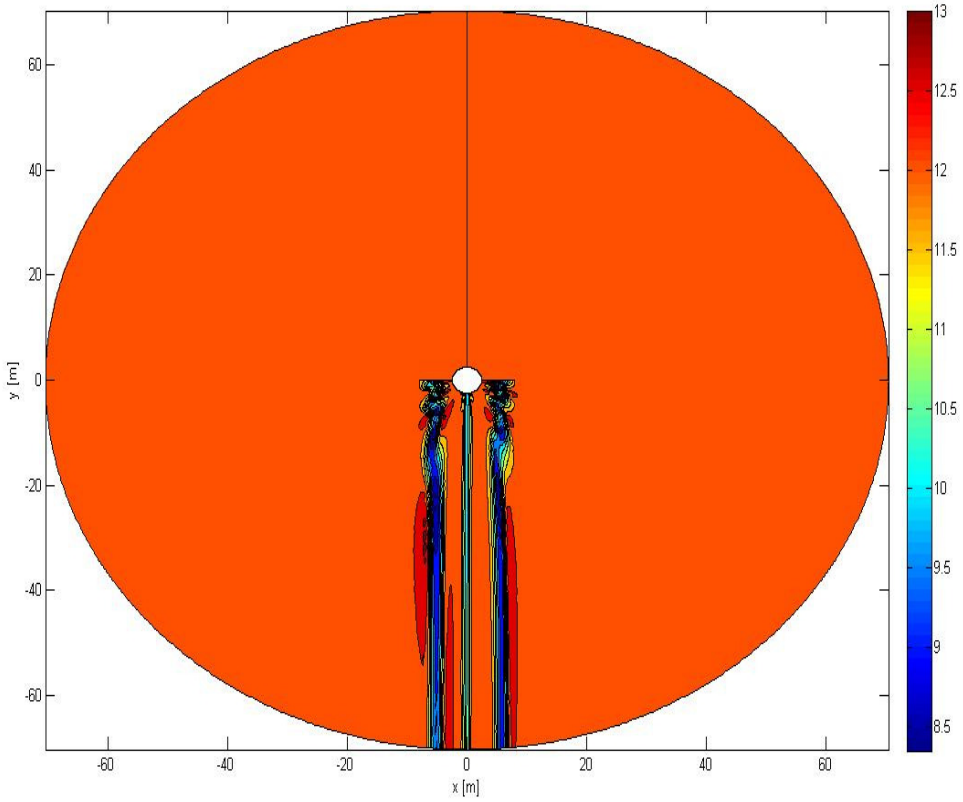

Figure 41 Wind velocity in rotor plane [m/s], ANSYS wind files with truss tower

Note that the velocity deficit is about 0.5 m/s higher with the truss tower configuration compared to the tubular tower. The modification of the wind field from 2D to 3D changes the geometry of the tower shadow. The modification fails to incorporate the slope of the corner columns: i.e. the horizontal distance from the corner columns to the rotor and the transverse distance between the corner columns are constant. Hence the transverse distance from x-axis to the tower shadow and the tower shadow width is constant along the

y-axis, and the average wind velocity deficit is constant: i.e. the geometry of the actual tower would be similar to four corner columns placed quadratic and vertical.

The velocity deficit right below the hub is due to the x-brace.

3.5.2 Blade Tip Displacement

Figure 42 shows the difference in blade tip displacement during five revolutions with the two tower configurations (matlab calculation 4).

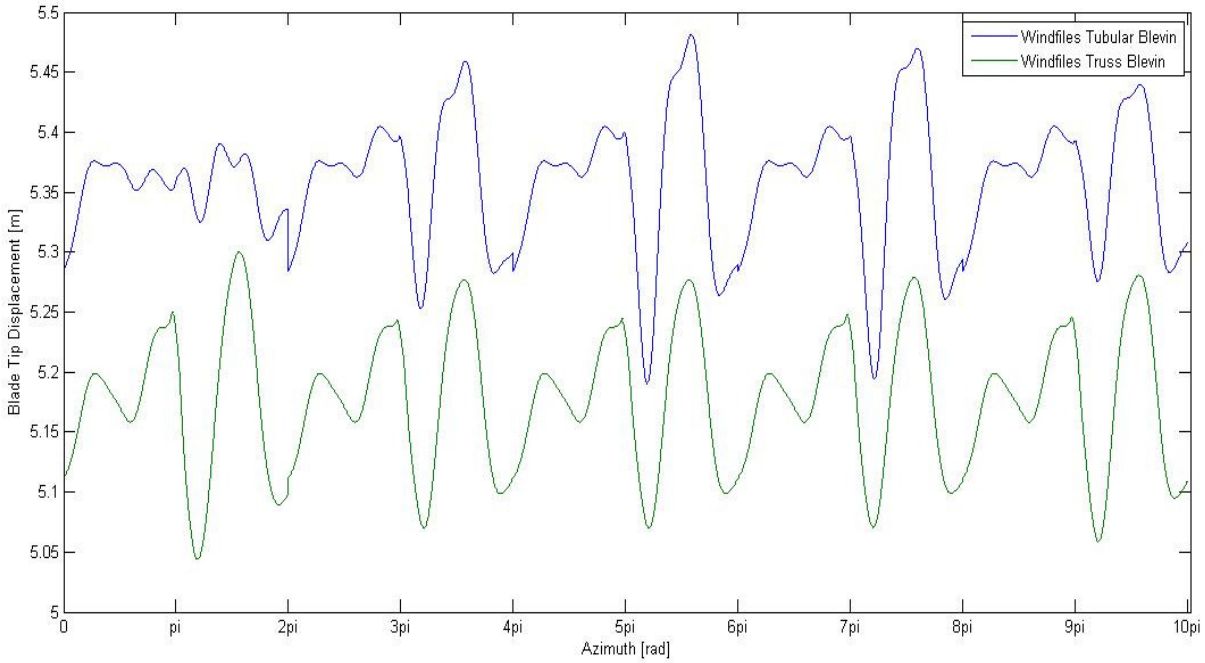

Figure 42 Blade tip deflection, ANSYS wind files with both towers

The blade tip deflection for a turbine with tubular tower is roughly 20 cm larger than for the truss tower. The frequency of the blade deflection variation is higher, and the amplitude of the fluctuations after the tower shadow varies significantly in the tubular tower case. This is connected to the effect of the vortex shedding.

The blade tip deflection are closer to being harmonic in the truss case. That may be because the force frequency due to the shedding is too high for the blade to react; i.e. the frequency lies significantly above the frequency of the first three modes. The effect may be seen in

higher order modes, but is assumed to provide very little contribution to the deflection and RFM.

The difference in blade tip displacement with calculations based on the first mode and based on the first three modes is shown for tubular tower (Figure 43) and truss tower (Figure 44).

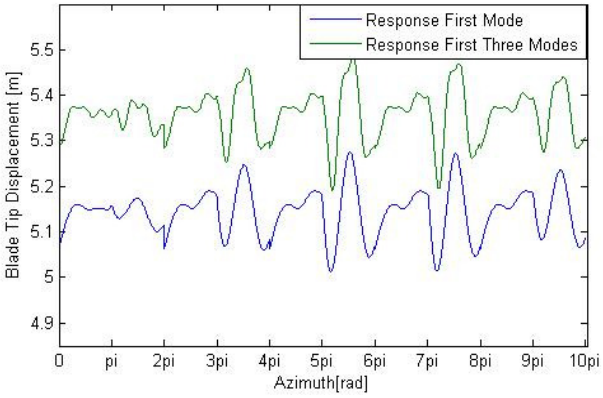

Figure 43 Blade tip displacement with Ansys wind files based on first three modes and merely first mode, tubular tower.

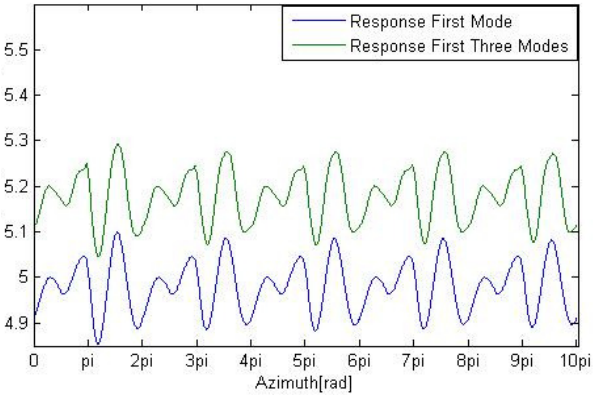

Figure 44 Blade tip displacement with ANSYS wind files based on first three modes and merely first mode, truss tower.

The upward shift of the curve due to higher order modes in the tubular tower lie around 20 cm. While for the truss tower, the difference is a few cm less. The perturbations are also of larger value in the tubular tower case. This is due to the effect of vortex shedding; the frequency is lower in the tubular tower configuration.

The difference in blade tip displacement in between the averaged Blevins model and the wind file case for tubular tower (Figure 45) and truss tower (Figure 46) are demonstrated during five revolutions.

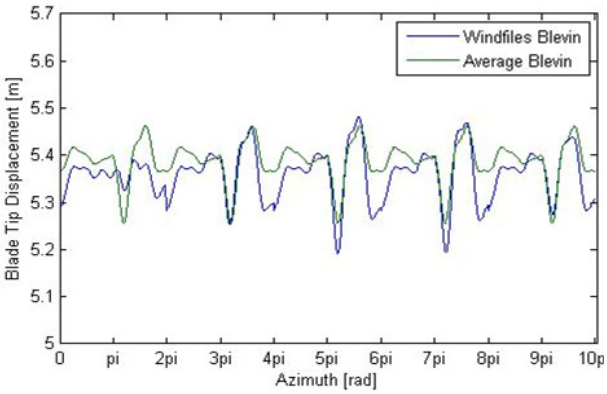

Figure 45 Difference in blade deflection between Blevins averaged model and wind file case, tubular tower

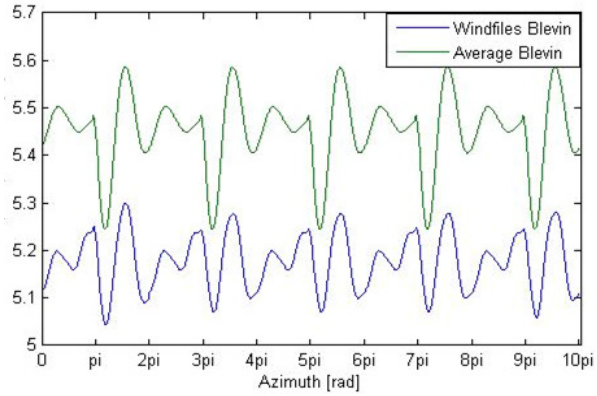

Figure 46 Difference in blade deflection between Blevins averaged model and wind file case, truss tower

Blade deflections roughly agree in the tubular tower case. The average Blevins model overestimates the blade deflection and the dip due to tower shadow during the first revolution compared to the result from the wind files. The second dip and fifth dip seems to agree quite well. However, in the third and fourth revolution the averaged Blevins underestimates the dip.

In the truss case the two models produced two distinct results for blade deflection. The tip displacement from the averaged Blevins model lies about 30 cm above the results from the wind file case, and the response from the averaged model has higher amplitudes. Hence, the modification of the wind field from 2D to 3D has a large influence on the results.

3.5.3 Root Flapwise Bending Moment

Figure 47 shows the difference in root flapwise bending moment between the two tower cases based on the wind files.

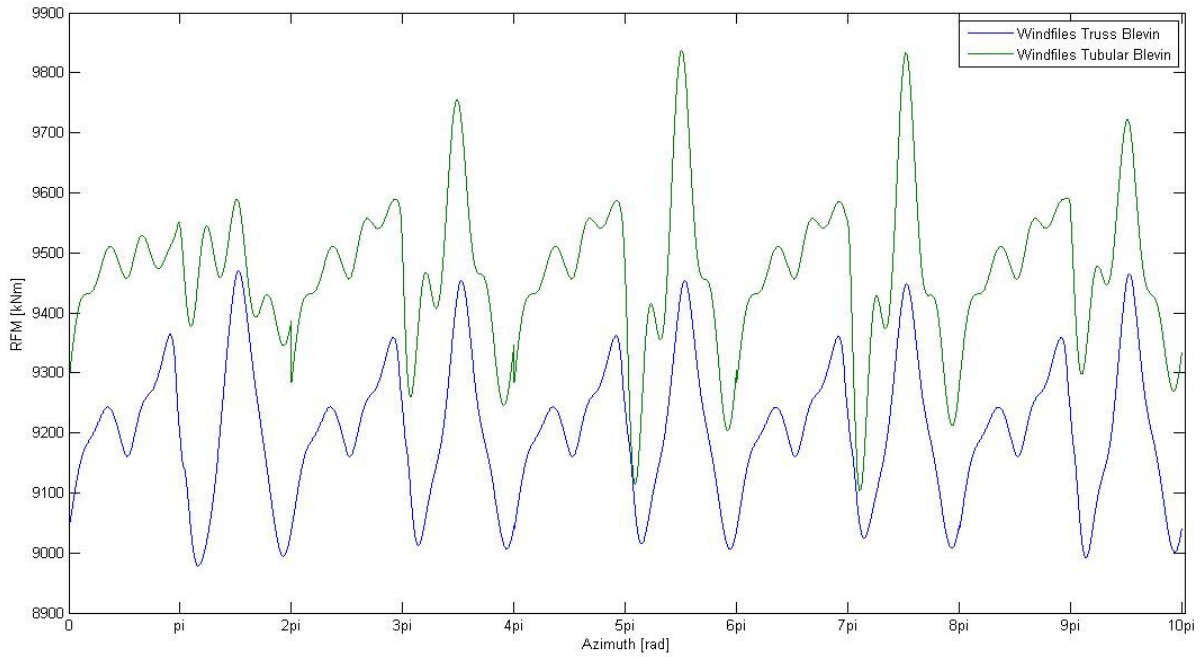

Figure 47 Root flapwise bending moment, ANSYS wind files with Both Towers

The bending moment for the turbine with tubular tower is up to about 400 kNm larger than in the truss tower case. The deflection was larger in the tubular case, and because the upward shift of curves from the contribution from the higher modes was about the same in both the tubular and the truss case, the bending moment is, as expected, larger in the tubular tower case.

The RFM value for the tubular tower case varies from 9100 to 9800 kNm, a difference of 700 kNm. With the truss tower configuration, the bending moment varies from 9000 to 9450 kNm, a difference of 450 kNm.

The high frequency perturbation from the third mode is visible in the tubular tower configuration. The frequency of the force dips with vortices from the tubular tower case is assumed to be closer to the natural frequency of the third mode.

RFM show a steeper drop after tower shadow and have larger amplitude in the tubular case. The truss tower configuration results in lower and more harmonic movement of RFM. As a result, the fatigue loading is believed to be higher in the tubular tower case.

The difference in root flapwise bending moment between the Blevins averaged model and results calculated from the wind files with tubular and truss towers are displayed in Figure 48 and Figure 49 respectively.

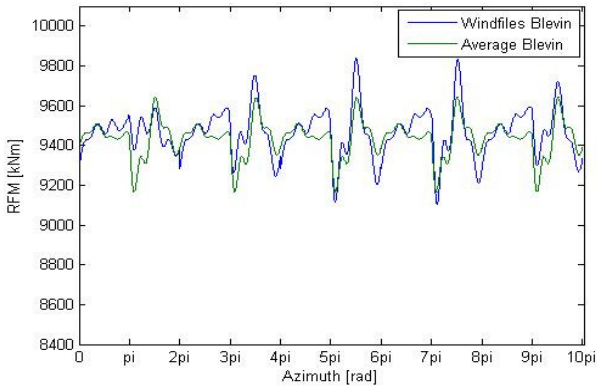

Figure 48 Root flapwise bending moment, ANSYS wind files and averaged Blevins model with tubular tower

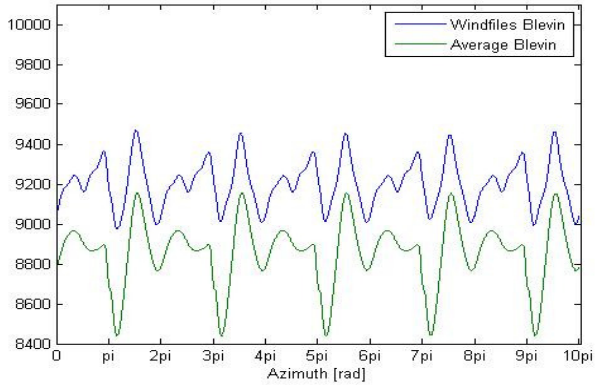

Figure 49 Root flapwise bending moment, ANSYS wind files and averaged Blevins model with truss tower

With a tubular tower, the amplitude in the root bending moment is up to 200 kNm larger when calculated from the wind files. This has to do with the increased wind speed close to the tower, creating a larger force drop as the blade enters the area of velocity deficit. Otherwise, the RFM based on the wind file case overall roughly coincide with the results from the average Blevin model.

For a wind turbine with a truss tower, the response based on the wind files give about 300 kNm larger bending moments than the average Blevin. Calculations based on the averaged Blevin give bigger amplitudes than in the wind file calculations. This change is due to the modification of the wind field in the wind file case; the modification fails to incorporate change in velocity deficit and wake width along the tower axis. As a result, the blade experiences a wake with a lower velocity deficit in total.

3.6 Wind Tunnel Experiment Wind Profile

Chapter 3.6 presents results based on wind velocity profile from wind tunnel experiment at NTNU [27].

3.6.1 Wind Velocity in Rotor Plane

Figure 50 illustrates the wind speed in the rotor plane for tubular tower wake with modified parameters to match the result from [27].

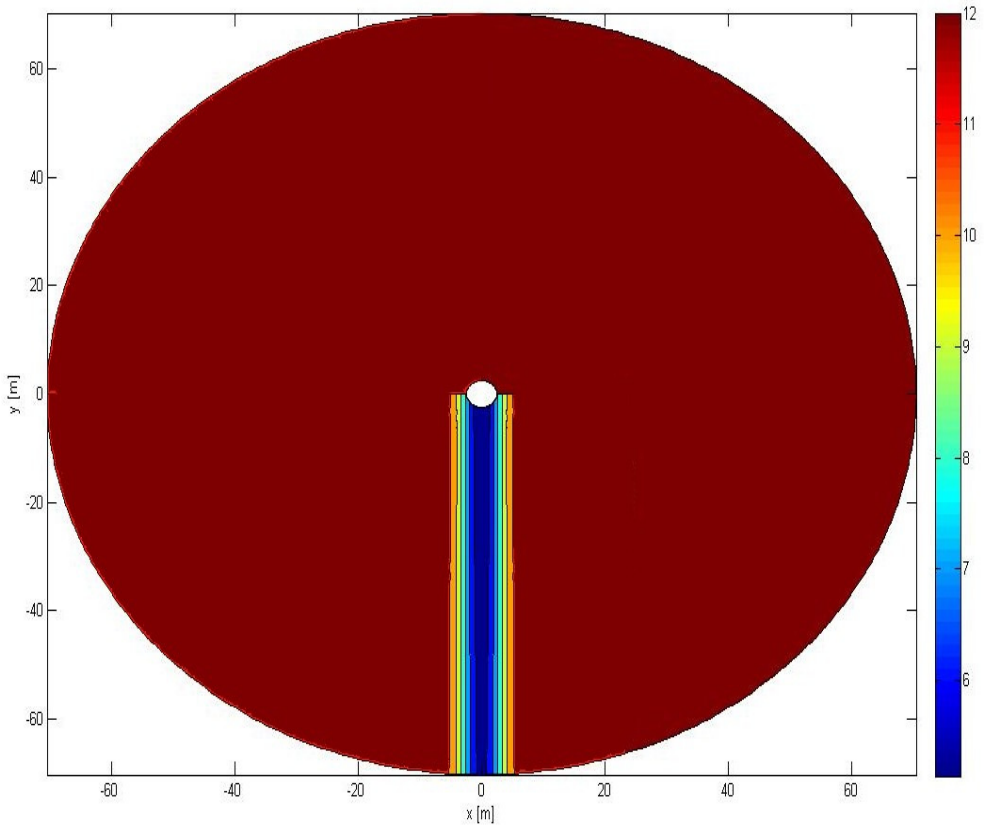

Figure 50 Wind Velocity in rotor plane [m/s], wind tunnel experiment with tubular tower

The velocity deficit behind this tower is about 7m/s, 3.5m/s higher than in the previous averaged Blevins model (section 3.4). Also, the wake width in this case is about twice the value of the previous result for the tubular tower.

The wind speeds in rotor plane with a truss tower is presented in Figure 51.

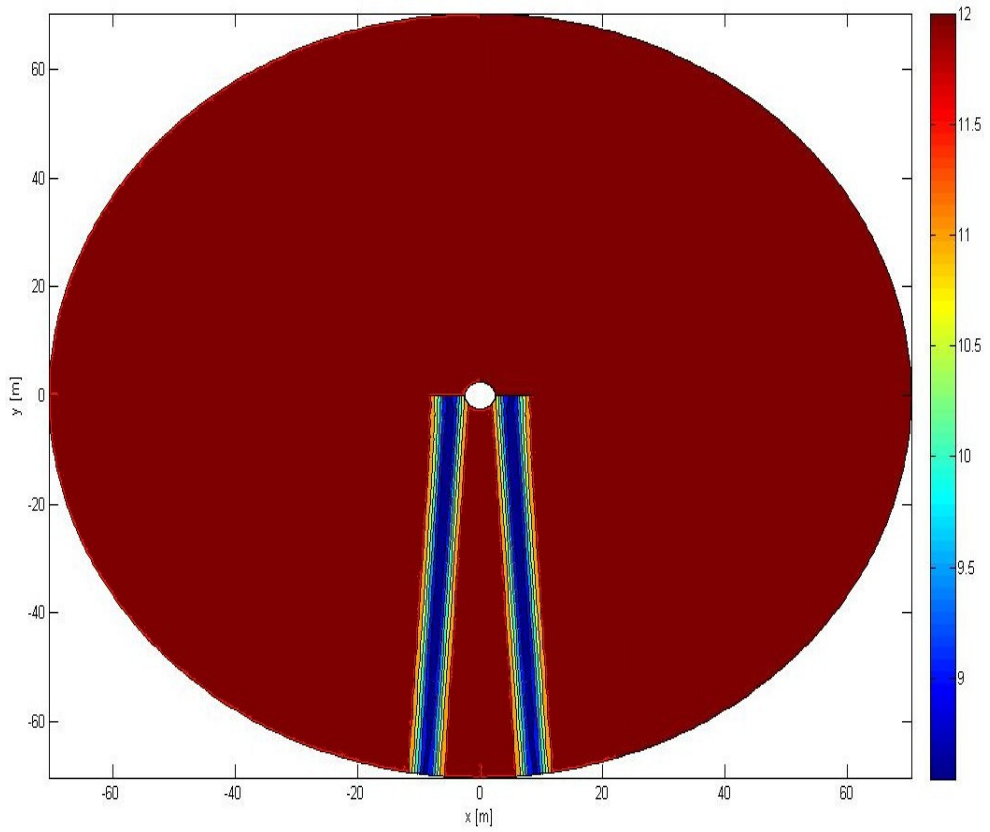

Figure 51 Wind velocity in rotor plane [m/s], wind tunnel experiment with truss tower

The velocity deficit is about 3.5 m/s, 0.7m/s lower than the results from section 3.4. The wake width in this section is about twice the result from the previous model.

3.6.2 Blade Tip Displacement

The blade tip deflections for both tubular and truss tower is presented in the two tower cases (Figure 52).

is the blade displacement from Blevins averaged model (Section 3.4). Note that this model uses input from the study by Hagen et al. [11].

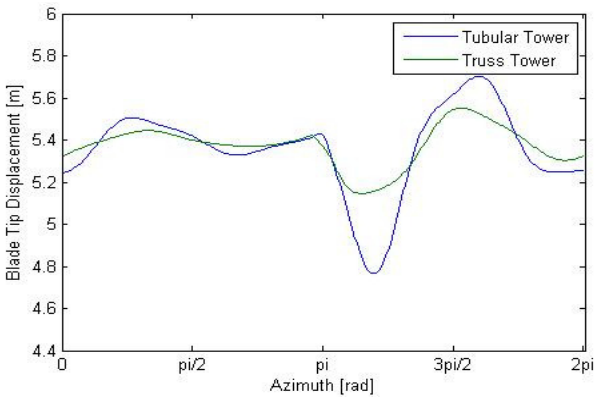

Figure 52 Blade tip displacement, wind tunnel experiment with both towers

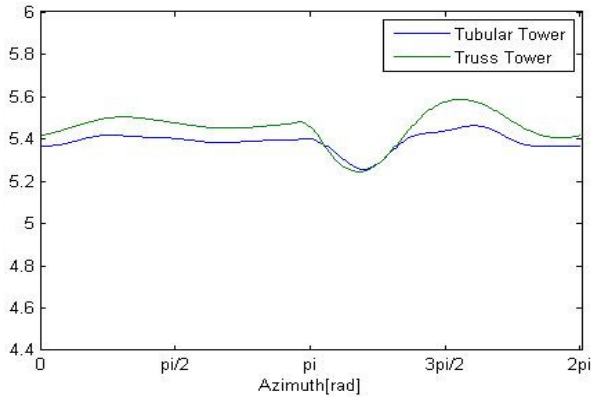

Figure 53 Blade tip displacement, Blevins averaged model with both towers

In the wind tunnel case, the amplitude of the blade deflection due to tower shadow is about 40 cm larger with a tubular tower compared to the truss tower. As a result, the fluctuations have higher amplitude than in the truss tower case.

The Blevins averaged model showed that the truss tower case had about 10 cm higher amplitude than with the tubular tower.

The total value of the deflection amplitude for the tubular tower is about 60 cm in the wind tunnel case and roughly 15 cm for the Blevin averaged case. The difference is due to the increased wake width and velocity in the wind tunnel case.

The truss tower configuration displays deflection amplitude of 30 cm in the wind tunnel case and 25 cm in Blevins averaged model. Hence, even though the velocity deficit is lower in the wind tunnel case, the amplitude is larger. This is due to the tower shadow width; the blades experience velocity deficit during a longer time period, contributing to higher amplitude.

3.6.3 Root Flapwise Bending Moment

Figure 54 shows the difference in root flapwise bending moment between the two tower cases calculated with results based on the wind tunnel experiment. The result from the previous Blevins averaged model is displayed again for comparison (Figure 55).

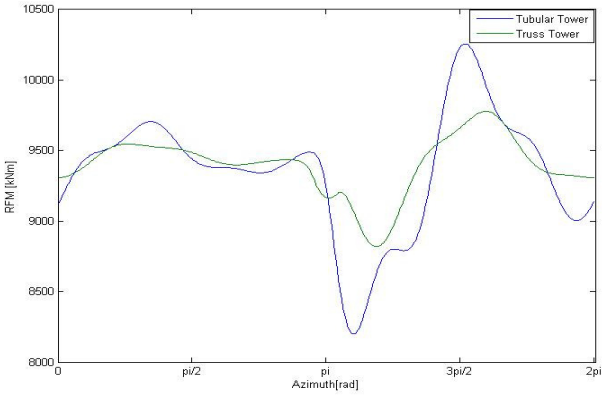

Figure 54 Root flapwise bending moment, wind tunnel experiment with both towers

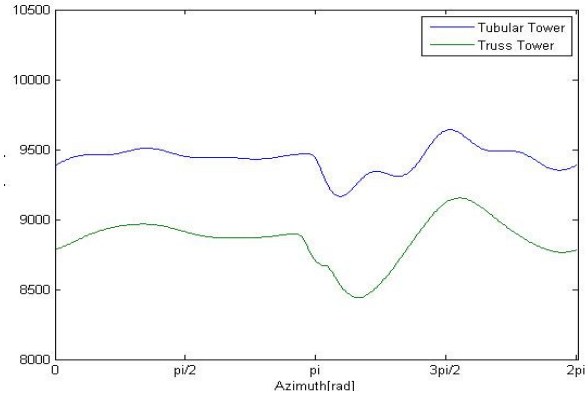

Figure 55 Root flapwise bending moment, Blevins averaged model with both towers

The tubular tower configuration shows a steeper drop in RFM when calculated from the wind tunnel experiment. The bending moment varies from about 8200 kNm to 10200 kNm in this case, a difference in RFM of about 2000 kNm within one revolution. With Blevins model the range is from 9200 to 9700 kNm, a difference of 500kNm. The large tip deflection in the wind file case is the cause of this effect.

The variation in RFM with a truss tower configuration is from 8800 to 9700 kNm in the wind tunnel case, a difference of 900 kNm. With Blevins model, the RFM varies from 8400 kNm to 9200 kNm, a difference of 800 kNm. Again, larger tip deflection with the wind tunnel case is the source of this effect.

With a truss tower, the RFM value from the wind tunnel lie roughly about 500 kNm above the results from Blevins averaged model. This has to do with the contribution from the higher order modes in averaged Blevins model, changing the curvature of the blade.

The tubular tower configuration has a longer recovery time visualized by the larger fluctuating blade deflections and RFM as they pass through the tower shadow region. The fluctuating loads seen by the tubular tower configurations contribute to high fatigue loading of the structure. Hence, based on this model, the truss tower would be the natural best choice in terms of tower shadow influence.

A summary of the RFM results are given in Table 3:

Table 3 RFM Results from Matlab Calculations

Case	Tower	Min RFM [kNm]	Max RFM [kNm]	Δ [kNm]
Averaged Blevin	Tubular	9200	9700	500
Wind file	Tubular	9100	9800	700
Wind tunnel	Tubular	8200	10200	2000
Averaged Blevin	Truss	8400	9200	800
Wind file	Truss	9000	9450	450
Wind tunnel	Truss	8800	9700	900

3.7 Adjusted Stiffness and Mass

Chapter 3.7 presents the difference in response when modifying the blade stiffness in both flapwise and edgewise directions and the blade mass. The original blade stiffness and mass reference is 100%, while reductions of this value make up the alterations. Chapter 3.8 presents the dynamic response when modifying merely the blade stiffness. The other structural properties of the blade have been kept unchanged. The analysis has been made based on the averaged Blevin model.

Adjusting the stiffness reduces the natural frequency of the blade (see
Table 4). When adjusting both the blade stiffness and -mass, the natural frequency actually increases (see Table 5). This is due to the unchanged parameters of the blade; the longitudinal stiffness, torsional stiffness, modulus of elasticity, and cross sectional area. The two adjustment cases changes the eigenmodes of the blade; the eigenmodes are presented in appendix A-10.

Table 4 Natural frequency, modified stiffness (EI)

EI adjustment	Frequency First Mode [Hz]	Frequency Second Mode [Hz]	Frequency Third Mode [Hz]
No adjustment	3.24	6.48	8.75
95% EI	3.20	6.32	8.63
90% EI	3.15	6.15	8.50
80% EI	3.04	5.80	8.22
70% EI	2.91	5.41	7.90

Table 5 Natural frequency, modified stiffness (EI) and mass (m)

EI & m Adjustment	Frequency First Mode [Hz]	Frequency Second Mode [Hz]	Frequency Third Mode [Hz]
No adjustment	3.24	6.48	8.75
95% EI & m	3.28	6.48	8.85
90% EI & m	3.32	6.49	8.96
80% EI & m	3.40	6.49	9.19
70% EI & m	3.48	6.50	9.43

3.7.1 Blade Tip Displacement

Figure 56 and Figure 57 shows the blade tip deflection with decreasing stiffness and mass in the tubular tower case and truss tower case, respectively.

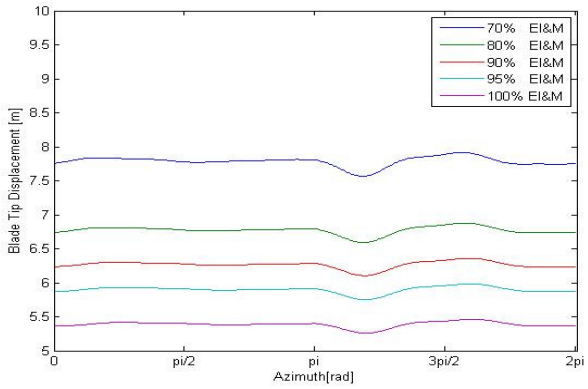

Figure 56 Blade tip displacement with modified stiffness and mass, tubular tower

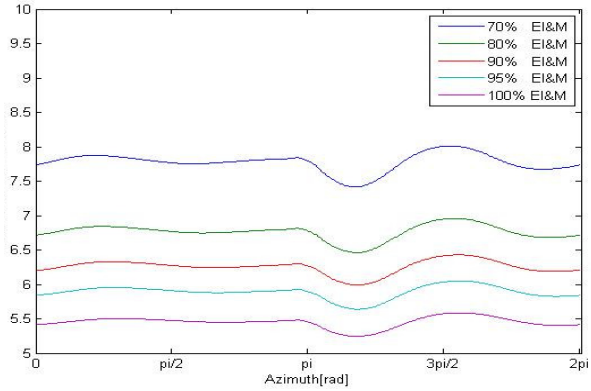

Figure 57 Blade tip displacement with modified stiffness and mass, truss tower

For decreasing stiffness and mass values up to 90%, the tip deflection seems to vary gradually. Then there is less difference between 90 and 80% adjustment, and an increase between 80 and 70% adjustment.

3.7.2 Root Flapwise Bending Moment

Figure 58 and Figure 59 show the effect of decreasing blade mass and stiffness on the root flapwise bending moment in with tubular tower and truss tower, respectively. The bending moment seems to increase until the stiffness value drops to between 80 and 70% of original stiffness.

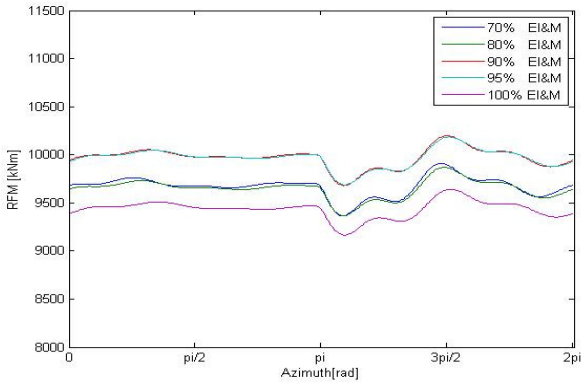

Figure 58 Root flapwise bending moment with modified stiffness and mass, tubular tower

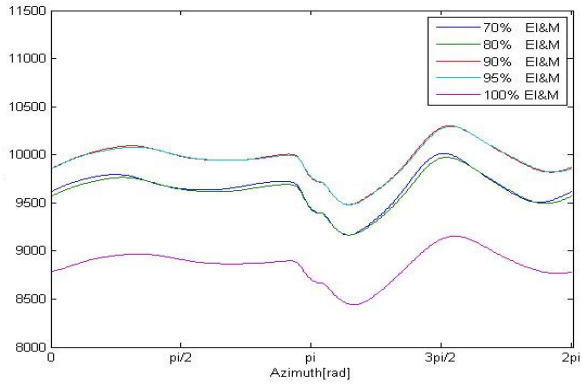

Figure 59 Root flapwise bending moment with modified stiffness and Mass, truss tower

For the both tower cases, the RFM increases between 100% and 95% mass and stiffness values. 95% and 90% adjustment give about the same RFM. The same is the case for 80% and 70%.

The value of RFM fluctuation pattern during a revolution is about the same in all cases.

3.8 Adjusted Stiffness

The following chapter presents the difference in response when modifying the blade stiffness. The other structural properties of the blade are unchanged. As before, the averaged Blevin model is used.

3.8.1 Blade Tip Displacement

Figure 60 and Figure 61 show the difference in blade tip displacement when modifying the blade stiffness, *EI*, in the tubular- and truss cases.

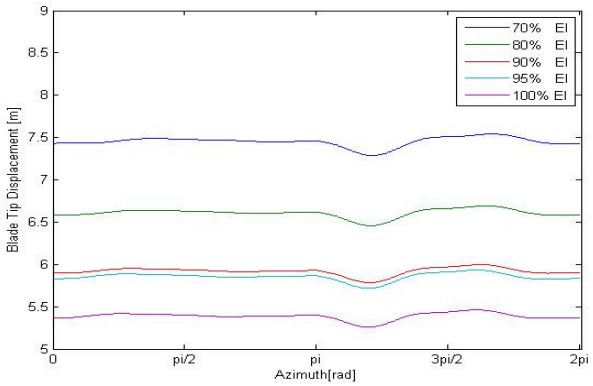

Figure 60 Blade tip displacement with modified blade stiffness, tubular tower

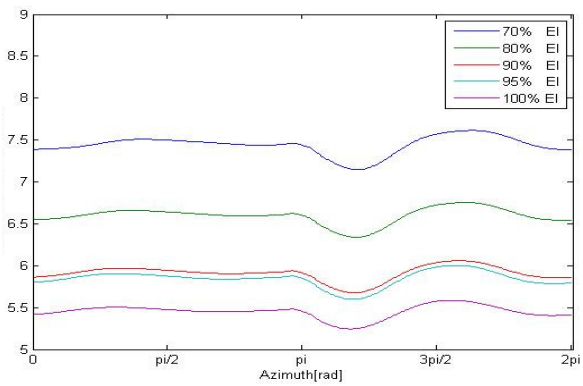

Figure 61 Blade tip displacement with modified blade stiffness, truss tower

Adjusting the stiffness gives a large impact on the blade deflection. Note that the tip deflection with 95% stiffness is only a few cm lower than the tip deflection with 90 % stiffness. This is believed to be due to change in eigenmode with 95% stiffness.

3.8.2 Root Flapwise Bending Moment

The difference in root flapwise bending moment in the tubular tower case (Figure 62) and in the truss tower case (Figure 63) are presented:

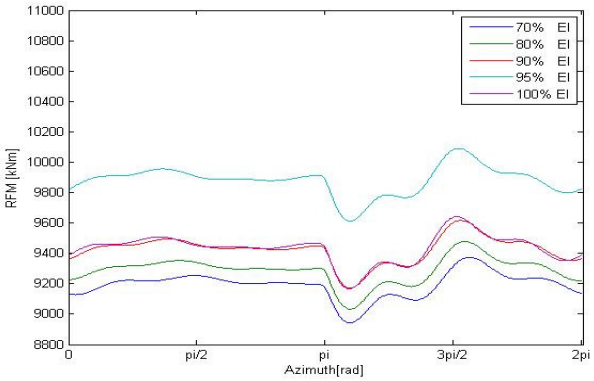

Figure 62 Root flapwise bending moment with modified stiffness, tubular tower

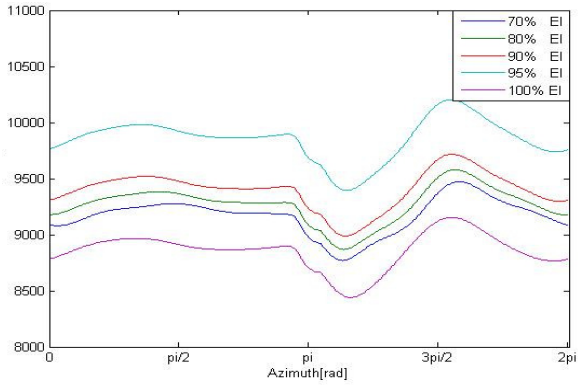

Figure 63 Root flapwise bending moment with modified stiffness, truss tower

In both cases the bending moment seems to increase with stiffness reduced to about 95%, decreasing the stiffness further cause the bending moment to decrease rapidly. Note that the RFM fluctuation does not increase noteworthy when adjusting the stiffness.

4 Discussion

The induction factors and aerodynamic forces for free stream velocity found agree with what Frøyd et al [28] found, and can be trusted. The centrifugal loading scheme used in this study is similar to methods described by Burton [13] and Hansen [16], and give reson for validity of results for the effect of centrifugal loading.

It is difficult to determine which of the three wind distribution cases that are providing the most realistic display of the wind field behind a full scale wind turbine. The averaged Blevins model does not incorporate the effect of vortex shedding and turbulent inflow, and is therefore providing results for a time-independent theoretical case. In reality, the wind flow is far from being constant. The input parameters from Hagen et al. [11] used in this model needs verification to be trusted.

The wind file case provides results with the vortex effects, though the wind profile modification going from 2D to 3D will provide some inaccuracy in the tubular case. In the truss case, the entire shape of the wake is different, and is not providing valid results for the given truss tower geometry. Also, the resulting wind profiles from the study by Hagen et al. [11] need verification to be trusted. Despite the uncertainties, the model proves that vortex shedding has a large influence on RFM in the tubular tower case. However, in the truss case, the effect of vortex shedding is small.

Blevins averaged model and the wind file case give different results in case of tip deflection and RFM. When comparing the tip deflection and RFM with tubular tower configuration, it is obvious that the vortex shedding gives larger fluctuations in RFM and tip deflection. Hence the averaged model will underestimate the load on the blade. Designing a blade based on the RFM from averaged Blevins model means a large safety factor both in terms of maximal- and fatigue loading.

The wind tunnel experiment is considered to give the most viable results for the averaged wind field behind the towers. The results in terms of RFM agrees with what Reiso et al [27] found. However, the study is conducted in small scale. When employing the results in a full scale case, the changed Reynolds number will affect the velocity field behind the cylinder. The vortex shedding and possible turbulence in the wake will have influence on the wind velocity and wake width. But it is uncertain to what extent the wind profile would be affected. In addition, the wind tunnel experiment case is based on a time averaged model, which fails to incorporate the effect of vortex shedding. Based on the difference between averaged Blevins model and the wind file case, this would give rise to uncertainties in terms of blade dynamic response.

The value of the aerodynamic damping is merely a guess, and gives rise to uncertainties when it comes to the course of blade displacement after the tower shadow.

Adjusting the blade stiffness could represent changing the blade material. The deflection of the blade becomes larger, but the fluctuation in RFM due to the tower shadow does not increase to the same extent. Hence, a less stiff blade could be a good option in terms of fatigue loading. In reality, the other structural properties of the blade would change with another material, affecting the eigenmodes and hence the eigenmodes and natural frequency of the blade.

Adjusting both the stiffness and mass could be thought of as adjusting the thickness of the blade material. Also here, a less stiff blade would be a more suitable choice in terms of fatigue loading. Structural properties that have been kept constant are the cross sectional area, elastic modulus, shear modulus of elasticity, and torsional stiffness. Adjusting the thickness of the material would have an impact on these properties, resulting in different eigenmodes, and natural frequency of the blade, hence have an influence on the blade dynamic response. The two adjustment cases do not give viable results as to what would be the properties of an optimal blade.

5 Conclusion

The intention of this work has been to investigate the blade dynamic response of a downwind turbine with both a tubular and a truss tower, in terms of blade deflection and RFM. Three different wind profiles have been used; averaged Blevin, wind files from ANSYS and wind velocity profiles from wind tunnel experiments.

The three different cases give ambiguous results in both blade deflection and RFM. Based on Blevins averaged model, the tubular tower configuration would be a better choice in terms of fatigue loading. However, this model should not be trusted until the input data have been verified. In addition, time averaging the wind field provides some uncertainties in terms of blade deflection and RFM.

Based on the wind file case, the better tower option is the truss tower. However, the modification from 2D to 3D changes the geometry of the truss tower, and provides a result with some uncertainty.

The wind tunnel case indicates that the truss tower is the best option regarding fatigue loading. The time averaged model and modification to full scale will though provide some uncertainties in this result as well.

The wind file case and wind tunnel case agree that the truss tower would be a better option with regards to the tower shadow effect. As the averaged Blevins model is assumed to be the most uncertain way of modeling the wind field; the study indicates that a truss tower should be used in downwind turbines. However, further investigation is necessary to make a final conclusion.

The model developed to determine the dynamic response is believed to provide valid results. The uncertainties are concerning the wind velocity input.

6 Recommendations for further work

There are some uncertainties connected with the wind field behind the different towers. The two different studies this work is based on provide different results. It is recommended that the wind field behind two towers with geometry for a 10 MW wind turbine is determined, to give a final result as to which is the better tower choice concerning fatigue loading; a full scale wind tunnel test.

Based on the reduction in wind speed upstream of the tower, it would be interesting to compare an upwind and a downwind turbine in terms of fatigue loading.

Adjusting the stiffness should be analyzed with realistic structural properties to be able to decide what kind of blade properties would give the optimal dynamic response in terms of fatigue loading for a downwind turbine.

References

1. Salthaug, L., *About truss towers*, M. Salthaug, Editor. 2011: Stavanger.
2. DWIA. *Wind Turbine Towers* 2003 19.09.2003 [cited 2011 08.04.2011]; Available from: http://guidedtour.windpower.org/en/tour/wtrb/tower.htm.
3. Talisman. *Windward*. 2007 [cited 2011 31.05.2011]; Available from: http://www.beatricewind.co.uk/Uploads/Downloads/Windward_5_newsletter.pdf.
4. NAOWPI. *Offshore Wind Turbine Foundations- Current & Future Prototypes*. 2009 09.09 [cited 2011 10.03]; Available from: http://offshorewind.net/Other_Pages/Turbine-Foundations.html.
5. Aasheim, E., *Dynamic Response Analysis of Fixed Offshore Wind Turbines*, in *Fakultet for Ingeniørvitenskap og Teknologi*. 2009, NTNU: Trondheim. p. 8,50.
6. Manwell, J.F., J.G. McGowan, and A.L. Rogers, *Wind energy explained: theory, design and application*. 2002, New York: Wiley. 84-110.
7. Haugset, S.K., *An introduction to the BLADE ELEMENT MOMENTUM METHOD.* 2007: p. 19, 23, 40-45.
8. Krogstad, P.-Å., *An introduction to aerodynamics*, in *TEP4545, Lecture notes*. 2010, NTNU: Trondheim.
9. Cartage. *Boundary Layers*. 2011 [cited 2011 06.06.2011]; Available from: http://www.cartage.org.lb/en/themes/sciences/physics/mechanics/fluidmechanics/RealFluids/BoundaryLayers/BoundaryLayers.htm.
10. Breinig, M. *Turbulence*. Elements of Physics I 2011 [cited 2011 08.06.2011]; Lecture notes]. Available from: http://labman.phys.utk.edu/phys221/modules/m9/turbulence.htm.
11. Hagen, T.R., M. Reiso, and M. Muskulus, *Numerical Analysis of Turbulent Flow Past a Truss Tower for Offshore Wind Turbines*, in *Department of Civil and Transport Engineering*. 2011, Norwegian University of Science and Technology: Trondheim.
12. Blevins, R.D., *Flow-Induced Vibrations*. 1990: Van Nostrand Reinhold. p. 177-178.
13. Burton, T., *Wind energy: handbook*. 2001, Chichester: J. Wiley. xxiv, 617 s.
14. Holmås, T., *Email: Assignment Sway*, M. Salthaug, Editor. 2010.

15. Ekberg, A. *Damage accumulation*. Fatigue and Fracture 2004 [cited 2011 31.05.2011]; Available from: http://www.am.chalmers.se/~anek/teaching/fatfract/.
16. Hansen, M.O.L., *Aerodynamics of Wind Turbines (2nd Edition)*. 2010, Earthscan. p. p. 109.
17. Frøyd, L., *Rotor design for a 10MW Offshore Wind Turbine*, in *Department of Energy and Process Engineering*. 2011, Norwegian University of Science and Technology: Trondheim.
18. Merz, K., *Conseptual Design of Stall-Regulated Rotors for Offshore Wind Turbines*. 2011, NTNU: Trondheim.
19. MathWorks. *Product Documentation*. Eig, Eigenvalues and eigenvectors 2010 [cited 2011 05.03]; Available from: http://www.mathworks.com/help/techdoc/ref/eig.html.
20. Moe, G., *Dynamics of multi-degree of freedom structures*. 2011, NTNU: Trondheim.
21. MathWorks, *MATLAB*. 2010.
22. Cook, R.D., *Concepts and applications of finite element analysis*. 2002, New York: Wiley. p. 27-29, 49-50.
23. Przemieniecki, J.S., *Theory of matrix structural analysis*. 1968, New York: McGraw-Hill.
24. Jonkman, J., et al., *Definition of a 5-MW Reference Wind Turbine for Offshore System Development*, NREL, Editor. 2009.
25. Thomassen, P. and D. Zwick, *Offshore Wind and Tidal Reference Turbines*. 2011, NTNU: Trondheim.
26. Bossanyi, E.A. *GH Bladed Theory Manual*. 2003 [cited 2011 02.06.2011].
27. Reiso, M., M. Muskulus, and G. Moe, *Tower Shadow-Experiment Comparing Wake Behind Tubular and Truss Towers*. 2011, Norwegian University of Science and Technology (NTNU): Trondheim.
28. Frøyd, L. and O. Dahlhaug, *A Conseptional Design Method For Parametric Study of Offshore Wind Turbines*. 2011, NTNU: Trondheim.

Appendix A-1: MATLAB Script for Blevins model, Tubular Tower

```
clear all
clc
%%%%%%%%%%%%%%%%%%%%%%%%%%%%%Input%%%%%%%%%%%%%%%%%%%%%%%%%%%%%%%%%%%%%%%%%%%%%%%%
load Data                       %Structural data
load Tubular
Hr=2.5;                         %Hub radius[m]
D=4;                            %Monopile diameter[m]
V0=12;                          %Mean free stream velocity[m/s]
betta=2.5*pi/180;               %Cone angle[rad]
Cd=0.399;                       %Drag coefficient[-]
x0=6.709;                       %Downstream location of virtual wake origin[m]
%%%%%%%%%%%%%%%%%%%%%%%%%%%%%%%%%%%%%%%%%%%%%%%%%%%%%%%%%%%%%%%%%%%%%%%%%%%%%%%%%%
az=linspace(0,2*pi,360);     %Azimuth angles[rad]

Radius=Blade.Radius*cos(betta);         %Blade Radius[m]


for k=1:max(size(Radius))
    x(k)=3*D+Radius(k)*sin(betta);    %Downstream distance [m]
    b(k)=0.23*sqrt(Cd*D*(x(k)+x0));   %Shadow half width [m]
    c(k)=1.02*V0*sqrt(Cd*D/(x(k)+x0));%Velocity deficit at centerline [m/s]
end

for i=1:max(size(Radius))
    for j=1:max(size(az))
        x(i,j)=Radius(i)*sin(az(j));    %y value (rotor plane) [m]
        y(i,j)=Radius(i)*cos(az(j));    %z value (rotor plane) [m]

        if az(j)>pi/2 && az(j)<3*pi/2
            V(i,j)=V0-c(i)*exp(-0.69*((y(i,j))^2)/((b(i))^2));
            %Velocity in tower shadow [m/s]

        else
            V(i,j)=V0;  %Velocity outside tower shadow [m/s]
        end
    end
end

%%%%%%%%%%%%%%%%%%%%%%%%%%%%%%%SAVING%%%%%%%%%%%%%%%%%%%%%%%%%%%%%%%%%%%%%%%%%%%%
Tubular.Rotorwind=V;
save Tubular.mat Tubular
%%%%%%%%%%%%%%%%%%%%%%%%%%%%%%%%PLOT%%%%%%%%%%%%%%%%%%%%%%%%%%%%%%%%%%%%%%%%%%%%%
contourf(x,y,V)
colorbar
xlabel('x [m]')
ylabel('y [m]')
```

Appendix A-2: MATLAB Script for Blevins model, Truss Tower

```
clear all
clc

%%%%%%%%%%%%%%%%%%%%%%%%%%%%%Input%%%%%%%%%%%%%%%%%%%%%%%%%%%%%%%%%%%%%%%%%%%%
load Data                    %Structural data
load Truss
Bb=28.1;                     %Tower bottom(base) width[m]
Bt=4;                        %Tower top width[m]
D=4;                         %Monopile diameter[m]
D_t=1.35;                    %Corner column diameter [m]
H=170;                       %Tower height [m]
betta=2.5*pi/180;            %Cone angle[rad]
V0=12;                       %Mean free stream velocity[m/s]
Cd=0.608;                    %Drag coefficient [-]
x0=15.314;                   %Downstream location of virtual wake origin[m]
%%%%%%%%%%%%%%%%%%%%%%%%%%%%%%%%%%%%%%%%%%%%%%%%%%%%%%%%%%%%%%%%%%%%%%%%%%%%%%%
Radius=Blade.Radius*cos(betta);        %Blade Radius[m]

az=linspace(0,2*pi,360);     %Azimuth angles[rad]


for k=1:max(size(Radius))
    %Rear corner columns
    xa(k)=3*D+((Bt)/2)+Radius(k)*sin(betta);    %Downstream distance[m]
    ba(k)=0.23*sqrt(Cd*D_t*(xa(k)+x0));         %Shadow half width [m]
    ca(k)=1.02*V0*sqrt(Cd*D_t/(xa(k)+x0));%Velocity deficit centerline[m/s]

    %Foremost corner columns
    xb(k)=3*D-((Bt)/2)+Radius(k)*sin(betta); %Downstream distance[m]
    bb(k)=0.23*sqrt(Cd*D_t*(xb(k)+x0));      %Shadow half width [m]
    cb(k)=1.02*V0*sqrt(Cd*D_t/(xb(k)+x0));%Velocity deficit centerline[m/s]

    Zt(k)=0.5*Bt+((0.5*Bb-0.5*Bt)*Radius(k)*cos(betta))/H;
    %Horisontal distance from x axis to tower shadow [m]
end


for i=1:max(size(Radius))
    for j=1:max(size(az))
        y1(i,j)=Radius(i)*sin(az(j))-(Zt(i)+D_t/2);
        %distance in y- direction from first tower shadow part[m]
        y2(i,j)=Radius(i)*sin(az(j))+(Zt(i)+D_t/2);
        %distance in y- direction from second tower shadow part[m]

        xc(i,j)=Radius(i)*sin(az(j)); %x value (rotor plane) [m]
        yc(i,j)=Radius(i)*cos(az(j)); %y value (rotor plane) [m]

        if Radius(i)>Zt(1)
        if az(j)>pi/2 && az(j)<pi
            Vda(i,j)=ca(i)*exp(-0.69*(y1(i,j)^2)/(ba(i)^2));
            Vdb(i,j)=cb(i)*exp(-0.69*(y1(i,j)^2)/(bb(i)^2));
            %Velocity deficit in 1.st tower shadow [m/s]
        elseif az(j)>pi && az(j)<3*pi/2
            Vda(i,j)=ca(i)*exp(-0.69*(y2(i,j)^2)/(ba(i)^2));
            Vdb(i,j)=cb(i)*exp(-0.69*(y2(i,j)^2)/(bb(i)^2));
```

```
            %Velocity deficit in 2.nd tower shadow [m/s]
        else
            Vda(i,j)=0; %Velocity deficit outside tower shadow[m/s]
            Vdb(i,j)=0; %Velocity deficit outside tower shadow[m/s]
        end
        end
   V(i,j)=V0-(Vda(i,j)+Vdb(i,j));%Velocity distribution in rotor plane[m/s]
    end
end

%%%%%%%%%%%%%%%%%%%%%%%%%%%%%%%%SAVING%%%%%%%%%%%%%%%%%%%%%%%%%%%%%%%%%%%%
 Truss.Rotorwind=V;
 save Truss.mat Truss
%%%%%%%%%%%%%%%%%%%%%%%%%%%%%%%%%%PLOT%%%%%%%%%%%%%%%%%%%%%%%%%%%%%%%%%%%%
 contourf(xc,yc,V)
 colorbar
 xlabel('x [m]')
 ylabel('y [m]')
```

Appendix A-3: MATLAB Script for wind velocity distribution in rotor plane for tubular tower, wind file case

```
clear all
clc

%files=dir('rake*');    %localize files cntaining wind velocities
betta=2.5*pi/180;       %Cone angle [rad]

%for i=1:length(files)
%   Wind(i)=importdata(files(i).name,' ',1); %Imports wind files
%end

load Wind
load blad               %Turbine blade data
%load WindFluent
r=Blade.Radius*cos(betta);
az=linspace(0,2*pi,1000);
y1=-70.5:0.1:70.5;      %Transverse distance [m]

%Vindfiles(6000,1)=struct;
for j=1:5               %Number of Revolutions
for k=1:1000

    k1=k+1000*(j-1);

V1(k1,:)=interp1(Wind(1,k1).data(:,3),Wind(1,k1).data(:,5),y1,'linear','ext
rap');
    %Interpolates the wind speeds based on distance from the tower

        for i=1:max(size(r))
        xb(i,k)=r(i)*sin(az(k));    %Y value [m]
        yb(i,k)=r(i)*cos(-az(k));   %X value [m]
        end

        V2(:,k)=interp1(y1,V1(k1,:),xb(:,k)); %Wind velocity in wake

        if az(k)<pi/2
        V2(:,k)=12;         %Wind velocity outside wake
        end
        if az(k)>3*pi/2
        V2(:,k)=12;         %Wind velocity outside wake
        end
end
WindFluent.Tubular.R(:,1000*(j-1)+1:1000*j)=V2;
%Saves wind velocity distribution for the revolution
end
save WindFluent.mat WindFluent
%%%%%%%%%%%%%%%%%%%%%%%%%%%%PLOT%%%%%%%%%%%%%%%%%%%%%%%%%%%%%%%%%%%%%%%%%%
contourf(xb,yb,V2);
colorbar
xlabel('x [m]')
ylabel('y [m]')
```

Appendix A-4: MATLAB Script for wind velocity distribution in rotor plane for truss tower, wind file case

```
clear all
clc

%files=dir('rake*');    %localize files cntaining wind velocities
betta=2.5*pi/180;       %Cone angle [rad]
%for i=1:length(files)
%   Wind(i)=importdata(files(i).name,' ',1);    %Imports wind files
%end
load Wind
load Blad           %Turbine blade data
%load WindFluent
r=Blade.Radius*cos(betta);  %Blade radius [m]
az=linspace(0,2*pi,1000);   %Azimuth angle [rad]
y1=-70.5:0.1:70.5;          %Transverse distance [m]
%Vindfiles(5960,1)=struct;

for j=1:5      %Number of Revolutions

for k=1:1000
    k1=k+1000*(j-1);

V1(k1,:)=interp1(Wind(1,k1).data(:,3),Wind(1,k1).data(:,5),y1,'linear','ext
rap');
    %Interpolates the wind speeds based on distance from the tower

        for i=1:max(size(r))
        xb(i,k)=r(i)*sin(az(k));    %Y value [m]
        yb(i,k)=r(i)*cos(-az(k));   %X value [m]
        end

        V2(:,k)=interp1(y1,V1(k1,:),xb(:,k)); %Velocity distribution in
tower shadow
        if az(k)<pi/2
        V2(:,k)=12;     %Velocity distribution outside tower shadow
        end
        if az(k)>3*pi/2
        V2(:,k)=12;     %Velocity distribution outside tower shadow
        end

end

WindFluent.Truss.R(:,1000*(j-1)+1:1000*j)=V2;
%Saves wind velocity distribution for the revolution

end
save WindFluent.mat WindFluent
%%%%%%%%%%%%%%%%%%%%%%%%%%%%PLOT%%%%%%%%%%%%%%%%%%%%%%%%%%%%%%%%%%%%%%%%%%
contourf(xb,yb,V2);
colorbar
xlabel('x [m]')
ylabel('y [m]')
```

Appendix A-5: MATLAB Script for induction Factors, Lift- and Drag Coefficients

```
clear all
clc
%%%%%%%%%%%%%%%%%%%%%%%%%%%%%%%%INPUT%%%%%%%%%%%%%%%%%%%%%%%%%%%%%%%%%%%%%%%%
w=1.2566;                       %Rotor speed[rad/sek]
U=12;                           %Free stream wind velocity [m/s]
az=0:2*pi/(359):2*pi;           %Azimut angles[rad]
load Truss                      %Wind welocity rotorplane [m/s] (tubular tower)
load Tubular                    %%Wind welocity rotorplane [m/s] (tubular
tower)
load Data                       %Strucural blade data
t=0;                            %Tower choice. (set 1 for tubular, 0 for truss)
B=3;                            %Number of blades[-]
R=68;                           %Blade radius[m]
betta=2.5*pi/180;               %Cone angle[rad]
%%%%%%%%%%%%%%%%%%%%%%%%%%%%%%%%%%%%%%%%%%%%%%%%%%%%%%%%%%%%%%%%%%%%%%%%%%%%
Radius=linspace(Blade.Radius(1),Blade.Radius(end-1),39);
%Sectional radius [m]

ax=1/3*ones(max(size(Radius)),1);   %Initialize axsial induction factor
ar=zeros(max(size(Radius)),1);      %Initialize tangential induction factor

if t==1
    Ur=Tubular.Rotorwind;
elseif t==0
    Ur=Truss.Rotorwind;
end
%Wind velocities in rotor plane[m/s] (tubular or truss tower)

%%%%%%%%%%%%%%%%%%%%%%%%Iteration procedyre%%%%%%%%%%%%%%%%%%%%%%%%%%%%%%%%
for j=1:10 %Number of iterations

 for i=1:max(size(Radius))

     phi1(i)=(atan((1-ax(i,j))*U/((1+ar(i,j))*w*Radius(i))));
     %Local air flow angle [rad]
     alfa1(i)=phi1(i)*180/pi-Blade.Twist(i);
     %Angle of attack(AoA) [deg]
     f(i)=B/2*(1-(Radius(i)/R))/((Radius(i)/R)*sin(phi1(i)));
     %Input in tip loff factor
     F(i)=real((2/pi)*acos(exp(-(f(i)))));
     %Tip loss factor

     [ab,cv] = searchclosest(Aero(1,i).AoA,alfa1(i));
     Cla(i)=Aero(1,i).Prop(ab,1);
     Cda(i)=Aero(1,i).Prop(ab,2);

     %For each section, the function look up the aoa nearest to the coputed
     %aoa. Then finds the appurtenant Cl and Cd

     Cn(i)=Cla(i)*cos(phi1(i))+Cda(i)*sin(phi1(i)); %Cn coefficient[-]
     Ct(i)=Cla(i)*sin(phi1(i))+Cda(i)*cos(phi1(i)); %Ct coefficient[-]

     sy(i)=B*Blade.Chord(i)/(2*pi*Radius(i)); %Solidity[-]

     ax(i,j+1)=1/(4*F(i)*(sin(phi1(i))^2)/(sy(i)*Cn(i))+1);
```

```
     %Axial induction factor[-]

     if ax(i,j+1)>0.2
         K(i)=4*F(i)*(sin(phi1(i)))^2/(sy(i)*Cn(i));
         ax(i,j+1)=0.5*(2+K(i)*(1-2*0.2)-sqrt((K(i)*(1-
2*ax(i,j+1))+2)^2+4*(K(i)*(0.2^2)-1)));
     end
     %Glauerts correction

     ar(i,j+1)=abs(1/(4*F(i)*sin(phi1(i))*cos(phi1(i))/(sy(i)*Ct(i))-1));
     %Tangential induction factor
     end
end
 clear i


 a=ax(:,end);   %Final axial induction factor[-]
 am=ar(:,end);  %Final tangential induction factor[-]


%%%%%%%%%Lift and drag coeffients during a revolution%%%%%%%%%%%%%%%%%%%%%%%

for l=1:max(size(az))
    for k=1:max(size(Radius))

        phit(k,l)=atan((1-a(k))*Ur(k,l)/((1+am(k))*w*Radius(k)));
        %Relative vind angle
        alfa(k,l)=phit(k,l)*180/pi-Blade.Twist(k);               %AoA

     [ba,vc] = searchclosest(Aero(1,k).AoA,alfa(k,l));
     Clb(k,l)=Aero(1,k).Prop(ba,1);     %Lift Coefficient
     Cdb(k,l)=Aero(1,k).Prop(ba,2);     %Drag coefficient
    end
end

%%%%%%%%%%%%%%%%%%%%%%%%%SAVING%%%%%%%%%%%%%%%%%%%%%%%%%%%%%%%%%%%%%%%%%%%%%
if t==1
    Tubular.Cl=Clb;
    Tubular.Cd=Cdb;
    Tubular.phi=phit;
    Tubular.a=a;
    Tubular.am=am;
    Tubular.F=F;
    save Tubular.mat Tubular
elseif t==0
    Truss.Cl=Clb;
    Truss.Cd=Cdb;
    Truss.phi=phit;
    Truss.a=a;
    Truss.am=am;
    Truss.F=F;
    save Truss.mat Truss
end
%%%%%%%%%%%%%%%%%%%%%%%%%PLOT%%%%%%%%%%%%%%%%%%%%%%%%%%%%%%%%%%%%%%%%%%%%%%

plot(Radius,a,Radius,am)
legend('Axial','Tangential')
xlabel('Blade Radius(m)')
ylabel('Induction Factor [-]')
```

Appendix A-6: MATLAB Script for Aerodynamic Forces

```
clear all
clc
%%%%%%%%%%%%%%%%%%%%%%%%%%INPUT%%%%%%%%%%%%%%%%%%%%%%%%%%%%%%%%%%%%%%%%%%%%%%%%%
az=0:2*pi/(360-1):2*pi;     %Azimuth[rad]
rho=1.225;                  %Air density [kg/m3]
w=1.2566;                   %Rotational speed[rad/sec]
load data                   %Structural data
load Truss
%Wind speeds, relative vind angle, and Cl and Cd for truss tower
load Tubular
%Wind speeds, relative vind angle, and Cl and Cd for tubular tower
t=0;                        %Set 1 for Tubular tower, 0 for truss tower.
betta=2.5*pi/180;           %Cone angle[rad]
%%%%%%%%%%%%%%%%%%%%%%%%%%%%%%%%%%%%%%%%%%%%%%%%%%%%%%%%%%%%%%%%%%%%%%%%%%%%%%%%
r=Blade.Radius*cos(betta); %Sectional radius[m]

if t==1;
    Ur=Tubular.Rotorwind;
    phi=Tubular.phi;
    Cl=Tubular.Cl;
    Cd=Tubular.Cd;
    a=Tubular.a;
    am=Tubular.am;
    F=Tubular.F;
elseif t==0;
    Ur=Truss.Rotorwind;
    phi=Truss.phi;
    Cl=Truss.Cl;
    Cd=Truss.Cd;
    a=Truss.a;
    am=Truss.am;
    F=Truss.F;
end



for j=1:max(size(az))
    for i=1:max(size(r))
    Urel(i,j)=sqrt((Ur(i,j)*(1-a(i)))^2+((1+am(i))*w*r(i))^2);
    %Relative wind speed [m/s]

    Cn(i,j)=Cl(i,j)*cos(phi(i,j))+Cd(i,j)*(sin(phi(i,j)));    %[N/m]
    Ct(i,j)=Cl(i,j)*sin(phi(i,j))-Cd(i,j)*cos(phi(i,j));      %[N/m]

    Pz(i,j)=F(i)*Cn(i,j)*0.5*rho*(Urel(i,j)^2)*Blade.Chord(i)*cos(betta);
    %Flapwise aerodynamic loading
    Py(i,j)=F(i)*Ct(i,j)*0.5*rho*(Urel(i,j)^2)*Blade.Chord(i);
    %Edgewise aerodynamic loading
    end
end

 %%%%%%%%%%%%%%%%%%%%%%%%%%%SAVING%%%%%%%%%%%%%%%%%%%%%%%%%%%%%%%%%%%%%%%%%%%%%
 if t==1;
    Tubular.Pz=Pz;
    Tubular.Py=Py;
```

```
    save Tubular.mat Tubular
elseif t==0;
    Truss.Pz=Pz;
    Truss.Py=Py;
    save Truss.mat Truss
 end

 %%%%%%%%%%%%%%%%%%%%%%%%%%PLOT%%%%%%%%%%%%%%%%%%%%%%%%%%%%%%%%%%%%%%%%%%%%
 plot(Blade.Span,Pz(:,1)/1000,Blade.Span,Py(:,1)/1000)
 legend('Axial','Tangential')
 xlabel('Blade Radius [m]')
 ylabel('Aerodynamic Forces [kN/m]')
```

Appendix A-7: MATLAB Script for Dynamic Response

```
clear all
clc
%%%%%%%%%%%%%%%%%%%%%%%%%%%%INPUT%%%%%%%%%%%%%%%%%%%%%%%%%%%%%%%%%%%%%%%%%
load data                   %Structural data
load Tubular                %Aerodynamic forces Tubular tower
nSections=38;               %Number of sections[-]
pp=3;                       %for plotting. 1=x,2=y,3=z
az=linspace(0,2*pi,360);    %Azimuth angle
w=1.2566;                   %Rotational speed[rad/sec]
betta=2.5*pi/180;           %Cone angle[rad]
mch=1;                      %Choose which mode to plot response
%%%%%%%%%%%%%%%%%%%%%%%%%%%%%%%%%%Calculations%%%%%%%%%%%%%%%%%%%%%%%%%%%

    Pzs=Tubular.Pz;  %loading in z-direction[N/m]
    Pys=Tubular.Py;

L=Blade.Span(end)/nSections;                        %Section length[m]
x1=0:Blade.Span(end)/nSections:Blade.Span(end); %Node placements

x=zeros(1,nSections);
for i=2:max(size(x1))-1
    x(i)=x1(i)+(x1(i+1)-x1(i))/2;                   %Section placement
end
x(1)=x1(2)/2;
clear i

EIy=interp1(Blade.Span,Blade.EIflap,x);     %Stiffness[N*m^2]
EIz=interp1(Blade.Span,Blade.EIedge,x);     %Stiffness[N*m^2]
GJ=interp1(Blade.Span,Blade.GJ,x);          %Torsional stiffness[N*m^2]
G=1e9;                                %Shear modulus of elasticity[N/m^2]
J=GJ/(G);                             %Torsional stiffness constant[m^4/rad]
E1=interp1(Blade.Span,Blade.EIflap,x);   %Stiffness in flap direction[Nm^2]
E2=interp1(Blade.Span,Blade.IAflap,x);   %Second moment of area[m^4]
E=E1/E2;                                 %Modulus of elasticity[N/m^2]
Iy=interp1(Blade.Span,Blade.IAflap,x);   %Second moment of area[m^4]
Iz=interp1(Blade.Span,Blade.IAedge,x);   %Second moment of area[m^4]
A=interp1(Blade.Span,Blade.A,x)/10;      %Area[m]
AE=A*E;
m1s=interp1(Blade.Span,Blade.Mass,x);    %Distributed mass[kg/m]
ky=0.5;                                  %Timoshenko Shear coefficient
miy=interp1(Blade.Span,Blade.IMflap,x); %Mass moment of inertia[kg*m^2]
miz=interp1(Blade.Span,Blade.IMedge,x); %Mass moment of inertia[kg*m^2]



K=zeros(6*nSections+6);     %Initialise
M=zeros(6*nSections+6);     %Initialise
T1=zeros(12);               %Initialise
T2=zeros(12);               %Initialise

for i=1:max(size(x));
%%%%%%%%%%%%%%%%%%%%%%%%%%%%%%%%Stiffness matrix%%%%%%%%%%%%%%%%%%%%%%%%%
    phiy(i)=12*EIz(i)*ky/(A(i)*G*(L^2));
    X(i)=AE(i)/(L^3);
    Y1(i)=12*EIz(i)/((1+phiy(i))*L^3);
    Y2(i)=6*EIz(i)/((1+phiy(i))*L^2);
    Y3(i)=(4+phiy(i))*EIz(i)/((1+phiy(i))*L);
```

```
    Y4(i)=(2-phiy(i))*EIz(i)/((1+phiy(i))*L);
    S(i)=GJ(i)/L;
    phiz(i)=12*EIy(i)*ky/(A(i)*G*(L^2));
    Z1(i)=12*EIy(i)/((1+phiz(i))*L^3);
    Z2(i)=6*EIy(i)/((1+phiz(i))*L^2);
    Z3(i)=(4+phiz(i))*EIy(i)/((1+phiz(i))*L);
    Z4(i)=(2-phiz(i))*EIy(i)/((1+phiz(i))*L);

    %Stiffness matrix
    km =[X(i),0,0,0,0,0,-X(i),0,0,0,0,0;
       0,Y1(i),0,0,0,Y2(i),0,-Y1(i),0,0,0,Y2(i);
       0,0,Z1(i),0,-Z2(i),0,0,0,-Z1(i),0,-Z2(i),0;
       0,0,0,S(i),0,0,0,0,0,-S(i),0,0;
       0,0,-Z2(i),0,Z3(i),0,0,0,Z2(i),0,Z4(i),0;
       0,Y2(i),0,0,0,Y3(i),0,-Y2(i),0,0,0,Y4(i)
       -X(i),0,0,0,0,0,X(i),0,0,0,0,0;
       0,-Y1(i),0,0,0,-Y2(i),0,Y1(i),0,0,0,-Y2(i);
       0,0,-Z1(i),0,Z2(i),0,0,0,Z1(i),0,Z2(i),0;
       0,0,0,-S(i),0,0,0,0,0,S(i),0,0;
       0,0,-Z2(i),0,Z4(i),0,0,0,Z2(i),0,Z3(i),0;
       0,Y2(i),0,0,0,Y4(i),0,-Y2(i),0,0,0,Y3(i)];

   mt(i)=m1s(i)*L; %Section mass[kg]

   %Mass matrix
   mm=mt(i)*[1/3,0,0,0,0,0,1/6,0,0,0,0,0;

0,(13/35)+6*Iz(i)/(5*A(i)*L^2),0,0,0,(11*L)/210+(Iy(i))/(10*A(i)*L),0,9/70-
(6*Iz(i))/(5*A(i)*L^2),0,0,0,-13*L/420+(Iz(i))/(10*A(i)*L);
      0,0,(13/35)+6*Iy(i)/(5*A(i)*L^2),0,(-11*L/210)-
(Iy(i)/(10*A(i)*L)),0,0,0,9/70-(6*Iy(i))/(5*A(i)*L^2),0,13*L/420-
(Iy(i))/(10*A(i)*L),0;
      0,0,0,J(i)/(3*A(i)),0,0,0,0,0,J(i)/(6*A(i)),0,0;
      0,0,(-11*L/210)-
(Iy(i)/(10*A(i)*L)),0,(L^2/105)+(2*Iy(i))/(15*A(i)),0,0,0,-
13*L/420+(Iz(i))/(10*A(i)*L),0,-L^2/140-(Iy(i))/(30*A(i)),0;

0,(11*L)/210+(Iy(i))/(10*A(i)*L),0,0,0,(L^2/105)+(2*Iz(i))/(15*A(i)),0,13*L
/420-(Iz(i))/(10*A(i)*L),0,0,0,-L^2/140-Iz(i)/(30*A(i));
      1/6,0,0,0,0,0,1/3,0,0,0,0,0;
      0,9/70-(6*Iz(i))/(5*A(i)*L^2),0,0,0,13*L/420-
(Iz(i))/(10*A(i)*L),0,13/35+6*Iz(i)/(5*A(i)*L^2),0,0,0,-11*L/210-
Iz(i)/(10*A(i)*L);
      0,0,9/70-(6*Iy(i))/(5*A(i)*L^2),0,-
13*L/420+(Iz(i))/(10*A(i)*L),0,0,0,13/35+6*Iz(i)/(5*A(i)*L^2),0,11*L/210+Iy
(i)/(10*A(i)*L),0;
      0,0,0,J(i)/(6*A(i)),0,0,0,0,0,J(i)/(3*A(i)),0,0;
      0,0,13*L/420-(Iy(i))/(10*A(i)*L),0,-L^2/140-
(Iy(i))/(30*A(i)),0,0,0,11*L/210+Iy(i)/(10*A(i)*L),0,L^2/105+2*Iy(i)/(15*A(
i)),0;
      0,-13*L/420+(Iz(i))/(10*A(i)*L),0,0,0,-L^2/140-Iz(i)/(30*A(i)),0,-
11*L/210-Iz(i)/(10*A(i)*L),0,0,0,L^2/105+2*Iz(i)/(15*A(i))];

 %Assembly
  K(((i-1)*6+1):(12+(i-1)*6),(i-1)*6+1:12+(i-1)*6)=K(((i-1)*6+1):(12+(i-
1)*6),(i-1)*6+1:12+(i-1)*6)+km;
  M(((i-1)*6+1):(12+(i-1)*6),(i-1)*6+1:12+(i-1)*6)=M(((i-1)*6+1):(12+(i-
1)*6),(i-1)*6+1:12+(i-1)*6)+mm;
end
clear i
```

```
K = K(7:end,7:end);     %Removes (condensates) fixed degrees of freedom
M = M(7:end,7:end);     %Removes (condensates) fixed degrees of freedom


[VB,DB] = eig(K,M,'chol'); %Solves the generalized eigen problem


for i=1:max(size(x))
   eigenfreq(i)=sqrt(DB(i,i));      %Eigenfrequencies
   phitrans(i,:)=VB(6*(i-1)+pp,:);  %Mode shapes in chosen translational
degree of freedom
end
clear i
eigenfreq=sort(eigenfreq);          %Sorts Eigenfrequencies

for j=1:min(size(phitrans))
    if abs(max(phitrans(:,j)))>abs(min(phitrans(:,j)))      %normalizing
mode shape vectors(max value=1)
        phinorm(:,j)=phitrans(:,j)/(max(phitrans(:,j))+1);
    else
        phinorm(:,j)=phitrans(:,j)/(min(phitrans(:,j))+1);
    end
    phiplot(1,j)=0;                                         %Zero at fixed end
    phiplot(2:min(size(phitrans))+1,j)=phinorm(:,j);    %Mode shape
end
clear j

%%%%%%%%%%%%%%%%%%%%%%%%%%%%%%Mode shape plots%%%%%%%%%%%%%%%%%%%%%%%%%%%%%%
for j=1:3
  subplot(3,1,j)
    axis([-1.1,1.1,0,max(x1)*1.1]);
    plot(x1,phiplot(:,j));
    grid
end
clear j
%%%%%%%%%%%%%%%%%%%%%%%%%%%%%%%%%%%%%%%%%%%%%%%%%%%%%%%%%%%%%%%%%%%%%%%%%%%
for b=1:7 %Number of iterations for determening centrifugal force
    load d_bladetrt.dat %Blade tip deflection [m]

    P=zeros(nSections*6+6,1);   %Initialise
for j=1:360
    for i=2:max(size(x1))-1
        d_ang(i,j)=asin(d_bladetrt(i,j)/(x1(i))); %Deflection angle [rad]

    P(6*(i-1)+3,j)=Pzs(i,j)*L-
m1s(i)*L*(w^2)*x(i)*cos(d_ang(i,j)+betta)*sin(d_ang(i,j)+betta);
    P(6*(i-1)+2,j)=Pys(i,j)*L;
    P(6*(i-1)+1,j)=m1s(i)*L*(w^2)*x(i)*(cos(d_ang(i,j)+betta))^2;
    %Load matrix[N]
    end
    for o=max(size(x1))-1:max(size(x1))
    P(6*(o-1)+3,j)=Pzs(o,j)*L/2-
m1s(i)*L/2*(w^2)*x(i)*cos(d_ang(i,j)+betta)*sin(d_ang(i,j)+betta);
%Total load matrix[N]
    P(6*(o-1)+2,j)=Pys(o,j)*L/2;
    P(6*(i-1)+1,j)=L/2*m1s(i)*(w^2)*x(i)*(cos(betta+d_ang(i,j)))^2;
    %Total load matrix[N]
```

```
    end

end
clear i j o

P=P(7:end,:);      %Removes (condensates) loads at fixed degrees of freedom
%%%%%%%%%%%%%%%%%%%%%%%%%Dynamic response%%%%%%%%%%%%%%%%%%%%%%%%%%%%%%%%%%

    m=transpose(VB)*M*VB;   %Generalized mass
    k=transpose(VB)*K*VB;   %Generalized stiffness

    c=zeros(nSections*6);
    for i=1:max(size(eigenfreq))
    c1t(i,i)=2*m(i,i)*eigenfreq(i)*0.0048+1.2; %1.st mode damping
    c2t(i,i)=2*m(i,i)*eigenfreq(i)*0.0048+1.2; %2.nd mode damping
    end
    clear i

     m=diag(m);
     k=diag(k);
     c1t=diag(c1t);
     c2t=diag(c2t);

    for i=1:360
        p1(:,i)=transpose(VB)*P(:,i);   %Generalized load
    end
    clear i

pt=linspace(0,5,360);           %Time steps for load vector[s]

%%%%%%%%%%%%%%%%%%%%%%%%%%%%first mode%%%%%%%%%%%%%%%%%%%%%%%%%%%%%%%%%%%%%
if mch==1;
m1=m(1);    %Generalized mass first mode
k1=k(1);    %Generalized stiffness first mode
c1=c1t(1);  %Generalized damping first mode
p=p1(1,:);  %Generalized loading first mode

save -ascii m.dat m1
save -ascii c.dat c1
save -ascii k.dat k1

tspan=linspace(0,5,360);        %Time span[s]
if pp==3 %Flap direction
    y0=[244.3146    2.8697];        %Intital conditions
elseif pp==2 %Edge direction
    y0=[242.1715    2.4675];        %Intital conditions
end

[t,y] = ode45(@(t,y) fcn45(t,y,pt,p),tspan,y0);%Solves ODE with time
dependent load

%plot(tspan,y(:,1))

for i=1:360
hop1(:,i)=phiplot(:,1)*y(i,1); %Deflections first mode
end
clear i
%plot(hop1(end,:));
```

```
save -ascii d_bladetrt.dat hop1
end
end
%%%%%%%%%%%%%%%%%%%%%%%%%second mode%%%%%%%%%%%%%%%%%%%%%%%%%%%%%%%%%%%%%%%%
if mch==2;
m2=m(2);     %Generalized mass second mode
k2=k(2);     %Generalized stiffness second mode
c2=c2t(2);   %Generalized damping second mode
p=p1(2,:);   %%Generalized load second mode

save -ascii m.dat m2
save -ascii c.dat c2
save -ascii k.dat k2

tspan=linspace(0,5,360);
if pp==3 %Flap direction
    y0=[11.6156    2.0038];
elseif pp==2 %Edge direction
    y0=[11.5009    3.8461];
end

[t1,y1] = ode45(@(t1,y1) fcn45(t1,y1,pt,p),tspan,y0);
%Solves ODE with time dependent load

%plot(tspan,y1(:,1))

for i=1:360
    hop2(:,i)=phiplot(:,2)*y1(i,1); %Deflections second mode
end
%clear i
%plot(hop2(end,:));
end
%%%%%%%%%%%%%%%%%%%%%%%%%Third mode%%%%%%%%%%%%%%%%%%%%%%%%%%%%%%%%%%%%%%%%%
if mch==3;
m2=m(3);     %Generalized mass third mode
k2=k(3);     %Generalized stiffness third mode
c2=c2t(3);   %Generalized damping third mode
p=p1(3,:);   %%Generalized load third mode

save -ascii m.dat m2
save -ascii c.dat c2
save -ascii k.dat k2

tspan=linspace(0,5,360);

if pp==3
    y0=[-6.6629    1.8983];
elseif pp==2
    y0=[-10.2085    2.6521];
end
[t2,y2] = ode45(@(t2,y2) fcn45(t2,y2,pt,p),tspan,y0);

%plot(tspan,y2(:,1))

for i=1:360
    hop3(:,i)=phiplot(:,3)*y2(i,1); %Deflections third mode
end
clear i j
%plot(hop3(end,:));
```

```
end
%%%%%%%%%%%%%%%%%%%%%%%%%%%%%%%%%%%%%%%%%%%%%%%%%%%%%%%%%%%%%%%%%%%%%%%%%%%%%%%

%%%%%%%%%%%%%%%%%%%%%%%%%%%%%%%%%%%%%%%%%%%%%%%%%%%%%%%%%%%%%%%%%%%%%%%%%%%%%%%
%%%%%%%%%%%%%%%%%%%%%%%%%%%%%%%%%%%%Saving%%%%%%%%%%%%%%%%%%%%%%%%%%%%%%%%%%%%%
if pp==3
if mch==1
Tubular.Response.Flap.Mode1=hop1;
end
if mch==2
Tubular.Response.Flap.Mode2=hop2;
end
if mch==3
Tubular.Response.Flap.Mode3=hop3;
end
elseif pp==2
%Tubular.Response.Edge.Mode1=hop1;
%Tubular.Response.Edge.Mode2=hop2;
%Tubular.Response.Edge.Mode3=hop3;
end
save Tubular.mat Tubular
```

Appendix A-8: MATLAB Script for Bending Moment

```
clear all
clc

load Data       %Structural data
load Tubular    %Dynamic response tubular tower
load Truss      %Dynamic response truss tower

nSections=38;   %Number of sections
L=Blade.Span(end)/nSections;                      %Section length[m]
x1=0:Blade.Span(end)/nSections:Blade.Span(end); %Node placements
az=linspace(0,2*pi,360);                          %Azimuth


EIbmy=interp1(Blade.Span,Blade.EIflap,x1);
for j=1:360

hop1_yd(:,j)=gradient(Tubular.Response.Flap.Mode1(:,j)+Tubular.Response.Fla
p.Mode2(:,j)+Tubular.Response.Flap.Mode3(:,j),L);
    hop1_ydd(:,j)=gradient(hop1_yd(:,j),L); %d^2w/dx^2
    for i=1:max(size(x1))
        Mfl(i,j)=EIbmy(i)*hop1_ydd(i,j);  %Bending moment tubular tower[Nm]
    end
end



for j=1:360

hop1_ydT(:,j)=gradient(Truss.Response.Flap.Mode1(:,j)+Truss.Response.Flap.M
ode2(:,j)+Truss.Response.Flap.Mode3(:,j),L);
    hop1_yddT(:,j)=gradient(hop1_ydT(:,j),L); %d^2w/dx^2
    for i=1:max(size(x1))
        MflT(i,j)=EIbmy(i)*hop1_yddT(i,j);  %Bending moment truss tower[Nm]
    end
end

%%%%%%%%%%%%%%%%%%%%%%%%%%%%%%%%%%%%PLOT%%%%%%%%%%%%%%%%%%%%%%%%%%%%%%%%%%%%
plot(az,Mfl(2,:)/1000,az,MflT(2,:)/1000)
set(gca,'XTick',0:pi/2:2*pi)
set(gca,'XTickLabel',{'0','pi/2','pi','3pi/2','2pi'})
legend('Tubular Tower','Truss Tower')
xlabel('RFM [kNm]')
ylabel('Azimuth[rad]')
```

Appendix A-9 Input Data for Structural Matrices

R [m]	A [m^2]	E [N/m^2]	Iy [m^4]	Iz [m^4]	M [kg/m]	G [N/m^2]	K [m^4/rad]	ky [-]	kz[-]
1.38	9.58	9.49E+09	1.88E+00	1.92E+00	924.69	1.00E+09	6.87E+00	0.50	0.50
2.84	9.93	9.49E+09	1.53E+00	1.72E+00	827.61	1.00E+09	6.50E+00	0.50	0.50
4.29	10.31	9.49E+09	1.55E+00	1.40E+00	676.12	1.00E+09	4.59E+00	0.50	0.50
5.75	10.49	9.49E+09	1.35E+00	1.54E+00	607.82	1.00E+09	3.92E+00	0.50	0.50
7.21	10.40	9.49E+09	1.19E+00	1.71E+00	562.94	1.00E+09	3.34E+00	0.50	0.50
8.67	10.08	9.49E+09	1.02E+00	1.88E+00	535.03	1.00E+09	2.84E+00	0.50	0.50
10.13	9.61	9.49E+09	8.67E-01	2.03E+00	519.42	1.00E+09	2.41E+00	0.50	0.50
11.59	9.04	9.49E+09	7.33E-01	2.18E+00	503.57	1.00E+09	2.03E+00	0.50	0.50
13.05	8.42	9.49E+09	6.14E-01	2.33E+00	486.03	1.00E+09	1.68E+00	0.50	0.50
14.51	7.39	9.49E+09	4.90E-01	2.24E+00	475.10	1.00E+09	1.37E+00	0.50	0.50
15.97	6.61	9.49E+09	3.94E-01	2.17E+00	463.13	1.00E+09	1.14E+00	0.50	0.50
17.43	5.98	9.49E+09	3.09E-01	2.09E+00	441.22	1.00E+09	9.62E-01	0.50	0.50
18.89	5.36	9.49E+09	2.50E-01	2.02E+00	434.86	1.00E+09	8.18E-01	0.50	0.50
20.35	4.79	9.49E+09	1.96E-01	1.91E+00	419.13	1.00E+09	6.92E-01	0.50	0.50
22.78	4.13	9.49E+09	1.49E-01	1.75E+00	406.50	1.00E+09	5.46E-01	0.50	0.50
25.21	3.61	9.49E+09	1.16E-01	1.55E+00	393.30	1.00E+09	4.46E-01	0.50	0.50
27.64	3.17	9.49E+09	9.22E-02	1.37E+00	390.47	1.00E+09	3.82E-01	0.50	0.50
30.08	2.79	9.49E+09	7.30E-02	1.19E+00	378.02	1.00E+09	3.18E-01	0.50	0.50
32.51	2.46	9.49E+09	5.87E-02	1.04E+00	370.18	1.00E+09	2.68E-01	0.50	0.50
34.94	2.18	9.49E+09	4.62E-02	8.76E-01	347.50	1.00E+09	2.18E-01	0.50	0.50
37.37	1.94	9.49E+09	3.64E-02	7.29E-01	321.21	1.00E+09	1.75E-01	0.50	0.50
39.81	1.73	9.49E+09	2.88E-02	6.03E-01	293.88	1.00E+09	1.40E-01	0.50	0.50
42.24	1.55	9.49E+09	2.28E-02	4.98E-01	266.30	1.00E+09	1.12E-01	0.50	0.50
44.67	1.40	9.49E+09	1.78E-02	4.10E-01	233.76	1.00E+09	8.73E-02	0.50	0.50
47.10	1.27	9.49E+09	1.38E-02	3.28E-01	202.94	1.00E+09	6.64E-02	0.50	0.50
49.54	1.15	9.49E+09	1.07E-02	2.68E-01	172.54	1.00E+09	5.00E-02	0.50	0.50
51.97	1.05	9.49E+09	8.54E-03	2.20E-01	149.55	1.00E+09	3.86E-02	0.50	0.50
54.40	0.97	9.49E+09	6.97E-03	1.80E-01	131.16	1.00E+09	3.02E-02	0.50	0.50
56.44	0.90	9.49E+09	5.90E-03	1.51E-01	116.86	1.00E+09	2.45E-02	0.50	0.50
58.49	0.82	9.49E+09	4.74E-03	1.19E-01	103.01	1.00E+09	1.91E-02	0.50	0.50
60.53	0.72	9.49E+09	3.63E-03	8.84E-02	89.53	1.00E+09	1.43E-02	0.50	0.50
62.57	0.61	9.49E+09	2.66E-03	6.33E-02	79.18	1.00E+09	1.07E-02	0.50	0.50
64.62	0.47	9.49E+09	1.51E-03	3.66E-02	63.62	1.00E+09	6.76E-03	0.50	0.50
65.30	0.41	9.49E+09	1.19E-03	2.87E-02	58.79	1.00E+09	5.54E-03	0.50	0.50
65.98	0.34	9.49E+09	8.68E-04	2.08E-02	52.98	1.00E+09	4.25E-03	0.50	0.50
66.66	0.27	9.49E+09	5.50E-04	1.30E-02	45.63	1.00E+09	2.89E-03	0.50	0.50
67.34	0.17	9.49E+09	2.57E-04	6.00E-03	35.68	1.00E+09	1.51E-03	0.50	0.50
68.02	0.09	9.49E+09	8.88E-05	2.02E-03	25.35	1.00E+09	6.02E-04	0.50	0.50

Appendix A-10 Eigenmodes with structural adjustments

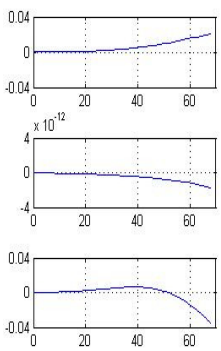

Figure 64
Eigenmodes, 100% EI

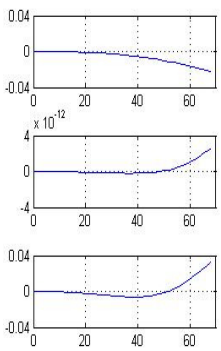

Figure 65
Eigenmodes, 95% EI

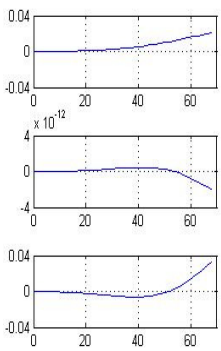

Figure 66
Eigenmodes, 90% EI

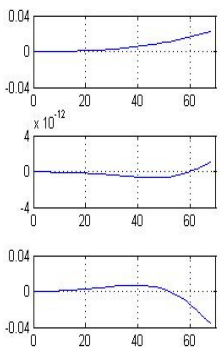

Figure 67
Eigenmodes, 80% EI

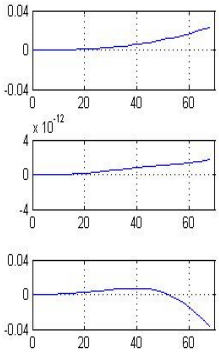

Figure 68
Eigenmodes, 70 % EI

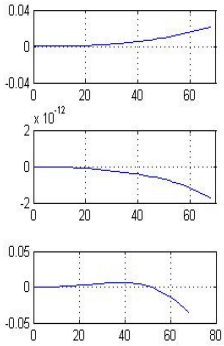

Figure 69
Eigenmodes, 100% EI & m

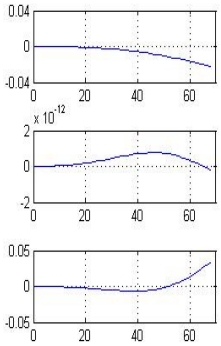

Figure 70
Eigenmodes, 95 % EI & m

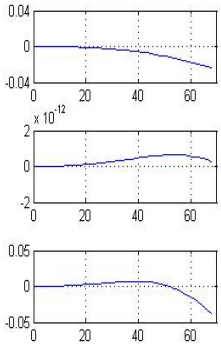

Figure 71
Eigenmodes, 90% EI & m

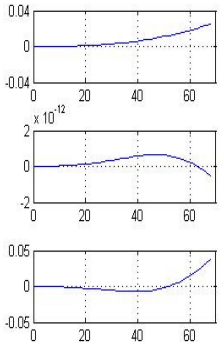

Figure 72
Eigenmodes, 80 % EI & m

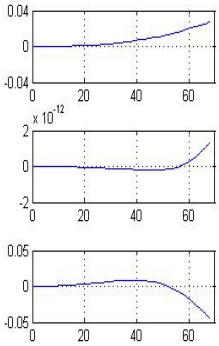

Figure 73
Eigenmodes, 70 % EI & m

Appendix A-11 MATLAB script for plotting blade tip deflection with reduced stiffness

```
clear all
clc

load Truss70  %Dynamic response with 70% of original stiffness, truss tower
load Truss80  %Dynamic response with 70% of original stiffness, truss tower
load Truss90  %Dynamic response with 90% of original stiffness, truss tower
load Truss95  %Dynamic response with 95% of original stiffness, truss tower
load Truss100 %Dynamic response with 100% of original stiffness, truss
tower

load Tubular70  %Dynamic response with 70% of original stiffness, tubular t
load Tubular80  %Dynamic response with 80% of original stiffness, tubular t
load Tubular90  %Dynamic response with 90% of original stiffness, tubular t
load Tubular95  %Dynamic response with 95% of original stiffness, tubular t
load Tubular100 %Dynamic response with 100% of original stiffness, tubular
t

az=linspace(0,2*pi,360); %Azimuth angle

%%%%%%%%%%%%%%%%%%%%%%%%%%%%%%%%%PLOTTING%%%%%%%%%%%%%%%%%%%%%%%%%%%%%%%%%
%PLOT: Adjusted stiffness, truss tower
plot(az,Truss70.Response.Flap70.Mode1(end,:)+Truss70.Response.Flap70.Mode2(
end,:)+Truss70.Response.Flap70.Mode3(end,:),az,Truss80.Response.Flap80.Mode
1(end,:)+Truss80.Response.Flap80.Mode2(end,:)+Truss80.Response.Flap80.Mode3
(end,:),az,Truss90.Response.Flap90.Mode1(end,:)+Truss90.Response.Flap90.Mod
e2(end,:)+Truss90.Response.Flap90.Mode3(end,:),az,Truss95.Response.Flap95.M
ode1(end,:)+Truss95.Response.Flap95.Mode2(end,:)+Truss95.Response.Flap95.Mo
de3(end,:),az,Truss100.Response.Flap.Mode1(end,:)+Truss100.Response.Flap.Mo
de2(end,:)+Truss100.Response.Flap.Mode3(end,:));

%PLOT: Adjusted stiffness tubular tower
%plot(az,Tubular70.Response.Flap70.Mode1(end,:)+Tubular70.Response.Flap70.M
ode2(end,:)+Tubular70.Response.Flap70.Mode3(end,:),az,Tubular80.Response.Fl
ap80.Mode1(end,:)+Tubular80.Response.Flap80.Mode2(end,:)+Tubular80.Response
.Flap80.Mode3(end,:),az,Tubular90.Response.Flap90.Mode1(end,:)+Tubular90.Re
sponse.Flap90.Mode2(end,:)+Tubular90.Response.Flap90.Mode3(end,:),az,Tubula
r95.Response.Flap95.Mode1(end,:)+Tubular95.Response.Flap95.Mode2(end,:)+Tub
ular95.Response.Flap95.Mode3(end,:),az,Tubular100.Response.Flap.Mode1(end,:
)+Tubular100.Response.Flap.Mode2(end,:)+Tubular100.Response.Flap.Mode3(end,
:));

%PLOT: Differenci in dynamic response without adjustment between the two
%towers:
%plot(az,Tubular100.Response.Flap.Mode1(end,:)+Tubular100.Response.Flap.Mod
e2(end,:)+Tubular100.Response.Flap.Mode3(end,:),az,Truss100.Response.Flap.M
ode1(end,:)+Truss100.Response.Flap.Mode2(end,:)+Truss100.Response.Flap.Mode
3(end,:))

%PLOT: Dynamic response based on first mode and three first modes without
%adjustment, Tubular tower
%plot(az,Tubular100.Response.Flap.Mode1(end,:),az,Tubular100.Response.Flap.
Mode1(end,:)+Tubular100.Response.Flap.Mode2(end,:)+Tubular100.Response.Flap
.Mode3(end,:))

%PLOT: Dynamic response based on first mode and three first modes without
%adjustment, Truss tower
```

```
%plot(az,Truss100.Response.Flap.Mode1(end,:),az,Truss100.Response.Flap.Mode
1(end,:)+Truss100.Response.Flap.Mode2(end,:)+Truss100.Response.Flap.Mode3(e
nd,:));

set(gca,'XTick',0:pi/2:2*pi)
set(gca,'XTickLabel',{'0','pi/2','pi','3pi/2','2pi'})
ylabel('Blade Tip Displacement [m]')
xlabel('Azimuth[rad]')
legend('70%   EI','80%   EI','90%   EI','95%   EI','100% EI')
%legend('Tubular Tower','Truss Tower');
%legend('Response Frist Mode','Response Frist Three Modes')
```

Appendix A-12 MATLAB script for plotting RFM with reduced stiffness

```
clear all
clc

load Data
load Truss70 %Dynamic response with 70% of original stiffness, truss tower
load Truss80 %Dynamic response with 80% of original stiffness, truss tower
load Truss90 %Dynamic response with 90% of original stiffness, truss tower
load Truss95 %Dynamic response with 95% of original stiffness, truss tower
load Truss100%Dynamic response with 100% of original stiffness, truss tower

load Tubular70 %Dynamic response with 70% of original stiffness, tubular t
load Tubular80 %Dynamic response with 80% of original stiffness, tubular t
load Tubular90 %Dynamic response with 90% of original stiffness, tubular t
load Tubular95 %Dynamic response with 95% of original stiffness, tubular t
load Tubular100%Dynamic response with 100% of original stiffness, tubular t

nSections=38;
L=Blade.Span(end)/nSections;                    %Section length[m]
x1=0:Blade.Span(end)/nSections:Blade.Span(end); %Node placements [m]
az=linspace(0,2*pi,360);                       %Azimuth angle[rad]


EIbmy70=interp1(Blade.Span,Blade.EIflap*0.7,x1);    %
EIbmy80=interp1(Blade.Span,Blade.EIflap*0.8,x1);    %
EIbmy90=interp1(Blade.Span,Blade.EIflap*0.9,x1);    %Reduced blade stiffnes
EIbmy95=interp1(Blade.Span,Blade.EIflap*0.95,x1);   %
EIbmy100=interp1(Blade.Span,Blade.EIflap,x1);       %


for j=1:360
    %%%%%%%%%%%%%%%%%%Gradients%%%%%%%%%%%%%%%%%%%%%%%%%%%%%%%%%%%%%%%%%%%%

hop1_yd70(:,j)=gradient(Tubular70.Response.Flap70.Mode1(:,j)+Tubular70.Resp
onse.Flap70.Mode2(:,j)+Tubular70.Response.Flap70.Mode3(:,j),L);
    hop1_ydd70(:,j)=gradient(hop1_yd70(:,j),L);


hop1_yd80(:,j)=gradient(Tubular80.Response.Flap80.Mode1(:,j)+Tubular80.Resp
onse.Flap80.Mode2(:,j)+Tubular80.Response.Flap80.Mode3(:,j),L);
    hop1_ydd80(:,j)=gradient(hop1_yd80(:,j),L);


hop1_yd90(:,j)=gradient(Tubular90.Response.Flap90.Mode1(:,j)+Tubular90.Resp
onse.Flap90.Mode2(:,j)+Tubular90.Response.Flap90.Mode3(:,j),L);
    hop1_ydd90(:,j)=gradient(hop1_yd90(:,j),L);


hop1_yd95(:,j)=gradient(Tubular95.Response.Flap95.Mode1(:,j)+Tubular95.Resp
onse.Flap95.Mode2(:,j)+Tubular95.Response.Flap95.Mode3(:,j),L);
    hop1_ydd95(:,j)=gradient(hop1_yd95(:,j),L);


hop1_yd100(:,j)=gradient(Tubular100.Response.Flap.Mode1(:,j)+Tubular100.Res
ponse.Flap.Mode2(:,j)+Tubular100.Response.Flap.Mode3(:,j),L);
    hop1_ydd100(:,j)=gradient(hop1_yd100(:,j),L);
```

```
hop1_ydTr70(:,j)=gradient(Truss70.Response.Flap70.Mode1(:,j)+Truss70.Respon
se.Flap70.Mode2(:,j)+Truss70.Response.Flap70.Mode3(:,j),L);
    hop1_yddTr70(:,j)=gradient(hop1_ydTr70(:,j),L);


hop1_ydTr80(:,j)=gradient(Truss80.Response.Flap80.Mode1(:,j)+Truss80.Respon
se.Flap80.Mode2(:,j)+Truss80.Response.Flap80.Mode3(:,j),L);
    hop1_yddTr80(:,j)=gradient(hop1_ydTr80(:,j),L);


hop1_ydTr90(:,j)=gradient(Truss90.Response.Flap90.Mode1(:,j)+Truss90.Respon
se.Flap90.Mode2(:,j)+Truss90.Response.Flap90.Mode3(:,j),L);
    hop1_yddTr90(:,j)=gradient(hop1_ydTr90(:,j),L);


hop1_ydTr95(:,j)=gradient(Truss95.Response.Flap95.Mode1(:,j)+Truss95.Respon
se.Flap95.Mode2(:,j)+Truss95.Response.Flap95.Mode3(:,j),L);
    hop1_yddTr95(:,j)=gradient(hop1_ydTr95(:,j),L);


hop1_ydTr100(:,j)=gradient(Truss100.Response.Flap.Mode1(:,j)+Truss100.Respo
nse.Flap.Mode2(:,j)+Truss100.Response.Flap.Mode3(:,j),L);
    hop1_yddTr100(:,j)=gradient(hop1_ydTr100(:,j),L);

    for i=1:max(size(x1))
        %%%%%%%%%%%%%%%%%%%%%%%%%TUBULAR TOWER%%%%%%%%%%%%%%%%%%%%%%%%%%%%
        Mfl70(i,j)=EIbmy70(i)*hop1_ydd70(i,j);          %RFM 70% stiffness
        Mfl80(i,j)=EIbmy80(i)*hop1_ydd80(i,j);          %RFM 80% stiffness
        Mfl90(i,j)=EIbmy90(i)*hop1_ydd90(i,j);          %RFM 90% stiffness
        Mfl95(i,j)=EIbmy95(i)*hop1_ydd95(i,j);          %RFM 95% stiffness
        Mfl100(i,j)=EIbmy100(i)*hop1_ydd100(i,j);       %RFM 100% stiffness

        %%%%%%%%%%%%%%%%%%%%%%%%%TRUSS TOWER%%%%%%%%%%%%%%%%%%%%%%%%%%%%%%
        MflTr70(i,j)=EIbmy70(i)*hop1_yddTr70(i,j);      %RFM 70% stiffness
        MflTr80(i,j)=EIbmy80(i)*hop1_yddTr80(i,j);      %RFM 80% stiffness
        MflTr90(i,j)=EIbmy90(i)*hop1_yddTr90(i,j);      %RFM 90% stiffness
        MflTr95(i,j)=EIbmy95(i)*hop1_yddTr95(i,j);      %RFM 95% stiffness
        MflTr100(i,j)=EIbmy100(i)*hop1_yddTr100(i,j);   %RFM 100% stiffness
    end
end

%PLOT: RFM tubular tower
plot(az,Mfl70(2,:)/1000,az,Mfl80(2,:)/1000,az,Mfl90(2,:)/1000,az,Mfl95(2,:)
/1000,az,Mfl100(2,:)/1000)
%PLOT: RFM truss tower
%plot(az,MflTr70(2,:)/1000,az,MflTr80(2,:)/1000,az,MflTr90(2,:)/1000,az,Mfl
Tr95(2,:)/1000,az,MflTr100(2,:)/1000)

%PLOT: Difference in RFM between towers. No adjustment
%plot(az,Mfl100(2,:)/1000,az,MflTr100(2,:)/1000)

set(gca,'XTick',0:pi/2:2*pi)
set(gca,'XTickLabel',{'0','pi/2','pi','3pi/2','2pi'})
ylabel('RFM [kNm]')
xlabel('Azimuth[rad]')
legend('70%   EI','80%   EI','90%   EI','95%   EI','100% EI')
%legend('Tubular Tower','Truss Tower');
```